

**Comprehensive phosphoproteomics of heart development  
identifies Mic85 as a new component of the mitochondrial  
MICOS complex**

*Dissertation zur Erlangung des Doktorgrades*

**Doctor philosophiae naturalis (Dr. phil. nat.)**

*vorgelegt beim*

Fachbereich Biowissenschaften (FB 15)

der Johann Wolfgang Goethe-Universität

in Frankfurt am Main



*von*

**Sriram Aravamudhan**

aus Chennai, Indien

Frankfurt am Main, 2015

(D 30)

Die vorliegende Arbeit wurde am Max-Planck-Institut für Herz- und Lungenforschung (W.G. Kerckhoff Institut) in Bad Nauheim angefertigt



und vom Fachbereich 15 der Johann Wolfgang Goethe - Universität als Dissertation angenommen.

**Dekanin:** Prof. Dr. Meike Piepenbring  
Fachbereich Biowissenschaften (FB 15)  
Johann Wolfgang Goethe-Universität, Frankfurt am Main

**Erstgutachterin:** Prof. Dr. Anna Starzinski-Powitz  
Institut für Zellbiologie und Neurowissenschaft  
Johann Wolfgang Goethe-Universität, Frankfurt am Main

**Zweitgutachter:** Prof. Dr. Dr. Thomas Braun  
Abteilung für Entwicklung und Umbau des Herzens  
Max-Planck-Institut für Herz- und Lungenforschung, Bad Nauheim

**Doktorvater:** Prof. Dr. Marcus Krüger  
CECAD Forschungszentrum  
Universität zu Köln, Köln

**Datum der Disputation:**

## ERKLÄRUNG

Ich erkläre hiermit, dass ich mich bisher keiner Doktorprüfung im Mathematisch-Naturwissenschaftlichen Bereich unterzogen habe.

Frankfurt am Main, den

.....

(Unterschrift)

## Versicherung

Ich erkläre hiermit, dass ich die vorgelegte Dissertation über

**Comprehensive phosphoproteomics of heart development identifies Mic85 as a new component of the mitochondrial MICOS complex**

selbständig angefertigt und mich anderer Hilfsmittel als der in ihr angegebenen nicht bedient habe, insbesondere, dass alle Entlehnungen aus anderen Schriften mit Angabe der betreffenden Schrift gekennzeichnet sind.

Ich versichere, die Grundsätze der guten wissenschaftlichen Praxis beachtet, und nicht die Hilfe einer kommerziellen Promotionsvermittlung in Anspruch genommen zu haben.

Vorliegende Ergebnisse der Arbeit werden in folgendem Publikationsorgan veröffentlicht:

**Aravamudhan S**, et al. Comprehensive phosphoproteomics of heart development identifies Mic85 as a new component of mitochondrial MICOS complex. *(Manuskript in Arbeit)*

Frankfurt am Main, den

.....

(Unterschrift)

## ACKNOWLEDGEMENTS

I take this opportunity to express my gratitude to all those who have been instrumental in providing their full encouragement and support towards the successful completion of my thesis.

I would like to thank Prof. Dr. Dr. Thomas Braun and Prof. Dr. Marcus Krüger for giving me this opportunity to pursue my PhD in the Biomolecular Mass Spectrometry division at the Max Planck Institute for Heart and Lung Research. I highly appreciate their constant mentoring and tremendous support right from the beginning, without which this project would not have materialized.

I extend my deep gratitude towards my thesis committee chair Prof. Dr. Anna Starzinski-Powitz for her valuable feedback and suggestions, and to Prof. Dr. Meike Piepenbring, the Dean of Faculty of Biological Sciences (FB 15) at the Goethe University, Frankfurt am Main, for supporting my doctoral graduation.

I would like to thank my peers, especially Hendrik Nolte, Natalie Al-Furoukh, Kerstin Wilhelm and Ramesh Kumar Krishnan for their valuable input towards the project, and Soraya Hölper and Krishnamoorthy Sreenivasan for healthy scientific discussions. I also extend my sincere thanks to the laboratory technicians Sylvia Jeratsch and Ellen Borowski for their timely assistance.

Finally, I am very grateful to my parents, my brother and my wife for their continuous moral support, love and encouragement which keeps me motivated and flying high in my career.

Sriram Aravamudhan

## ABSTRACT

Dissecting the complexities of mammalian heart development and regenerative capacity require thorough understanding of the underlying molecular mechanisms through the expression pattern of proteins and post-translational modifications. To obtain insights into activated signaling pathways that control the cellular phenotype during postnatal heart development, we generated a comprehensive map of phosphorylation sites. In total we identified 21,261 phosphorylation sites and 8985 proteins in developing mouse hearts by mass spectrometry. The in-vivo SILAC (stable isotope labeling of amino acids in cell culture) approach allowed robust quantification of phosphorylation sites and proteins, which are regulated during heart development. We found several activated pathways involved in cell cycle regulation and detected numerous kinases and transcription factors to be regulated on protein and phosphopeptide level. Most strikingly, we identified a novel mitochondrial protein, known previously as Perm1, as a highly phosphorylated factor regulated during heart development. We renamed Perm1 as MICOS complex subunit Mic85 since it shows robust physical interaction with MICOS complex subunits, including Mitofilin (Mic60), Chchd3 (Mic19), Chchd6 (Mic25) and the outer membrane protein Samm50. Moreover, Mic85 is localized to the mitochondrial inner membrane facing the intermembrane space and the dynamics of Mic85 protein expression is regulated by the ubiquitin-proteasomal system through phosphorylation of casein kinase 2 on its PEST motif. Silencing of Mic85 in cultured neonatal cardiomyocytes impairs mitochondrial morphology and compromises oxidative capacity. Our findings support a clear role for Mic85 in the maintenance of mitochondrial architecture and in its contribution to enhanced energetics during developing and adult mouse cardiomyocytes. The transgenic Mic85 knockout mouse generated with a GFP knock-in will support future *in vivo* investigations on the integrity of mitochondria and the function of Mic85 in cardiac development.

# CONTENTS

<b>Abbreviations</b> .....	10
<b>1. Introduction</b> .....	12
1.1 <i>Mus musculus</i> as a model organism for cardiovascular research .....	12
1.1.1 Background on mouse as a model organism.....	12
1.1.2 Mouse as a model system for heart development .....	13
1.2 Morphogenesis of the mouse heart.....	14
1.3 Regenerative potential of the neonatal mouse heart.....	16
1.4 Role of protein phosphorylation in the cardiovascular system .....	17
1.5 Mitochondrial bioenergetics in cardiac development .....	19
1.5.1 Post-natal changes in cardiomyocyte bioenergetics.....	19
1.5.2 Respiratory chain and oxidative phosphorylation.....	20
1.6 The mitochondrial contact site and cristae organizing system (MICOS) complex .....	21
1.7 Mass spectrometry-based proteomics.....	23
1.7.1 Shotgun proteomics .....	24
1.7.2 Quantitative methods in MS-based proteomics .....	27
1.7.3 Mass spectrometry-based phosphoproteomics.....	31
1.8 Mass spectrometry instrumentation.....	32
1.8.1 Quadrupole TOF and LTQ Orbitrap instruments.....	32
1.8.2 The Exactive series mass spectrometers.....	34
1.9 Aim of the thesis.....	36
<b>2. Materials and Methods</b> .....	38
2.1 Materials and chemicals for biochemistry methods.....	38
2.2 Materials and chemicals for mass spectrometry methods .....	40
2.3 Materials and chemicals for molecular biology methods .....	40
2.4 Materials and chemicals for cell culture methods .....	41
2.5 Enzymes.....	42
2.6 Kits .....	42
2.7 Antibodies.....	43
2.7.1 Primary antibodies .....	43
2.7.2 Secondary antibodies .....	44

2.8 Primers .....	44
2.9 Buffers .....	44
2.10 Devices used .....	48
2.11 Working with the model organism <i>Mus musculus</i> .....	49
2.11.1 SILAC mice colony.....	49
2.11.2 Isolation of mouse heart .....	49
2.11.3 Isolation of mouse neonatal cardiomyocytes .....	49
2.12 Sample preparation methods for mass spectrometry .....	50
2.12.1 Protein extraction – tissue homogenization and cell lysis .....	50
2.12.2 Determination of protein concentration.....	50
2.12.3 In-solution digestion.....	50
2.12.4 In-gel digestion .....	51
2.12.5 Filter Aided Sample Preparation (FASP) .....	52
2.12.6 Strong Cation Exchange Chromatography (SCX) .....	53
2.12.7 Phosphopeptide enrichment using TiO <sub>2</sub> beads.....	54
2.13 Liquid Chromatography - Tandem Mass Spectrometry (LC-MS/MS).....	56
2.13.1 Reversed phase liquid chromatography (LC).....	56
2.13.2 Tandem mass spectrometry (MS/MS).....	56
2.13.3 Data processing with MaxQuant .....	57
2.14 Molecular biology methods.....	57
2.14.1 Bacterial culture and competent cell preparation .....	57
2.14.2 Polymerase chain reaction .....	58
2.14.3 A-tailing of PCR product .....	58
2.14.4 Enzymatic digestion and ligation.....	58
2.14.5 Bacterial transformation of plasmid.....	59
2.14.6 Plasmid DNA isolation .....	59
2.14.7 Agarose gel electrophoresis and DNA purification .....	60
2.14.8 RNA isolation .....	60
2.14.9 Reverse transcription .....	60
2.14.10 Real-time PCR .....	61
2.15 Cell culture and transfection methods.....	61
2.15.1 Culture and sub-culture.....	61
2.15.2 SILAC labelling .....	62
2.15.3 Stocking cells .....	62
2.15.4 Calcium phosphate transfection .....	62

2.15.5 Transfection with TurboFect .....	62
2.15.6 siRNA transfection .....	63
2.15.7 Treating cells with inhibitors .....	63
2.16 Biochemistry methods.....	63
2.16.1 Immunoprecipitation .....	63
2.16.2 Immunoblotting.....	64
2.16.3 Subcellular fractionation .....	64
2.16.4 Submitochondrial fractionation .....	65
2.16.5 In vitro kinase assay.....	65
2.17 Immunostaining methods .....	66
2.17.1 Immunofluorescence.....	66
2.17.2 Immunohistochemistry .....	66
2.18 Human heart tissues.....	67
2.19 Metabolic assay – oxygen consumption rate.....	67
<b>3. Results .....</b>	<b>68</b>
3.1 Proteome-wide mapping of phosphorylation sites and quantitative analysis of post-natal heart development .....	68
3.2 Cluster analysis reveals reduced phosphorylation of CDK1/2 substrates after P10.....	73
3.3 Key molecular players: kinases, phosphatases, transcription factors and ubiquitin ligases.....	75
3.4 Titin is dynamically phosphorylated during heart development .....	76
3.5 Mic85 is up-regulated during heart development and interacts with components of mitochondrial contact site (MICOS) complex .....	78
3.6 Mic85 is a mitochondrial inner membrane-associated protein facing the intermembrane space .....	82
3.7 Casein kinase 2 phosphorylation of PEST motif regulates the turnover of Mic85.....	84
3.8 Loss of Mic85 leads to reduced maximal oxidative capacity and altered mitochondrial morphology .....	88
<b>4. Discussion.....</b>	<b>91</b>
4.1 Significance of comprehensive phosphoproteomics analysis of heart development.....	91
4.2 SILAC mouse based <i>in vivo</i> quantification revealed downregulation of cell cycle progression after P10 .....	92
4.3 Mic85 is a novel member of MICOS complex and is possibly imported by the MIA pathway....	93
4.4 Mic85 is an important factor for mitochondria within high energy demanding cells .....	94



4.5 Mic85 is a mitochondrial membrane-associated intermembrane space protein.....	95
4.6 PEST phosphorylation mediated protein turnover controls Mic85 homeostasis .....	96
4.7 Mic85 contributes to increased energy demand of maturing cardiomyocytes.....	97
4.8 Generation of Mic85 knockout mouse for future <i>in vivo</i> studies .....	98
4.9 An overview of interdisciplinary collaborative projects.....	99
<b>5. Zusammenfassung .....</b>	<b>101</b>
5.1 Einführung .....	101
5.2 Ziele der Studie.....	103
5.3 Ergebnisse.....	103
5.4 Schlussfolgerung.....	106
<b>6. References.....</b>	<b>107</b>
<b>7. Curriculum Vitae .....</b>	<b>116</b>
<b>8. Publications.....</b>	<b>119</b>

## Abbreviations

<b>°C</b>	Degree Celsius
<b>μl</b>	Microliter
<b>ACN</b>	Acetonitrile
<b>ATP</b>	Adenosine triphosphate
<b>CDK</b>	Cyclin-dependent kinase
<b>cDNA</b>	Complementary deoxyribonucleic acid
<b>CID</b>	Collision-induced dissociation
<b>CK1</b>	Casein kinase I
<b>CK2</b>	Casein Kinase II
<b>Da</b>	Dalton
<b>DMEM</b>	Dulbecco's modified eagle's medium
<b>DMSO</b>	Dimethyl sulphoxide
<b>DNA</b>	Deoxyribonucleic acid
<b>DTT</b>	Dithiothreitol
<b>EDTA</b>	Ethylenediaminetetraacetic acid
<b>FBS</b>	Fetal bovine serum
<b>GFP</b>	Green fluorescence protein
<b>h</b>	Hours
<b>HCD</b>	Higher energy collisional dissociation
<b>HEK</b>	Human embryonic kidney
<b>IP</b>	Immunoprecipitation
<b>KD</b>	Knockdown
<b>LB</b>	Lysogeny broth
<b>LC</b>	Liquid chromatography
<b>M</b>	Molar

<b>mg</b>	Milligram
<b>MICOS</b>	Mitochondrial contact site complex
<b>min</b>	Minutes
<b>MS</b>	Mass spectrometry
<b>MS/MS</b>	Tandem mass spectrometry
<b>OS</b>	Osmotic shock
<b>P</b>	Post-natal day
<b>PBS</b>	Phosphate buffered saline
<b>PCR</b>	Polymerase chain reaction
<b>PK</b>	Proteinase K
<b>PMSF</b>	Phenylmethanesulphonyl fluoride
<b>ppm</b>	Parts per million
<b>PSG</b>	Penicillin-Streptomycin-L-Glutamine
<b>RIPA</b>	Radioimmunoprecipitation assay
<b>RNA</b>	Ribonucleic acid
<b>rpm</b>	Revolutions per minute
<b>SCX</b>	Strong cation exchange chromatography
<b>SDS</b>	Sodium dodecyl sulphate
<b>SILAC</b>	Stable isotope labelling of amino acids in cell culture
<b>siRNA</b>	Small interfering RNA
<b>TBB</b>	4,5,6,7-tetrabromobenzotriazole
<b>TBS-T</b>	Tris buffered saline – Tween 20
<b>TFA</b>	Trifluoroacetic acid
<b>UHPLC</b>	Ultra high pressure liquid chromatography
<b>WB</b>	Western blot
<b>WT</b>	Wild-type

# 1. Introduction

*“This organ deserves to be styled the starting point of life and the sun of our microcosm just as much as the sun deserves to be styled the heart of the world. For it is by the heart's vigorous beat that the blood is moved, perfected, activated, and protected from injury and coagulation” – William Harvey*

The heart is the key organ in humans and other animals and is a muscular pump that pumps blood through vessels of the circulatory system. The heart usually beats from 60-100 times per minute, about 100,000 times a day, about 30 million times per year and about 2.5 billion times in a 70-year lifetime. The pumped blood provides oxygen and nutrients to the body and removes metabolic wastes. The mammalian heart is made up of four chambers - two atria and two ventricles. Deoxygenated blood from the systemic circulation (circulation to all body parts except lungs) enters through the superior and inferior vena cava into the right atrium and passes on to the right ventricle. From there, the blood is pumped through the lungs into pulmonary circulation (circulatory system of lungs) where it gets oxygenated, then enters left atrium followed by left ventricle and then is pumped out through aorta into systemic circulation [1]. In a healthy heart, blood flows only in one direction since the valves in the heart efficiently prevent blood backflow. The heart is located in the center of the chest in the middle compartment of the mediastinum and it enclosed in a protective sac called pericardium [2]. Today, tremendous amount of research is focused on heart and its development in order to address the challenges of cardiovascular diseases and heart regeneration.

## **1.1 *Mus musculus* as a model organism for cardiovascular research**

### **1.1.1 Background on mouse as a model organism**

The mouse has developed into a widely used mammalian model system for genetic research over the past century because it has close genetic and physiological similarities to humans

and its genome can be easily manipulated. Although in the study of cell cycle and many developmental processes, yeast, worms and insects have been widely used as model organisms, mice are a more appropriate system in exploring complex physiological systems like immune, endocrine, cardiovascular and skeletal systems. Moreover, just like humans, mice also naturally develop diseases like atherosclerosis, hypertension, cancer and diabetes, making them suitable as disease models. Diseases like cystic fibrosis, Alzheimer and Parkinson disease which occur in humans but not in mice can be induced by overexpressing of disease related human genes in the mouse genome. In addition, the reasonable cost of maintenance of mice and their ability to reproduce rather quickly (every nine weeks) make them attractive model organisms for biomedical research.

In the early days, mouse models were developed by selecting and breeding mice to get the desired traits in the offspring. To produce models of genetic diseases, mice were exposed to DNA-damaging chemicals, a process known as chemical mutagenesis. In the recent decades, scientists have produced custom made mouse models with the help of advanced genetic technologies to study the function of targeted genes. One of the hallmarks in technology advancement has been the creation of transgenic mice in which a new gene is inserted into the animal's germline. Homologous recombination has allowed the development of "knock out" mice where an existing gene is replaced by a mutated variant, and "knock-in" mice where a mouse gene is altered or overexpressed in its natural location. More recently, the generation of DNA double-strand breaks (DSB) at specified loci using zinc-finger nucleases (ZFNs) [3], transcription activator-like effector nucleases (TALENs) [4] or the RNA-guided clustered regularly interspaced short palindromic repeat (CRISPR)/CRISPR-associated (Cas) [5] nuclease system have been used to genetically modify mice. For preservation and propagation of these valuable strains, state-of-the art technologies like cryopreservation, in vitro fertilization and ovary transplantation have been developed.

### **1.1.2 Mouse as a model system for heart development**

The heart is the first complex organ to develop and its constant pumping starts at embryonic day 6-7 after fertilization in mouse. Congenital cardiovascular diseases are the most common form of human birth defects, with 1 per 200 live births per year in North America.

Cardiovascular defects are of particular attention because a fully functional circulatory system is essential for the survival of the foetus through to the adult. However, little information is available on the origin of many congenital cardiovascular abnormalities in humans.

The mouse is a very useful model organism for heart development due to the availability of its detailed embryological information. Moreover, as described earlier, the mouse genome can be easily manipulated and analysed. Many critical time points during mouse gestation have been determined that can lead to embryonic death [6], of which most of them are related to defects in the development of the cardiovascular system. Several circulatory problems including inefficient pumping action of the heart and instability of blood vessel walls lead to embryonic morbidity and mortality. At birth when pulmonary circulation is established, inefficient remodeling of blood vessels also leads to circulatory problems [7].

In the mouse, there is an in-depth knowledge of single-gene mutations generated by targeted mutagenesis with the help of homologous recombination in embryonic stem cells [8-10]. Since the cardiovascular system is very sensitive and susceptible to disruption, many of these mutations have been shown to cause defects in heart development and in the vascular system. Therefore, the knowledge on these mutations and their effects in mice form a valuable source of information on the genetic control of cardiovascular development and the origin of cardiovascular diseases, making the mouse an excellent model organism for studying heart development and elucidating the origin of human cardiovascular defects.

## **1.2 Morphogenesis of the mouse heart**

Heart is the first organ to form in vertebrates and plays a crucial role in distributing oxygen and nutrients to the embryo. It consists of a contractile myocardium that is essential for its pumping action. Subsequent regionalization of the heart structure leads to the formation of four-chambered heart in adult birds and mammals. Cardiogenesis is a very sensitive process and any disturbance in the cells responsible for development of the heart leads to cardiac malformations and death of the embryo. An overview of the cellular processes of early cardiogenesis has been reviewed [11].

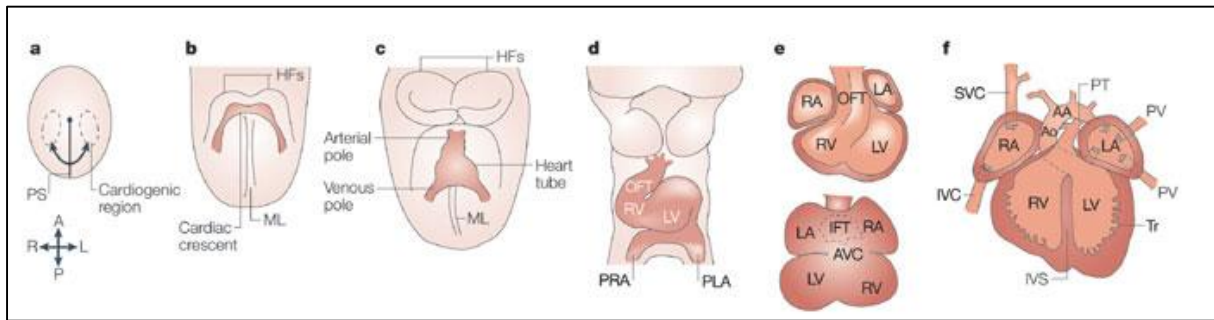


*Figure 1. Morphogenesis of the mouse heart, illustrating the early stages of cardiogenesis. PS: primitive streak; HF: head fold; ML: mid-line, PRA: primitive right atrium; PLA: primitive left atrium; RV: right ventricle; LV: left ventricle; OFT: outflow tract; RA: right atrium; LA: left atrium; IFT: inflow tract; AVC: atrioventricular canal; SVC: superior vena cava; IVC: inferior vena cava; Ao: aorta; AA: aortic arch; IVS: interventricular septum; Tr: trabeculae; PT: pulmonary trunk; PV: pulmonary vein; A- anterior axis; P-posterior axis; R-right axis; L-left axis (Buckingham et al., 2005 [11]).*

Myocardial cells are derived from the mesoderm, which itself develops from the primitive streak during gastrulation. In mouse and chick embryos, cardiac progenitor cells are present in the anterior part of the streak [12, 13] from where they migrate to the anterior of the embryo at embryonic day E6.5 (Fig. 1a). They form two groups of cells under the head fold (HF) on either side of the midline (ML) [13, 14], where differentiated myocardial cells are first detected at around E7.5 (Fig. 1b). The cells form a crescent shaped epithelium called cardiac crescent which fuses at the midline to form the early cardiac tube at E8 (Fig. 1c). The heart tube undergoes looping in the rightward direction, where its posterior side moves anteriorly. This occurs around E8.5 (Fig. 1d). The looping process and expansion of the myocardium leads to shaping of the heart and causes the formation of observable cardiac chambers, but the heart still being a tube. This occurs around E10.5 (Fig. 1f: upper panel-ventral view, lower panel-dorsal view). At E14.5, the fetal heart has separated chambers as a result of septation and they are connected to the pulmonary trunk (PT) and the aorta (Ao) (Fig. 1f). PT secures pulmonary circulation of blood and Ao secures systemic circulation of blood after birth. Oxygenated blood from the pulmonary circulation enters the left atrium and passes on to the left ventricle, from which it is pumped through aorta to the systemic circulation that serves the whole body. From the systemic circulation, deoxygenated blood enters the right atrium through the superior and inferior vena cava from which it is passed

onto the right ventricle. From there, the blood is pumped into the lungs for pulmonary circulation.

### 1.3 Regenerative potential of the neonatal mouse heart

Embryonic and neonatal heart development is achieved by rapid proliferation of cardiomyocytes until the first week after birth. After this time point cardiomyocytes exit from cell cycle and become binucleate [15, 16]. Post mitotic cardiomyocytes possess only a very limited capacity for regeneration since they are unable to replace dying cells in damaged heart [17, 18]. A previous study showed that embryonic mammalian heart is capable of showing a hyperplastic response to injury, suggesting that mammalian heart may retain a regenerative capacity in its early stage [19]. In addition, several studies have shown that the mammalian heart possesses a considerable capacity for cardiomyocyte renewal [20-23], though not sufficient to renew the contractile function after injury.

Interestingly, a recent study showed that hearts of newborn mice can regenerate within 21 days after surgical resection of ventricular apex [24]. The left ventricular apex corresponding to 15% of the ventricular myocardium of 1-day old mice was surgically resected. Histological analysis revealed that the apex gradually regenerated and was fully restored within 21 days post-surgery (Fig. 2A-D).



*Figure 2. Regeneration of the ventricular apex of neonatal mouse heart. (A-D) Hematoxylin and eosin (H&E) stainings of mouse heart at 1, 2, 7 and 21 days post-surgery. Arrow indicates the site of injury. (Adapted from Porrello et al., 2011 [24]).*

These results corroborated that the hearts of 1-day old mice can regenerate after partial surgical resection. However, this capacity was lost by 7 days post birth, suggesting that the



mammalian heart has a limited capacity for regeneration for a brief period after birth probably due to residual proliferative capacity of neonatal cardiomyocytes. To date, the molecular mechanisms and regulatory expression profiles of proteins and post-translational modifications that might control neonatal cardiomyocyte proliferation or the switch to maturation and differentiation are poorly described, although associated changes in metabolic activities have been recently claimed to determine acquisition of the post mitotic state of cardiomyocytes [25].

### 1.4 Role of protein phosphorylation in the cardiovascular system

Protein phosphorylation is often important for temporary modulation of protein function, enzyme activity and protein interactions. Reports on tissue-specific mouse and rat protein phosphorylation revealed specialized and interconnected phosphorylation networks within each tissue showing that proteins are regulated by phosphorylation independently of their expression [26, 27]. There have been several efforts to map phosphorylation sites but with minimum quantitative information.

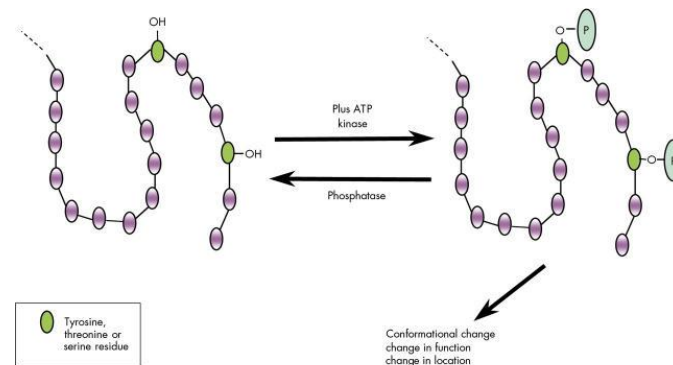


*Figure 3. Protein phosphorylation is a reversible mechanism and can have many downstream effects (Wheeler-Jones, 2005 [28])*

The role of phosphorylation of proteins and cell signalling in the cardiovascular system has been reviewed [28]. Phosphoregulation of proteins is a key component of signal transduction pathways, making them interesting targets for pharmacological studies. Moreover, protein phosphorylation plays an important role during cell proliferation, and cyclin dependent kinases (CDKs) show high dynamics of phosphorylation during the course of the cell cycle [29]. Notably, about 3% of the human genome encodes for protein kinases and phosphatases and mutations in these molecules have been implicated in human

diseases, showing the crucial role of these signalling elements in the cell [30]. Phosphorylation is a reversible mechanism; substrates are phosphorylated by kinases and dephosphorylated by phosphatases (Fig. 3).

The reversible phosphorylation events can induce a conformational change in a protein altering its biological activity, influence its physical interaction with other proteins and lead to a change in its localization. For example, phosphorylation of a protein by glycogen synthase kinase 3 (GSK3) normally inhibits the activity of its downstream target [31], whereas phosphorylation and activation of MEK by RAF kinase further phosphorylates and activates mitogen-activated protein kinase (MAPK) leading to recruitment of the MAPK kinase cascade [32]. Most of the signalling events in cells are mediated by kinases and since the substrates are cell specific, the effects of signalling in different tissues are diverse. Moreover, targeting kinases and phosphatases close to their target substrates in the cell ensures optimal regulation of phosphorylation [33]. Serine/threonine protein kinases phosphorylate serine or threonine residues in their protein substrates and are essential components of the signalling events required for normal functioning of the cardiovascular system. For example, protein kinase A (PKA) is an important mediator of adrenergic stimulation on heart and vasculature [34]. Similarly, protein kinase G (PKG) is an essential component of the pathway in which the vasodilator nitric oxide decreases vascular tone [35]. Besides, the function of protein kinase C (PKC) is significant in the cardiovascular system. PKC is an important mediator of myocardial preconditioning, where it protects against myocardial cell death either by phosphorylating proteins that activate protective genes or by phosphorylating and inhibiting proteins that promote cell death. Moreover, increased amount of the isoform PKC $\alpha$  impairs systolic and diastolic function in pathological hypertrophy [36-38].

Protein tyrosine kinases (PTKs) phosphorylate tyrosine residues within their substrates and represent only a minor fraction (2-3%) of all phosphorylations. PTKs are of two types, receptor tyrosine kinases (RTKs) of which 13 families are known and non-receptor PTKs of which 9 families are known [39]. RTKs play a crucial role in the cardiovascular system particularly in the initiation of signalling processes that control cell growth, proliferation and differentiation. For example, ErbB2 signalling in cardiomyocytes helps in the protection

against dilated cardiomyopathy. Importantly, patients treated with antibodies against ErbB2 for cancer treatment develop dysfunction of the heart as a side effect, showing the importance of these RTKs in normal cardiac behavior [40]. Non-receptor PTKs include JAK, FAK and Src kinase families. Many non-receptor PRKs are triggered by the G-protein coupled receptors to initiate their signalling events.

Thus, protein phosphorylation during heart development has a key function in regulating cell proliferation and signaling. It is also essential for the homeostasis of cardiac muscle proteins as shown by its influence on calcium-calmodulin signalling leading to the regulation of myocardial contraction and metabolism [41].

## **1.5 Mitochondrial bioenergetics in cardiac development**

### **1.5.1 Post-natal changes in cardiomyocyte bioenergetics**

A cellular compartment with highly dynamic protein changes is the mitochondrion and the heart function is highly dependent on the energy generated by mitochondria. After birth, cardiomyocytes undergo transition from hyperplasia to hypertrophy, a process called developmental hypertrophy [42]. Developmental cardiac hypertrophy and cardiomyocyte maturation are accompanied by an increase in mitochondrial biogenesis [43] and a switch in energy metabolism. Fetal cardiomyocytes generate ATP mainly through glycolysis and glucose oxidation [44]. After birth, there is an increased cardiac output and an increased energy demand [45]. This increased energy requirement is achieved by a switch in the energy metabolism from glycolysis to  $\beta$ -oxidation of lipids which produces more amounts of ATP than glycolysis [44, 46], and by an increase in mitochondrial number [47].

An upregulated expression of PGC1 $\alpha/\beta$  (Peroxisome proliferator-activated receptor gamma coactivator 1-alpha/beta) after birth leads to an increase in mitochondrial biogenesis [47]. Fetal mitochondria show a fragmented appearance whereas post-natal mitochondria are more elongated, this fusion being associated to the increased  $\beta$ -oxidation of lipids after birth [48, 49]. Mitofusin proteins have been known to be involved in the control of post-natal mitochondrial fusion and metabolic remodeling of the heart [50]. Mitochondria are dynamic organelles and have the ability to divide (fission) and fuse (fusion). Mitochondrial fission

leads to its fragmentation whereas the fusion activity leads to its elongation. A balance between the fission and fusion processes is crucial for the health of a cell [51]. The control of mitochondrial fission, fusion, biogenesis and respiratory complex is mainly controlled by peroxisome proliferator-activated receptors (PPARs) and their coactivators (PGCs), and also by estrogen related receptors (ERRs) and nuclear respiratory factors (NRFs) [52]. However, recently several other molecules including AMP-activated kinase (AMPK) [53], mammalian target of rapamycin complex 1 (mTORC1) [54], mitochondrial sirtuins [55] and transferrin receptor 1 (TFR1) [56] have been identified to be important to regulate mitochondrial activity.

### 1.5.2 Respiratory chain and oxidative phosphorylation

Oxidative phosphorylation is a metabolic pathway by which mitochondria use their enzymes to generate ATP. The electron transport chain in the mitochondrion is the site for oxidative phosphorylation. In the electron transport chain, electrons are transferred from electron donors to electron acceptors through redox reactions, and this is coupled to transfer of protons. This leads to the generation of an electrochemical proton gradient which drives the synthesis of chemical energy in the form of ATP. Oxygen is the final electron acceptor in this chain.

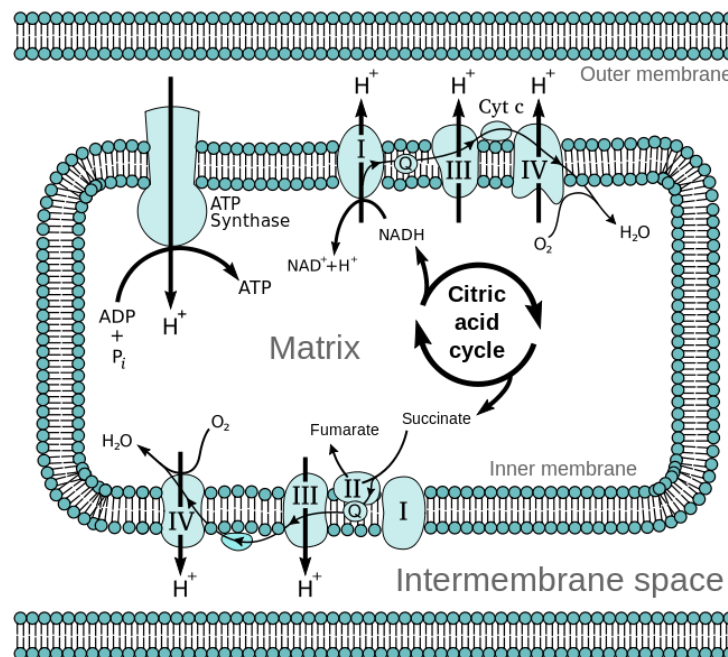


Figure 4. Overview of the electron transport chain in the mitochondrion (Fvasconcellos, 2007 [57])

The breakdown of carbohydrates through glycolysis and the  $\beta$ -oxidation of fatty acids generate acetyl-CoA. This compound is fed to the citric acid cycle [58] which reduces  $\text{NAD}^+$  to NADH, which in turn is transferred to the electron transport system. Components of this respiratory chain are present in four large protein complexes localized in the inner membrane of the mitochondria [59]. Electrons flow through this chain from NADH to  $\text{O}_2$  through three large protein complexes: NADH-Q oxidoreductase (Complex I), Q-cytochrome c oxidoreductase (Complex III) and cytochrome c oxidase (Complex IV). In complex I, electrons are transferred from NADH to ubiquinone. Complex III passes the electrons to cytochrome c and complex IV passes the electrons to  $\text{O}_2$  which gets reduced to  $\text{H}_2\text{O}$ , thereby completing the chain. Substrates like succinate that possess a stronger positive redox potential than NADH pass electrons to ubiquinone with the help of a fourth complex called succinate Q reductase (Complex II) instead of complex I. The complexes are embedded in the mitochondrial inner membrane, whereas ubiquinone and cytochrome c are mobile components. The flow of electrons through the protein complexes releases energy which is used for pumping of protons from the matrix to the intermembrane space through the inner membrane. This causes an electrochemical gradient across the membrane and generates potential energy. This energy allows protons to flow back across the membrane through an enzyme called ATP synthase, a process known as chemiosmosis [60]. The flow of protons causes a rotation of a part of this enzyme which is a mechanical rotor, which in turn generates ATP from ADP in a phosphorylation reaction [59].

Oxidative phosphorylation occurs in the cristae of the inner mitochondrial membrane which house a large protein complex that is crucial for inner membrane organization and formation of membrane contact sites, which is discussed in the following section.

## **1.6 The mitochondrial contact site and cristae organizing system (MICOS) complex**

Mitochondria contain two membranes, outer and inner, of different architecture and function [61]. The combined functioning of these two membranes is essential for protein import [62-64]. The components of the outer membrane help in controlling the shape of the organelle and in communicating with the rest of the cell. The inner membrane contains the

respiratory chain complexes, ATP synthase and enzymes for mitochondrial metabolism. The inner membrane is composed of an inner boundary membrane which is close to the outer membrane, and a membrane with invaginations called cristae [65, 66]. The connecting elements between the inner boundary membrane and crista membrane are tubular openings called crista junctions [67]. The contact sites between inner and outer mitochondrial membranes are essential for several functions including lipid transport, import of precursor proteins, metabolite channeling and membrane dynamics [63, 64, 66, 68].

Knowledge of the molecular machineries that regulate the interaction between inner and outer membranes is essential in understanding the complex structure of mitochondria. Several studies led to the identification of a large protein complex conserved from yeast to humans and important for inner membrane organization, maintenance of crista junctions and formation of membrane contact sites. This complex was named initially as the mitochondrial inner membrane organizing system (MINOS) [69] or the mitochondrial organizing structure (MitOS) [70]. Recently, to unify the nomenclature, this complex has been termed as the mitochondrial contact site and cristae organizing system (MICOS) comprising of various subunits from Mic10 to Mic60 [71] (Fig. 5A and Table 1). MicX represents a MICOS complex member where X denotes the molecular weight of the protein in kilo Daltons in the species it was identified.

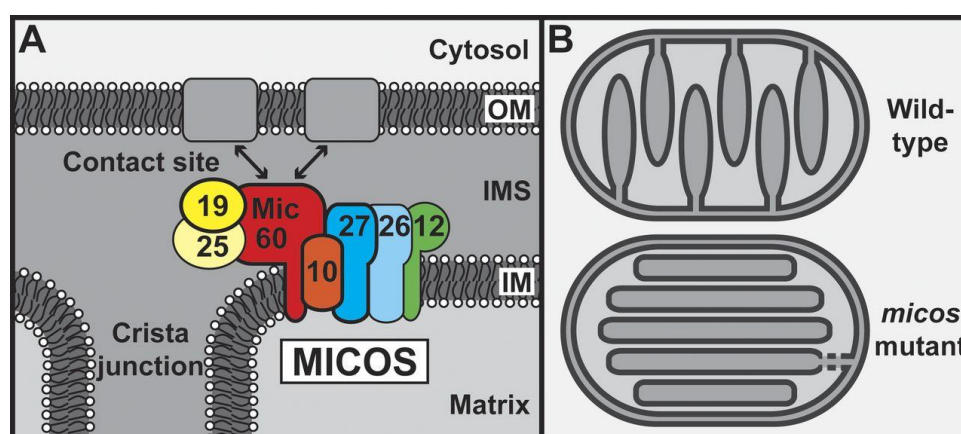


Figure 5. The MICOS complex. (A) The model of MICOS complex showing the various identified subunits. (B) Top panel shows the wild type architecture of mitochondrial inner membrane with intact cristae. Bottom panel shows the architecture of MICOS mutant mitochondria where most of the cristae are detached from the inner boundary membrane (Pfanner et al., 2014 [71]).

**Table 1: New nomenclature of MICOS subunits (Adapted from [71])**

<b>MICOS complex subunit</b>	<b>Former names in human</b>	<b>Former names in yeast</b>
Mic10	MINOS1, C1orf151	Mcs10, Mio10, Mos1
Mic12	Not identified	Aim5, Fmp51, Mcs12
Mic19	CHCHD3, MINOS3	Aim13, Mcs19
Mic25	CHCHD6, CHCM1	Not identified
Mic26	APOO, FAM121B	Mcs29, Mio27, Mos2
Mic27	APOOL, Cxorf33	Aim37, Mcs27
Mic60	IMMT (Mitofilin), MINOS2, HMP	Aim28, Fcj1, Fmp13

Mitofilin (Mic60) was the first component of the MICOS complex to be identified [72] and has been reported to be enriched in the crista junctions [73]. Mutants of Mic60 and other MICOS subunits show altered inner membrane architecture with loss of cristae junctions and reduced respiratory capacity (Fig. 5B) [72, 74-77]. It is reported that this complex interacts with many channel proteins and protein translocases located in the outer membrane, and defects lead to an impairment in the biogenesis of mitochondrial proteins [78-80]. Thus the MICOS/MINOS/MitOS complex plays a crucial role in maintenance of mitochondrial architecture, dynamics and biogenesis.

## **1.7 Mass spectrometry-based proteomics**

Mass spectrometry is a powerful tool and the method of choice for the unbiased identification and quantification of proteins and post-translational modifications in a biological sample, thereby addressing diverse biological questions in modern biology. The application of mass spectrometry for protein characterization became popular in the 1980's after the development of the two principal methods for ionization of proteins: matrix-assisted laser desorption/ionization (MALDI) and electrospray ionization (ESI). MALDI was developed by Franz Hillenkamp and Michael Karas when they ionized alanine mixed with tryptophan and irradiated with a pulse 266 nm laser [81]. Later in 1987 the breakthrough came when Koichi Tanaka made use of the 'ultrafine metal plus liquid matrix method' to ionize large biomolecules like carboxypeptidase A [82]. The first use of electrospray

ionization with mass spectrometry was reported in 1968 by Malcolm Dole and John Bennett Fenn was cited for its development [83, 84].

Two approaches are used in mass spectrometry-based proteomics for protein characterization: “top-down” approach where proteins are ionized either by ESI or MALDI and then subjected to the mass analyzer, and “bottom-up” approach where proteins are first enzymatically digested into peptides using a protease and then subjected to MS analysis and identified by tandem mass spectrometry, using which the parental proteins are identified by screening against the protein sequence database. Nowadays, bottom-up approach is the most widely used method in proteomics for detection of proteins and post-translational modifications or protein-protein interactions in a biological sample.

### **1.7.1 Shotgun proteomics**

Shotgun proteomics refers to the application of bottom-up proteomics techniques for the identification of proteins in complex biological samples using high performance liquid chromatography coupled to mass spectrometry (LC-MS) [85-87]. Though 2D-gel electrophoresis could resolve complex protein mixtures [88], shotgun proteomics emerged as a powerful method for low abundant proteins as well as membrane proteins [89].

Shotgun proteomics involves several stages of sample preparation before LC-MS analysis (Fig. 6). Cells or tissues of interest are lysed to extract the proteins in solution. Proteins are then digested using proteases like trypsin or LysC to generate peptides. Protein digestion could be performed on a complete sample in solution (in-solution digestion), after separation of proteins by SDS-PAGE (in-gel digestion), or in a filter (filter-aided sample preparation (FASP)).



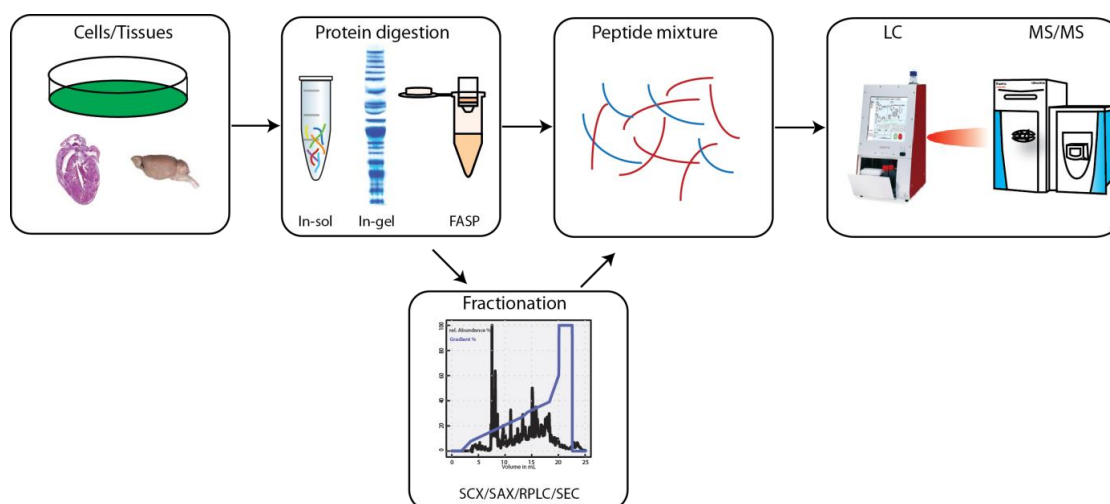


Figure 6. Shotgun proteomics workflow illustrating the various stages of sample preparation for mass spectrometric analysis

Digestion of proteins in solution [90] is the simplest and the most convenient method of protein digestion for mass spectrometry analysis. Typically, the total protein content in a biological sample is brought into solution using a denaturing buffer. In case of samples containing SDS detergent, proteins are precipitated using acetone. SDS must be removed from the sample as it imparts an overall negative charge on the proteins which later affects the ionization efficiency during electrospray ionization. The proteins are then resuspended typically in a urea-containing buffer, reduced to break the disulphide bonds, alkylated to block the free sulfhydryl groups from forming a disulphide bond again, and digested in solution using a suitable protease like LysC or trypsin. This method yields satisfactory protein identification when the complexity of biological sample is low. For samples with high dynamic range of protein abundance, this method yields a poor depth of protein coverage.

Digestion of proteins in gel was originally described in 1996 [91] but a more optimized protocol came up in 2006 [92]. Many proteomics studies depend on pre-separation of proteins using 1D or 2D gel electrophoresis [93]. Since protein bands are sharply separated based on molecular weight and each band is independently analysed by LC-MS after proteolytic digestion, the gel-based approach increases the dynamic range of analysis of protein mixtures. Increasing the number of gel slices for more complex proteomes could increase the depth of coverage of proteins and post-translational modifications. Also, low molecular weight impurities, buffer components and detergent are removed by gel

electrophoresis, leaving the protein sample clean for MS analysis. Moreover, polyacrylamide gels are a good resource for mass spectrometric protein characterization as they can handle femtomole amounts of proteins [94]. Besides these advantages, gel-based approaches do possess some limitations. Peptide recovery is a major issue due to the difficulty in complete extraction of peptides from the gel pieces after digestion. Also, casting the gels and extensive sample processing steps in this method increase the risk of exposure to human keratins and could increase the chemical noise in the analysis.

As described previously, in-solution and in-gel digestion methods have their own advantages and limitations. In-solution digestion minimizes sample handling and can be easily automated, but protein content may not be completely solubilized and digestion could be affected by interfering substances. On the other hand, in-gel digestion increases digestion efficiency by removing impurities, but the extent of peptide recovery is low, and the method cannot be easily automated. A universal sample preparation method called filter-aided sample preparation (FASP) was described in 2009 [95], which combines the advantages of in-solution and in-gel digestion methods. In FASP, the proteome is completely solubilized in sodium dodecyl sulphate which is the preferred reagent for total solubilization of cells or tissues. The SDS in the protein lysate is exchanged by urea on a filtration unit which has a molecular weight cutoff, thereby removing all the low molecular weight impurities. Reduction, alkylation and digestion of proteins all take place in the filter unit. Following digestion, only clean digested peptides flow through the filter while the remaining undigested proteins and any other high-molecular weight substances are retained in the filter. Hence, the FASP method facilitates an efficient solubilization of the proteome before digestion and a clean peptide output after digestion, making it the method of choice for single-run analyses and in-depth coverage of proteome.

After proteolytic digestion, the peptide mixture can be optionally fractionated offline using chromatographic methods like strong cation exchange chromatography (SCX), strong anion exchange chromatography (SAX) or reversed-phase liquid chromatography (RPLC). Alternatively, proteins can be fractionated by size exclusion chromatography (SEC) before digestion. Peptides are cleaned and desalted using C18 StageTips [96] and then separated by online reversed phase chromatography on a high performance liquid chromatography

(HPLC) system. In a HPLC instrument, the sample is forced through the column (made up of peptide binding material) by an organic liquid under pressure. The HPLC is coupled to a high resolution mass spectrometer having a nano electrospray source, where peptides are ionized. Ionized peptides are detected in MS scans, and their fragmented ions are detected in MS/MS scans (called tandem mass spectrometry). Detected spectra are produced as raw files which are analysed using the MaxQuant software, in which proteins are detected by database searching of peptides using the Andromeda search engine [97, 98].

Shotgun proteomics allows the identification of global proteome and facilitates the profiling of dynamic proteomes [99]. However, peptide identification does possess some limitations. It is difficult to assign those peptides which are shared by more than one protein, to a single protein. Moreover, paralogs in proteome samples and alternative splicing produce many identical protein subsequences.

### **1.7.2 Quantitative methods in MS-based proteomics**

An important aspect of proteomics is the quantification of differences in proteins and post-translational modifications between two different biological states. In spite of the rapid advancements in mass spectrometry and peptide separation techniques, the identification and quantification of the complete proteome is still challenging. Modern LC-MS/MS techniques have overcome the problems of classical protein quantification methods using radioactivity, dyes or fluorophores, however mass spectrometry is not inherently quantitative due to the diverse physicochemical properties exhibited by proteolytic peptides. Therefore, comparison of the abundance of individual peptides between experiments is inevitable for accurate quantification [100].

Proteome quantification can be achieved in several ways (Fig. 7). One quantitative approach is based on stable isotopes, in which a stable isotope labelled peptide is physico-chemically identical to its native counterpart and hence show the same chromatographic elution profile. The mass difference between the labelled and unlabeled peptides can be detected by the mass spectrometer and hence quantification is obtained by comparing their signal intensities (peak height). Stable isotopes can be induced into peptides either by metabolic labelling (during cell division and growth), chemical labelling of proteins or peptides, or using

spiked labelled synthetic peptides as an external standard [101]. Besides the labelling strategies, label-free methods of protein quantification have also emerged [102]. Label-free methods achieve quantification between different biological states by comparing the peptide's signal intensity obtained from mass spectrometry, or by comparison of the number of spectra (spectral counting) obtained for a peptide which is indicative of its abundance. Fig. 7 depicts the comparison of label-free method and different labelling techniques, showing the possible stages at which experimental variation and quantification error could occur. Evidently, the metabolic labelling method provides the most robust quantification since the labelled and non-labelled proteins are mixed at the very first stage of sample preparation and hence is minimally error prone.

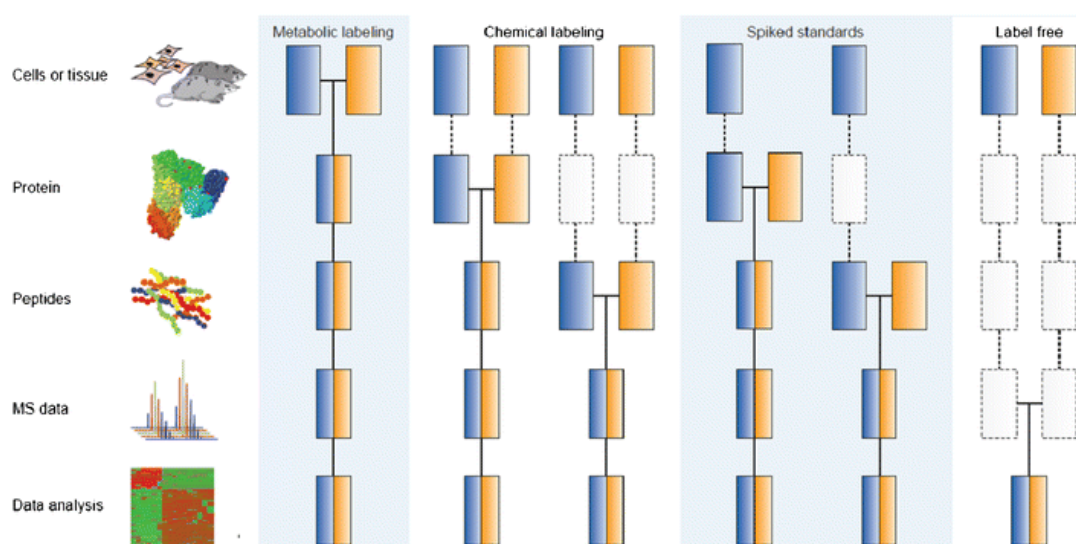


Figure 7. Quantitative methods in MS-based proteomics. Yellow and blue boxes represent two different experimental conditions. Dashed lines depict those stages where experimental variation and errors in quantification could occur (Bantscheff et al., 2012 [103]).

### 1.7.2.1 Stable isotope labelling by amino acids in cell culture (SILAC) based quantitative proteomics

Stable isotope labelling of amino acids in cell culture (SILAC) was described as a metabolic labelling technique in 2002 [104] for *in vivo* incorporation of labelled amino acids into proteins based on protein turnover [105]. Mammalian cells are cultured in a media lacking an essential amino acid, and replaced by a non-radioactive stable isotope-labelled counterpart. Moreover, dialyzed serum is used in the culture medium to make sure that the

supplied amino acids are the only source. Typically, cells are labelled with lysine and arginine containing heavy stable isotopes of carbon and/or nitrogen for about five cell doublings after which >99% labelling efficiency is obtained [104]. After tryptic digestion, the peptide mixture obtained contains all labelled peptides that can be used for quantification. In a SILAC experiment, cells are grown in light and heavy medium (and middle heavy medium for triple SILAC experiment) after which they are lysed, mixed and the entire sample preparation process is done together (Fig. 8a). Quantification is achieved by obtaining the ratios of peak intensities of light, middle and heavy peptides, which have a mass difference due to the heavier carbon/nitrogen in lysine and arginine of the middle and heavy peptides.

In 2011, a spike-in SILAC approach was described [106] where SILAC labelled sample is used as a reference standard to which experimental samples are compared. The SILAC-labelled sample is spiked-in equally to the non-labelled experimental samples, after which they are processed together. Peptide ratios between the sample and heavy spike-in standard are obtained and since the heavy standard is identical in all cases, the ratio of ratios gives the peptide fold-change (Fig. 8b).

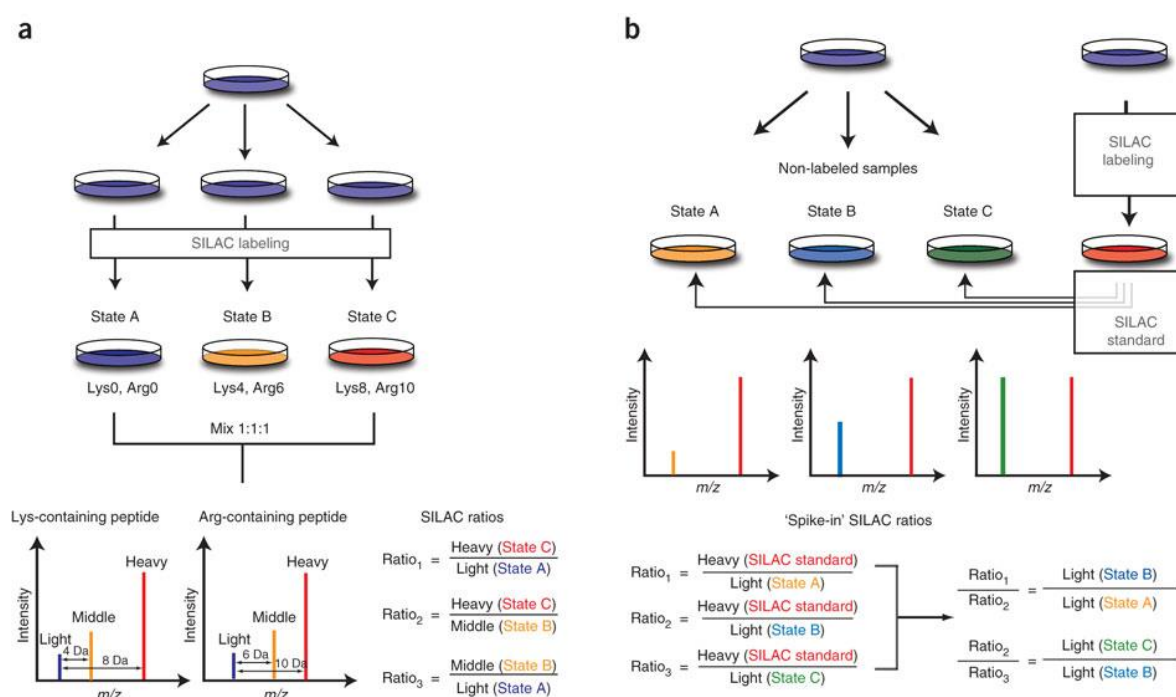


**Figure 8.** Workflows of classical SILAC and spike-in SILAC approaches. (a) Classical SILAC experiment where cell populations representing different experimental conditions are labelled and mixed together for LC-MS/MS analysis. (b) Spike-in SILAC experiment where heavy SILAC standard is spiked-in to light experimental conditions and then analyzed by LC-MS/MS (Geiger et al., 2011 [106]).

The advantage of spike-in SILAC approach is that the labelling is completely separated from the biological experiment. Moreover, the labelling process has no influence on the final result since it is identical in all experimental conditions and is only used as a reference standard for quantification. Moreover, there is no limit to the number of samples that can be analyzed as the experimental samples need not be labelled in this case. Most importantly, the spike-in SILAC method can be used for analysis of cells and tissues that cannot be SILAC labelled, thereby extending the boundaries of SILAC-based quantitative proteomics.

### 1.7.2.2 SILAC mouse for in vivo quantitative proteomics

The applicability of SILAC has been extended beyond cell culture to labelling of complete organisms [107]. In 2008, Krüger et al. completely labelled mice using a diet containing  $^{13}\text{C}_6$  substituted version of lysine [108]. SILAC mouse diet was prepared by mixing  $^{13}\text{C}_6$  lysine to a customized lysine-free mouse diet at a final concentration of 1%. The diet was pelleted under pressure and fed to mice for labelling over two generations (Fig. 9).

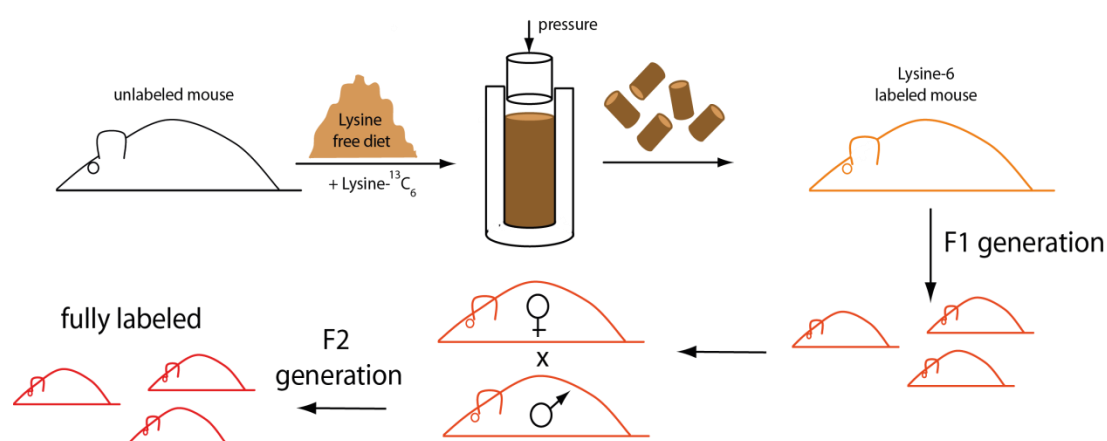


Figure 9. SILAC labelling of mice using a lysine free diet supplemented with heavy lysine (Adapted from Krüger et al., 2008 [108])

In comparison to the mice fed with normal diet, the SILAC mice consumed food similarly, had a similar body weight and possessed similar fertility. The mice were fed for four generations and the labelling was found to have no influence on normal development and physiology. Moreover, complete labelling efficiency was achieved in F2 generation mice.

Labelling with  $^{13}\text{C}_6$  lysine was preferred because lysine does not get converted to other amino acids. Also, the use of LysC as the protease for samples extracted from the SILAC mouse generates a mixture of all labelled peptides, making this method a powerful tool for *in vivo* quantification. Organs isolated from the SILAC mouse can be used as spike-in standards for various *in vivo* experimental conditions, such as comparison of wild-type and knockout mice. Besides organs, cells isolated from SILAC labelled tissues can serve as reference standard for those cell types which cannot be SILAC labelled in culture. Also, *in vivo* SILAC is highly advantageous in investigating cell types like intestinal epithelium which are difficult to be studied *ex vivo* [108]. Apart from proteome quantification, phosphopeptides enriched from the SILAC mouse serve as a spike-in standard for phosphoproteomics experiments involving tissue samples [109]. Thus, the SILAC mouse serves as a spike-in standard for *in vivo* quantitative proteomics of proteins and post-translational modifications.

### 1.7.3 Mass spectrometry-based phosphoproteomics

Recent advancements in high-resolution mass spectrometry-based proteomics has enabled site-specific identification of thousands of *in vivo* PTMs including phosphorylation, ubiquitination, methylation, acetylation and glycosylation, enabling system-wide characterization of signalling events [110]. Reversible phosphorylations play a very crucial role in many signalling pathways in the cell. Therefore, identification of phosphorylated proteins and mapping the sites of phosphorylation are essential in understanding the cellular processes. MS-based approaches have emerged as powerful tools for characterization of the global phosphoproteome [111]. The low abundance of phosphorylation sites in the proteome makes enrichment methods and pre-fractionation of samples essential prior to LC-MS/MS analysis. Phosphopeptide enrichment methods using strong cation exchange (SCX) chromatographic fractionation and titanium dioxide ( $\text{TiO}_2$ ) beads [112] together with improvements in mass spectrometry instrumentation and methods [113] have become a powerful tool for profiling phosphorylation sites in depth. About 6000 phosphorylation sites were identified in one of the first global phosphoproteomics studies using the SCX- $\text{TiO}_2$  approach [114]. More recently, it has been possible to identify as deep as 23,000 [115] and 36,000 [26] phosphorylation sites. Several other off-line and on-line peptide fractionation

techniques such as hydrophilic interaction chromatography (HILIC) [116], electrostatic repulsion-hydrophilic interaction chromatography (ERLIC) [117] and high-pH reversed-phase (HpH) fractionation [118] are also widely used to increase the depth of the proteome and phosphorylation sites. To rule out the possibility that observed phosphorylation changes might be a result of differential protein expression, it is important that the abundance of each phosphorylated site is normalized to the expression level of its parental protein [119].

## **1.8 Mass spectrometry instrumentation**

Mass spectrometry-based proteomics is applied for the analysis of complex peptide mixtures where proteolytic digested peptides are separated by liquid chromatography and ionized with an electrospray source for mass spectrometric (MS) and tandem mass spectrometric (MS/MS) analysis. In a relatively short time, tens of thousands of peptides are eluted and their intensities differ by several orders of magnitude [120, 121], making it inevitable for the mass spectrometers to have high speed, sensitivity, and resolution [122, 123]. In shotgun proteomics, four separation principles are applied in mass spectrometry: quadrupole mass filters, time of flight (TOF) [93] mass analysers, linear ion traps and Orbitrap analysers.

### **1.8.1 Quadrupole TOF and LTQ Orbitrap instruments**

Quadrupole TOF instruments are built with a quadrupole mass filter which either transmits the entire mass range of ions (MS mode) or a specific mass window of choice (MS/MS mode). In the MS/MS mode, ions are fragmented in the collision cell which are then analysed in the TOF section with high rate of repetition. In triple quadrupole instruments which are widely used in targeted proteomics [124-126], this TOF part is replaced by a final quadrupole section. In quadrupole TOF instruments, ions are separated almost instantaneously either by passing through the quadrupole in which only ions within a specified mass range have stable trajectories, or by passing through the TOF part. This is referred to as separation “in space”. On the other hand, linear ion trap instruments achieve peptide separation “in time” in the presence of radio frequency-direct current (RF-DC) field, whereby only certain ions can remain stable in the trap [127].



The Orbitrap mass analyzer was discovered by Makarov in 2000. It is an electrostatic device which contains a central, spindle shaped electrode around which ions injected at high energy orbit around [128-130]. The current generated by this axial motion of ions is detected by the detector and is Fourier Transformed (FT) to produce high resolution mass spectra. The first commercial use of the Orbitrap analyzer was made in a hybrid instrument in 2005 [131]. The combination of a low resolution linear ion trap and a high resolution Orbitrap analyzer emerged as 'LTQ Orbitrap' instruments which are widely used in proteomics [132, 133].

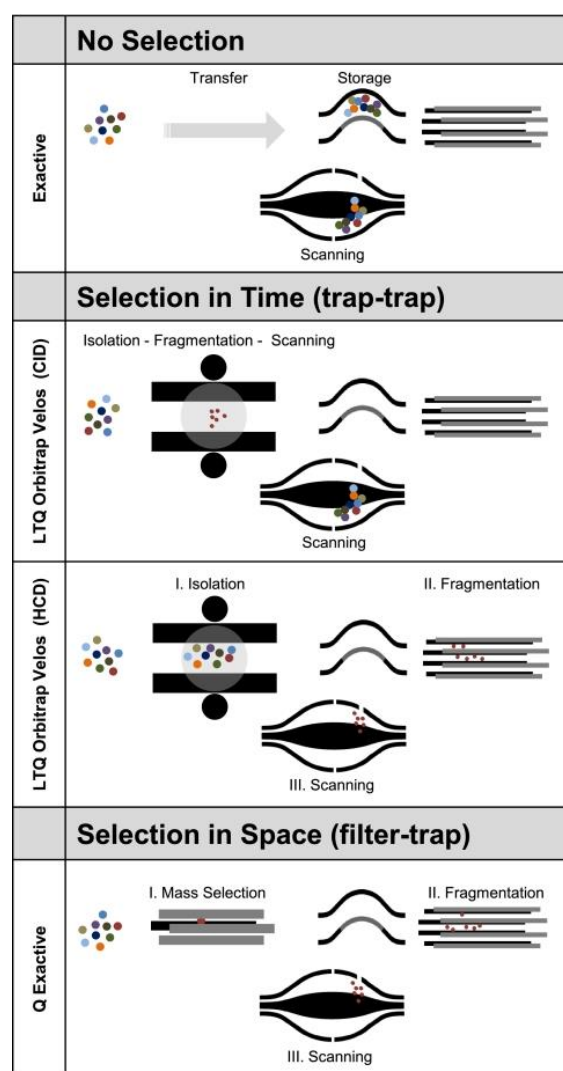


Figure 10. Mass spectrometers built with an Orbitrap mass analyzer (Michalski et al., 2011 [113])

LTQ Orbitrap instruments are characterized by multistage trapping (Fig. 10, middle panel). In the MS mode, the linear ion trap collects the ions and passes them to an intermediate C-trap which injects the ions into the Orbitrap mass analyzer for analysis at high resolution. In the MS/MS mode, the linear trap retains only those ions of a particular mass window, which are

then fragmented in the presence of a supplemental RF field and signals are recorded in low resolution. In the linear ion trap, both the high resolution MS scan and low resolution MS/MS scan can be obtained simultaneously. An improved linear ion trap Orbitrap instrument was introduced in 2009, called the LTQ Orbitrap Velos [134]. It is built with an S-lens which features a 10-fold improvement in the transmission of ions, a dual linear ion trap and a higher energy collisional dissociation (HCD) cell interfaced to the C-trap. The fragmented products of HCD are analysed in the Orbitrap with high mass accuracy [135]. In the collision-induced dissociation (CID) mode of the LTQ Orbitrap Velos, the LTQ and Orbitrap operate as separate mass spectrometers, while in the HCD mode precursor ion is selected for fragmentation in the HCD cell (Fig. 10, middle panel). The LTQ Orbitrap and LTQ Orbitrap Velos instruments provide diverse fragmentation options based on the analytical question of interest [136-138].

### 1.8.2 The Exactive series mass spectrometers

A standalone benchtop instrument called the “Exactive” was introduced in 2010 taking advantage of the small size of the Orbitrap analyzer. There is no mass selection made in this instrument (Fig. 10, top panel). The total ion population is collected in the C-trap which injects them into the Orbitrap analyzer. Hence, the applicability of this instrument is limited to All Ion Fragmentation (AIF), which refers to non-mass selective fragmentation of the complete mass range [139].

The Quadrupole Orbitrap instrument or the ‘Q Exactive’ was introduced in 2011 [113] which combines a quadrupole mass filter and an Orbitrap mass analyzer (Fig. 10, bottom panel). Due to the fast switching times of the quadrupole in the Q Exactive instrument, ions are selected almost instantaneously as only ions within a specified  $m/z$  (mass/charge) range have stable trajectories, and are also quickly fragmented in the HCD cell. Moreover, given the small size and advanced technology of the quadrupole, its combination with the Orbitrap mass analyzer is very robust. Also, the ‘in space’ separation of ions and recording of MS and MS/MS scans at high resolution in the Orbitrap facilitates multiplexed scan modes that is not feasible in the ion trap instruments. The Q Exactive instrument is coupled to an atmospheric pressure ion source (API) which is a nano electrospray ion source. It is built with an S-lens

[134], a bent flatapole, a quadrupole mass filter, a C-trap, an HCD fragmentation cell and an Orbitrap mass analyzer (Fig. 11).

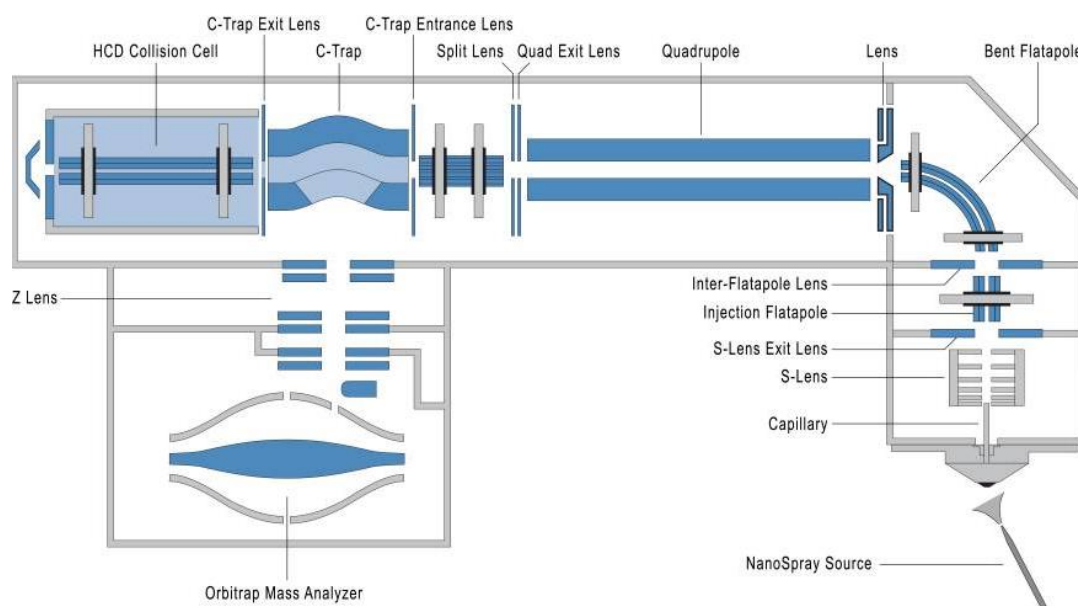


Figure 11. Build-up of the Q Exactive instrument that contains a combination of quadrupole mass filter and Orbitrap mass analyzer (Michalski et al., 2011 [113])

The nano electrospray source ionizes the peptide ions at atmospheric pressure which are sprayed through a transfer capillary into the S-lens. The ions exit the 'S-lens exit lens' and pass through an injection flatapole to a bent flatapole whose rods are separated by 2mm and oriented in such a way that ion clusters and droplets fly out of the flatapole. Ions are then transmitted through a lens into the hyperbolic quadrupole mass filter which isolates the ions of interest. The ions pass through the quadrupole's exit lens and a split lens which target the ion beam through an octapole into the C-trap. The C-trap is separated by a single diaphragm from the HCD lens and there is an axial field interface between them [134]. The axial field and offset of the radio frequency rods are adjusted to provide the collision energy required for fragmentation in the HCD cell. Multiple precursor ions are fragmented in the cell and the total ion population is transferred back to the C-trap and injected into the Orbitrap mass analyzer where they are detected in a single detection cycle. This facilitates multiplexing modes of operation of this instrument.

The problem of automatic gain control (AGC) of weak ion signals occurred by the combination of quadrupole and Orbitrap was solved by implementing an AGC pre-scan

where the full MS spectrum is scanned to predict the ion currents showing weak signals based on their proportion in the total ion current (predictive AGC). The Q Exactive instrument features parallel filling of ions in the HCD cell while ions of the previous detection cycle are still being analysed in the Orbitrap mass analyzer. The instrument therefore has high ion currents and hence enhanced speed and quality of the spectra. The image current obtained from the detector is processed using an enhanced Fourier Transformation (eFT) algorithm [140], thereby doubling the resolution of the spectra. With the isolation and fragmentation of ions being almost instantaneous, the cycle time in the Q Exactive instrument is achieved at the rate of 1s for a top10 HCD method. More than 2500 proteins could be identified from tryptic digested peptides from HeLa cell lysate using a 90 min chromatographic gradient [113]. Robust high performance and the ability to perform multiplexed operation at MS and MS/MS modes makes the Q Exactive a highly efficient mass spectrometer for complex proteomics analyses.

More recently, Q Exactive Plus and Q Exactive High Field (HF) mass spectrometers have been introduced [141]. They are an improved version of the Q Exactive and feature a low resolution mass filter incorporated within the injection flatpole so that unwanted ions do not enter deep into the instrument. Besides increased robustness, these instruments contain a segmented quadrupole that features enhanced isolation efficiency with a 2-fold improvement at narrow isolation windows. Moreover, the Q Exactive HF instrument is built with a more compact ultra-high field Orbitrap mass analyzer which enhances the field strength and doubles the resolution of the spectra. Given the almost instantaneous isolation and fragmentation of ions, this instrument features a cycle time of 1s for a top15 to top20 HCD method. About 5000 proteins could be identified from tryptic digested peptides from HeLa cell lysate using a 90 min chromatographic gradient, which is a 40% increase in comparison to the Q Exactive [141]. The Q Exactive Plus and Q Exactive HF instruments have emerged as efficient mass spectrometers for single-shot analysis of complex mixtures of proteins and post-translationally modified peptides.

## **1.9 Aim of the thesis**

Embryonic and neonatal heart development is achieved by proliferation of cardiomyocytes, which shortly after birth exit from cell cycle and lose the ability to proliferate. Post mitotic

cardiomyocytes possess only a very limited capacity for regeneration since they are unable to replace dying cells in damaged heart [17, 18]. Interestingly, a recent study showed that hearts of newborn mice can regenerate after surgical resection of ventricular apex probably due to residual proliferative capacity of neonatal cardiomyocytes [24]. Besides, phosphorylation during heart development has a key function and is essential for the regulation of myocardial contraction and metabolism [41], as protein phosphorylation is often important for temporary modulation of protein function, enzyme activity and protein interactions [26, 27]. Recent advancements in high-resolution mass spectrometry-based proteomics has enabled site-specific identification of hundred thousands of *in vivo* PTMs [110]. Moreover, phosphopeptide enrichment methods together with improvements in mass spectrometry instrumentation have become a powerful tool for profiling phosphorylation sites in depth [112, 113].

To date, the molecular mechanisms and regulatory expression profiles of proteins and post-translational modifications that might control neonatal cardiomyocyte proliferation or the switch to maturation and differentiation are poorly described, although associated changes in metabolic activities have been recently claimed to determine acquisition of the post mitotic state of cardiomyocytes [25]. In this study, we aimed to perform a global proteomics and phosphoproteomics study of post-natal heart development in mice using SILAC mouse based *in vivo* quantification, taking three time points P2, P10 and P20. We aimed to screen for proteins and components of signalling pathways that are differentially regulated between the neonatal proliferative phase of cardiomyocytes and the later matured phase.

Moreover, since the mitochondrion is a cellular compartment with highly dynamic protein changes and the functioning of heart is highly dependent on the energetics of cardiomyocyte mitochondria, we aimed to identify any novel mitochondrial proteins that show an interesting regulation during heart development and may be essential for the enhanced energetics of cardiomyocytes, and characterize such a protein using mass spectrometry-based interactome screening and subsequent biochemical approaches and loss of function studies.

## 2. Materials and Methods

### 2.1 Materials and chemicals for biochemistry methods

Lys6 mouse diet	Silantes
cOmplete protease inhibitor cocktail	Roche
PhosSTOP phosphatase inhibitor cocktail	Roche
N-ethylmaleimide	Sigma Aldrich
Needles and syringes	B.Braun
BSA protein standard	Sigma Aldrich
Dithiothreitol (DTT)	Sigma Aldrich
Iodacetamide	Sigma Aldrich
Ammonium bicarbonate (ABC)	Sigma Aldrich
Methanol	AppliChem
NuPAGE 4-12% Bis-Tris Gel	Life Technologies
NuPAGE LDS sample buffer 4x	Life Technologies
NuPAGE SDS MOPS running buffer	Life Technologies
InstantBlue	Expedeon
Ethanol	Carl Roth
Acetonitrile	Sigma Aldrich
Acetone	Carl Roth
Trifluoroacetic acid	Applied Biosystems
Microcon 30-kDa centrifugal filter unit	Merck Millipore
Sodium dodecyl sulphate (SDS)	Carl Roth
Urea	Sigma Aldrich
Thiourea	Sigma Aldrich
HEPES	Sigma Aldrich
Tris	Carl Roth
Hydrochloric acid	AppliChem

Resource S 15S column	GE Healthcare Life Sciences
Potassium phosphate	AppliChem
Potassium chloride	Carl Roth
Potassium hydrogen phosphate	Sigma Aldrich
Sodium chloride	AppliChem
Ammonia	Merck
Titansphere TiO <sub>2</sub> beads	GL Sciences Inc. Japan
3M Empore C8 extraction disk	Sigma Aldrich
3M Empore C18 extraction disk	Sigma Aldrich
Sepharose G beads	Life Technologies
Bicine	Sigma Aldrich
Bis-Tris	AppliChem
Tween-20	Carl Roth
Whatman (Rotilabo blotting) paper	Carl Roth
Nitrocellulose blotting membrane	GE Healthcare Life Sciences
RedAlert western blot stain 10x	EMD Millipore
Albumin bovine fraction	Serva
NP-40	Fluka
Sodium deoxycholate	Sigma Aldrich
Skim milk powder	Serva
Glass teflon homogenizer	Kontes Glass Co.
Sucrose	Carl Roth
Mannitol	Sigma Aldrich
Ethylenediaminetetraacetic acid (EDTA)	Carl Roth
Phenylmethanesulphonyl fluoride (PMSF)	Sigma Aldrich
Sodium carbonate	Carl Roth
Trichloroacetic acid	J.T. Baker Chemicals
Triton-X 100	Carl Roth
Casein kinase I	New England Biolabs
Casein kinase II	New England Biolabs
IKK kinase	Sigma Aldrich
$\gamma^{32}$ -ATP	Hartmann Analytic

X-ray film	GE Healthcare
Paraformaldehyde	Sigma Aldrich
Mowiol 4-88 reagent	Sigma Aldrich
Nunc Lab-Tek II chamber slide	Thermo Scientific
Fibronectin solution	Sigma Aldrich

## 2.2 Materials and chemicals for mass spectrometry methods

Fused-silica PicoTip Emitter	DNU-MS GbR
C18-AQ Reprosil Pur beads	Dr. Maisch GmbH
Nano electrospray ion source	Proxeon
LTQ Velos ESI positive ion calibration solution	Pierce
Methanol	AppliChem
Formic acid	Thermo Scientific
Acetonitrile	Sigma Aldrich

## 2.3 Materials and chemicals for molecular biology methods

DH5 $\alpha$ /DH10 $\beta$ bacterial cells	Life Technologies
LB bCarl Roth and agar	Sigma Aldrich
Glycerol	Sigma Aldrich
DMSO	Sigma Aldrich
dNTP mix	Life Technologies
<i>PfuUltra</i> High-Fidelity DNA polymerase AD	Agilent Technologies
DpnI restriction enzyme	New England Biolabs
T4 DNA ligation buffer 10x	Promega
T4 DNA ligase	Promega
2-propanol	Carl Roth
Agarose	Biozym
Ethidium bromide	AppliChem



TRIzol reagent	Life Technologies
Chloroform	Merck
Diethylpyrocarbonate (DEPC)	Sigma Aldrich
RQ1 DNase buffer	Promega
RQ1 DNase	Promega
RQ1 DNase stop solution	Promega
First strand buffer 5x	Promega
RNase IN	Promega
RNase H	Promega
Superscript II reverse transcriptase	Promega
Calcium chloride	AppliChem
Magnesium chloride	Carl Roth
Bacto-tryptone	BD Biosciences
Bacto-yeast extracts	BD Biosciences
Bacto-agar	BD Biosciences
Ampicillin	Sigma Aldrich
Kanamycin monosulphate	Sigma Aldrich
Tris-acetate	Sigma Aldrich
Glucose	Sigma Aldrich
Sodium hydroxide	Carl Roth
Potassium acetate	Carl Roth
Acetic acid	Carl Roth
KAPA SYBR Green fast qPCR master mix	Kapa Biosystems

## 2.4 Materials and chemicals for cell culture methods

DMEM medium	Sigma Aldrich
Fetal bovine serum (FBS)	Life Technologies
Penicillin-Streptomycin-Glutamine 100x	Sigma Aldrich
PBS tablets	Gibco (Life Technologies)
Trypsin EDTA	Sigma Aldrich

SILAC DMEM medium	Silantes
Dialyzed fetal bovine serum (dFBS)	Silantes
L-lysine	Sigma Aldrich
L-arginine	Sigma Aldrich
$^{13}\text{C}_6$ $^{15}\text{N}_2$ -L-Lysine HCl (Lys8)	Silantes
$^{13}\text{C}_6$ $^{15}\text{N}_4$ -L-Arginine HCl (Arg10)	Silantes
Dimethyl Sulphoxide (DMSO)	Sigma Aldrich
Sodium hydrogen phosphate	Carl Roth
Calcium chloride	AppliChem
TurboFect transfection reagent	Thermo Scientific
Opti-MEM medium	Gibco (Life Technologies)
Z-Leu-Leu-Leu-al (MG-132)	Sigma Aldrich
TBB	Sigma Aldrich
Cycloheximide	Sigma Aldrich
ON-TARGETplus non-targeting control siRNA	GE Dharmacon
ON-TARGETplus SMARTpool 2310042D19Rik siRNA	GE Dharmacon
DharmaFECT 2 transfection reagent	GE Dharmacon

## 2.5 Enzymes

Lysyl endopeptidase (LysC)	Wako
Sequencing grade Trypsin	Promega
Proteinase K	Sigma Aldrich
RNase A	Sigma Aldrich

## 2.6 Kits

Neonatal heart dissociation kit	Miltenyi Biotec
Neonatal cardiomyocyte isolation kit	Miltenyi Biotec

DC protein assay kit	Bio-Rad
Phusion High-Fidelity DNA polymerase kit	New England Biolabs
QIAquick Gel Extraction kit	Qiagen
NucleoBond Xtra Maxi Kit	Macherey Nagel
Epoxy embedding medium kit	Sigma Aldrich
SuperSignal West femto max. sensitivity substrate kit	Thermo Scientific

## 2.7 Antibodies

### 2.7.1 Primary antibodies

Antibody	Company	Catalog number	Application
c1orf170	Sigma Aldrich	#HPA031711	IP/WB/IHC
Mitofilin	Abcam	#ab110329	IP/WB
Chchd3	Abcam	#ab154500	IP/WB
Flag	Sigma Aldrich	#F1804	IF
Anti-Flag M2 affinity gel	Sigma Aldrich	#A2220	IP
Flag M2 peroxidase HRP	Sigma Aldrich	#A8592	WB
GFP	Evrogen	#AB121	IP
Pan-actin	Cell Signaling Technology	#4968	WB
Hsp60	Abcam	#ab46798	WB
GAPDH	Cell Signaling Technology	#14C10	WB
Rabbit Tom20	Santa Cruz	#FL-145	WB/IF/IHC
Mouse Tom20	Abcam	#ab56783	IHC
HA-HRP	Sigma Aldrich	#H6533	WB
Phospho Ser/Thr CK2 substrate	Cell Signaling Technology	#8738	WB
Fkbp10	Sigma Aldrich	#HPA051171	WB
Cofilin	Cell Signaling Technology	#3312	WB
Pdk3	Abcam	#ab182574	WB
Sarcomeric $\alpha$ -actinin	Sigma Aldrich	#A7811	IF
Alexa flour 488 Phalloidin	Life Technologies	#A12379	IHC

## 2.7.2 Secondary antibodies

Antibody	Company	Catalog number	Application
Anti-mouse Alexa flour 594	Life Technologies	#A-11005	IF
Anti-rabbit Alexa flour 594	Life Technologies	#A-11012	IF/IHC
Anti-mouse Alexa flour 488	Life Technologies	#A-11001	IF/IHC
Anti-rabbit Alexa flour 488	Life Technologies	#A-11008	IF
Anti-mouse IgG-peroxidase	Sigma Aldrich	#A5278	WB
Anti-rabbit IgG-peroxidase	Sigma Aldrich	#A9169	WB

## 2.8 Primers

Name of primer	Primer sequence (5'-3')	Application
Kpn1-Mic85-forward	AAAGGGAAAGGTACCATGGACAACCTCCAGTACAG	Cloning
Mic85-XhoI-reverse	TTCCCTTTCTCGAGGCAGCTGGGGTTTGA	Cloning
Mic85-forward	GAAACAGTCTTGCTCGCCAA	qPCR
Mic85-reverse	CTTGTCACCTGGGTTCGTCT	qPCR
Mic85 7-27 bp fwd	AACTTCCAGTACAGCGTCCAG	Sequencing
Mic85 510-529 bp fwd	TGACAGCCTCGAAGCTTCAC	Sequencing
Mic85 982-1002 bp fwd	TCTTTGTCCACACTTGCCTTC	Sequencing
Mic85 1480-1499 bp fwd	TCAGGAGAGTCCTGCCTAGG	Sequencing
Mic85 1879-1897 bp fwd	TGGCCTGACACATGCGAGT	Sequencing
Mic85 2007-2027 bp fwd	GCCTATTTCCATCCCTGAGGT	Sequencing
Mic85 310-325 bp rev	ACTGTGTGGACGTGCCGGCTACCTG	Sequencing

## 2.9 Buffers

SDS lysis buffer	4% SDS
	0.1M Tris/HCl pH 7.6

<b>RIPA lysis buffer</b>	100mM Tris/HCl pH 7.5 300mM NaCl 2% NP-40 2mM EDTA 0.2% Sodium deoxycholate
<b>Urea (UA) buffer</b>	6M Urea 2M Thiourea 0.1M HEPES pH 7.4
<b>Buffer A</b>	0.1% formic acid
<b>Buffer B</b>	80% acetonitrile 0.1% formic acid
<b>Buffer C</b>	5% Acetonitrile 1% Trifluoroacetic acid
<b>SCX Buffer A</b>	7mM KH <sub>2</sub> PO <sub>4</sub> 30% acetonitrile pH 2.65
<b>SCX Buffer B</b>	7mM KH <sub>2</sub> PO <sub>4</sub> 350mM KCl 30% acetonitrile pH 2.65
<b>SCX Buffer C</b>	50mM K <sub>2</sub> HPO <sub>4</sub> ·3H <sub>2</sub> O 500mM NaCl 30% acetonitrile pH 7.5

<b>Phospho binding buffer</b>	80% acetonitrile 6% trifluoroacetic acid
<b>Phospho wash buffer</b>	80% acetonitrile 3% trifluoroacetic acid
<b>Phospho elution buffer</b>	60% acetonitrile 40% ammonia (pH>11)
<b>KCM buffer 5x</b>	500 mM KCl 150 mM CaCl <sub>2</sub> 250 mM MgCl <sub>2</sub>
<b>LB (Luria-Bertani) medium per litre</b>	10g Bacto-tryptone 5g Bacto-yeast extracts 5g NaCl 950 ml deionized water added and dissolved, pH adjusted to 7.0 with 5N NaOH, filled upto 1l with deionized water, sterilized by autoclaving
<b>LB-Agar plate per litre</b>	10g Bacto-tryptone 5g Bacto-yeast extracts 5g NaCl 7g Bacto-agar Sterilized by autoclaving, cooled to 50-60°C and antibiotic added
<b>Antibiotics (1000x stocks)</b>	Ampicillin 50mg/ml in H <sub>2</sub> O

	Kanamycin monosulphate 10mg/ml in H <sub>2</sub> O
<b>Tris-EDTA (TE) buffer 10x</b>	100 mM Tris/HCl pH 7.6 10mM EDTA pH 8.0
<b>TAE buffer</b>	40mM Tris-acetate 1mM EDTA
<b>Mini prep solution A</b>	25mM Tris pH 8.0 10mM EDTA 50mM Glucose 10µg/ml RNase A
<b>Mini prep solution B</b>	0.2N NaOH 1% SDS
<b>Mini prep solution C</b>	3M Potassium acetate 8.9% Acetic acid
<b>HBS (HEPES Buffered Saline) 2x</b>	50 mM HEPES 280 mM NaCl 1.5 mM Na <sub>2</sub> HPO <sub>4</sub> pH 7.0 adjusted using HCl and filter sterilized
<b>Western blot transfer buffer 20x</b>	500mM Bicine 500mM Bis-Tris 20mM EDTA
<b>TBS-T</b>	50mM Tris/HCl pH 7.6 150mM NaCl 0.1% Tween-20

**Mito isolation buffer A**

220 mM Mannitol  
 70 mM Sucrose  
 20 mM HEPES pH 7.6  
 1mM EDTA  
 0.1% BSA

**Mito isolation buffer B**

220 mM Mannitol  
 70 mM Sucrose  
 20 mM HEPES pH 7.6  
 1mM EDTA

**2.10 Devices used**

FLUOstar galaxy spectrophotometer	BMG Labtech
SpeedVac concentrator plus	Eppendorf
Milli-Q water purification system	Merck Millipore
Thermomixer	Eppendorf
ÄKTA purifier	GE Healthcare Life Sciences
Easy nLC 1000 UHPLC	Thermo Scientific
Q Exactive mass spectrometer	Thermo Scientific
PCR labcycler	Sensquest
StepOne Plus real-time PCR system	Applied Biosystems
NanoDrop 2000c spectrophotometer	Peqlab
ChemiDoc MP imaging system	Bio-Rad
LSM700 confocal microscope	Zeiss
TCS SP8 confocal microscope	Leica microsystems
XFe96 Extracellular Flux Analyzer	Seahorse Bioscience
EM902 electron microscope	Carl Zeiss



## **2.11 Working with the model organism *Mus musculus***

### **2.11.1 SILAC mice colony**

For the generation of SILAC mice colony, C57BL/6 mice were fully labelled with  $^{13}\text{C}_6$  lysine containing mouse diet as described earlier [108], and maintained with this diet throughout their lifetime. Like unlabeled mice, the SILAC mice were also maintained at an ambient temperature of 20-22°C and in a 12h light-dark cycle.

### **2.11.2 Isolation of mouse heart**

P2 and P10 pups were sacrificed by decapitation and the heart tissue was isolated by cutting through the middle of the body. P20 and adult mice were sacrificed by cervical dislocation followed by decapitation and the heart tissue was isolated by opening the skin and the thoracic cavity. Isolated organs were washed in PBS to remove the blood and either snap frozen in liquid nitrogen or used directly in case of mitochondrial isolation.

### **2.11.3 Isolation of mouse neonatal cardiomyocytes**

For isolation of neonatal cardiomyocytes, heart tissues from P1, P2 and P3 pups were used. Neonatal hearts were dissociated into single-cell suspensions by a combination of mechanical dissociation and enzymatic degradation of the extracellular matrix, using the Neonatal Heart Dissociation Kit according to the manufacturer's protocol. Cardiomyocytes were enriched from the dissociated hearts using the Neonatal Cardiomyocyte Isolation Kit according to the manufacturer's instructions. Cultivation of beating cardiomyocytes was done in standard cell culture medium.

## 2.12 Sample preparation methods for mass spectrometry

### 2.12.1 Protein extraction – tissue homogenization and cell lysis

Frozen tissues were ground to a fine powder in liquid nitrogen using mortar and pestle and the powder was taken up in SDS (sodium dodecyl sulphate) lysis buffer, with the ratio of buffer to tissue being 15:1. The lysates were homogenized by shearing using a syringe followed by heating at 95°C for 5 min. Crude extracts were clarified by centrifugation at 13,000 rpm for 10 min. Cells were lysed in a similar way for use in SDS PAGE or western blot. For immunoprecipitation experiments, cells were lysed using RIPA buffer using protease inhibitors. Phosphatase inhibitors or N-ethylmaleimide were additionally used while studying phosphorylation or ubiquitination, respectively. RIPA lysates were homogenized on a rotating wheel at 4°C for 30 min. Crude extracts were clarified by centrifugation at 15,000 rpm at 4°C for 10 min.

### 2.12.2 Determination of protein concentration

Protein concentration was determined using the *DC* Protein assay according to the manufacturer's instructions using a FLUOstar galaxy spectrophotometer. This is a colorimetric assay very similar to the well-known Lowry assay [142]. It is a two-step process leading to color development, the first being the reaction of protein with an alkaline copper tartrate solution and the second being the reduction of Folin reagent by the copper treated protein. Proteins facilitate this reduction by loss of oxygen atoms primarily from tyrosine and tryptophan, thereby forming reduced species which show a characteristic blue color at an absorbance of 750 nm. Bovine serum albumin was used as the protein standard for this assay.

### 2.12.3 In-solution digestion

Protein digestion in solution was performed as described earlier [90]. Proteins in SDS lysis buffer were precipitated using ice-cold acetone at -20°C for 1 hour. The precipitated proteins

were pelleted by centrifugation at 15,000 rpm at 4°C for 10 min. The pellet was washed with 90% acetone to remove any remaining SDS and centrifuged at 15,000 rpm at 4°C for 10 min. The protein pellet was dissolved in Urea buffer (containing 8M urea) and incubated with 10mM DTT (dithiothreitol) for 30 min for reduction of the disulphide bonds. This was followed by treatment with 55mM iodacetamide in dark for 20 min to alkylate the free sulfhydryl groups of the cysteines. Proteins were then digested with LysC (which cuts at lysine) at the ratio of 1:100 overnight for samples containing Lys6 labelled proteins (from SILAC mouse). For all other samples, proteins were digested with LysC for 2-3 hours, diluted with 50mM ammonium bicarbonate (ABC) to 2M urea and digested with Trypsin (which cuts at lysine and arginine) at the ratio of 1:100 overnight. Enzymatic incubations were performed at room temperature. On the following day, digestion was stopped by mixing with equal volume of Buffer C and peptides were desalted on StageTips (Stop and go extraction tips) [96].

StageTips were made in-house by stacking two layers of C18 material in pipette tips. StageTips were equilibrated with 20µl 100% methanol (2600 rpm, 2 min) for activation, 20 µl Buffer B (2600 rpm, 2 min) for elution of any dirt in the C18 material, and twice with 20 µl Buffer A to remove any remaining acetonitrile from Buffer B. Digested peptides were then loaded onto the equilibrated StageTips and centrifuged at 2600 rpm for 5 min. Peptides bind to the C18 material through hydrophobic interactions. Bound peptides were washed with 20 µl Buffer A and the C18 material was dried using a syringe. StageTips were stored at 4°C until elution for measurement at the mass spectrometer.

#### **2.12.4 In-gel digestion**

To reduce the complexity of samples containing high dynamic range of proteins, proteins were separated based on their molecular weight by SDS-PAGE (Sodium dodecyl sulphate-polyacrylamide gel electrophoresis) using 4-12% Bis-Tris gel. After electrophoresis, proteins on the gel were stained using Instant Blue for 15 min on a shaker. Following this, the gel was washed with double distilled water (Milli-Q water) for 10 min. Each lane of the gel was cut into 12 slices (for whole proteome analysis) or 7 slices (for interactome screening) and digested in-gel as described previously [92]. In-gel digestion is performed in two days. On the first day, all buffers used until the addition of enzyme were discarded after each step. Firstly,

the gel pieces were destained by incubating twice with 100  $\mu$ l 50mM ABC for 20 min. Following this, the gel pieces were dehydrated by incubation with 100  $\mu$ l ethanol twice for 10 min and dried using SpeedVac for 5 min at 30°C. Proteins in the gel pieces were reduced with 100  $\mu$ l 10mM DTT at 56°C for 45 min with shaking at 600 rpm in a Thermomixer. The free SH groups in the reduced proteins were alkylated by treating the gel pieces with 100  $\mu$ l 55mM iodacetamide for 30 min in dark. Following this, the gel pieces were washed with 100  $\mu$ l 50mM ABC for 15 min, dehydrated with 100  $\mu$ l ethanol for 15 min, again washed with 100  $\mu$ l 50mM ABC for 15 min and dehydrated twice with 100  $\mu$ l ethanol for 15 min. The dehydrated gel pieces were dried using SpeedVac for 5 min at 30°C. Then 50  $\mu$ l 12ng/ $\mu$ l LysC or trypsin was added to the gel pieces, which were incubated in ice for 15 min for swelling. Then 80  $\mu$ l 50mM ABC was added and the gel pieces were incubated at 37°C overnight. On the following day, digested peptides in the gel pieces were eluted using increasing concentrations of acetonitrile (ACN) and the eluate from each step was collected in a new tube. Firstly, the gel pieces were incubated with 100  $\mu$ l 30% ACN / 3% trifluoroacetic acid (TFA) for 20 min to stop the enzymatic reaction, followed by twice with 100  $\mu$ l 70% ACN for 20 min and then twice with 100  $\mu$ l 100% ACN for 20 min. The final volume was concentrated by vacuum evaporation to ~80  $\mu$ l using a SpeedVac, mixed with 80  $\mu$ l Buffer C and desalted using StageTips as described earlier.

### **2.12.5 Filter Aided Sample Preparation (FASP)**

The FASP method of protein digestion was performed as described previously [95], using a Microcon YM-30 FASP filter. Samples were homogenized in SDS lysis buffer as described earlier. 1M DTT was added to a final concentration of 10 mM and the samples were heated at 70°C for 10 min. 4 ml UA buffer was used to pre-wet the FASP filter after which the DTT-treated sample was loaded onto the filter. The sample was mixed well with the UA buffer and centrifuged at 4000g for 15 min to concentrate the sample to 1500  $\mu$ l. The filtrate was discarded at each step. Two further wash steps, one with 4 ml UA and the other with 2 ml UA, were performed in a similar way to exchange the SDS buffer in the sample to UA buffer. Following this, 4 ml 55 mM iodacetamide in UA buffer was added to the concentrated sample, mixed well and incubated in dark for 20 min. The filter was centrifuged at 4000g for 20 min to concentrate the sample to 750  $\mu$ l. Then, 4 ml UA buffer was added, centrifuged at

4000g for 20 min to concentrate the sample to 750  $\mu$ l in order to wash out the remaining iodacetamide from the sample.

For digestion with LysC, 2 ml 50mM Tris/HCl (pH 8.5) was added, mixed thoroughly to avoid precipitation and further 2 ml 50mM Tris/HCl (pH 8.5) was added. The filtrate was discarded at each step. The filter was centrifuged at 4000g for 10 min to concentrate the sample to 750  $\mu$ l. Following this, two wash steps were performed with 4 ml 50mM Tris/HCl (pH 8.5) in a similar way to exchange the UA buffer in the sample to 50mM Tris/HCl (pH 8.5). The filter was transferred to a new falcon and filled with 50mM Tris/HCl (pH 8.5) just up to the brim. LysC was added at a ratio of 1:100 and the sample in the filter was incubated at room temperature for 3 h. Then, LysC was added again at the ratio of 1:100 and digestion was performed in the filter overnight at 30°C.

For digestion with trypsin, 4 ml 50mM ABC was added, mixed thoroughly and centrifuged at 4000g for 10 min to concentrate the sample to 750  $\mu$ l. The filtrate was discarded at each step. Following this, again 4 ml 50mM ABC was added and centrifuged at 4000g for 10 min to concentrate the sample to 750  $\mu$ l. Next 4 ml 20mM ABC was added and centrifuged at 4000g for 10 min to concentrate the sample to 750  $\mu$ l. The filter was transferred to a new falcon and filled with 20mM ABC just up to the brim. LysC was added at a ratio of 1:100 and the sample in the filter was incubated at room temperature for 3 h. Then, trypsin was added again at the ratio of 1:100 and digestion was performed in the filter overnight at 37°C.

On the following day, the sample in the filter was centrifuged at 4000g for 10 min and the filtrate was saved. The filter was washed with 4 ml Milli-Q water, centrifuged at 4000g for 10 min and the washed filtrate was collected on top of the already saved filtrate. This filtrate contained pure digested peptides.

### **2.12.6 Strong Cation Exchange Chromatography (SCX)**

Ion exchange chromatography is based on the principle of separation of ions based on affinity to the ion exchanger. In case of SCX, the stationary phase ion exchanger resin is negatively charged and has an affinity for positively charged ions. Hence negatively charged

ions bind weaker to the resin, while the strongly bound positively charged ions are eluted using an increasing salt gradient in the mobile phase. SCX is widely used for separation of phosphopeptides. At an acidic pH of 2.7, phosphopeptides carry an additional negative charge, due to which they bind weakly to the chromatographic column and elute in the early fractions. Moreover, the multiply phosphorylated peptides which are repelled by the column are collected in the flow through [111, 143]. The enrichment of phosphopeptides in the flow through and early fractions is because the strongly bound non-phosphopeptides are retained by the column.

For fractionation by SCX, the FASP-digested peptide solution was adjusted to a pH of 2.6 using TFA. Then, ACN was added to a final concentration of 30% and mixed thoroughly. Samples were centrifuged at 4000g for 5 min and the clear supernatant was used for SCX fractionation. A 1ml Resource S column was installed on an ÄKTA Purifier coupled to a fractionator. The column was pre-equilibrated by washing with 5 times its volume of SCX Buffer B followed by equal volume of SCX Buffer A. Pre-programmed methods in Unicorn software were used for sample loading and elution. Peptides were loaded onto the column and those with high negative charge like multiply phosphorylated peptides that do not bind to the column were collected in the flow-through. Peptides bound to the column were eluted using a 30-min increasing salt gradient with SCX Buffer B. Between two runs, the column was washed with 5 times its volume of SCX Buffer C, followed by equal volume of SCX Buffer B and then SCX Buffer A. The eluted fractions were pooled to a total of nine fractions based on the chromatogram.

### **2.12.7 Phosphopeptide enrichment using TiO<sub>2</sub> beads**

Titanium oxide-based solid phase material (Titansphere) contains porous Titania microspheres which possess a smooth and alkaline surface with amphoteric ion-exchange properties [144-147]. Moreover, titanium dioxide can selectively adsorb water-soluble organic phosphates [148-151]. Hence, titanium dioxide chromatography was described as an efficient method for enrichment of phosphopeptides prior to mass spectrometric analysis [152], however this method required O-methylation to enhance the efficiency of purification. Later, an improved method for enrichment of phosphopeptides from TiO<sub>2</sub>

without any prior chemical modification was described [153, 154]. This method described that the selectivity of TiO<sub>2</sub> beads for phosphopeptides was enhanced when the sample was loaded in a 2,5-dihydroxybenzoic acid (DHB) or phthalic acid solution with acetonitrile and trifluoroacetic acid (TFA), which prevented non-specific binding. Mono- and multi-phosphorylated peptides are then eluted using acetonitrile and ammonia (pH>11). The limitation of using DHB in the sample is that some of this acid also gets eluted from the TiO<sub>2</sub> beads together with the phosphorylated peptides, making the final sample for MS analysis unclean and detrimental for the mass spectrometer. Therefore, the protocol for TiO<sub>2</sub> based enrichment these days employs only acetonitrile and increased TFA concentration in the binding conditions, which works very efficiently and has resulted in the identification of >50,000 phosphorylation sites in an *in vitro* phosphoproteomics study [155] and >20,000 phosphorylation sites in an *in vivo* phosphoproteomics approach (this study). In a nutshell, the enrichment of phosphopeptides using TiO<sub>2</sub> beads is a highly efficient method for characterization of phosphoproteins using mass spectrometry.

Titanium dioxide (TiO<sub>2</sub>) beads were weighed as per the calculation of 5mg beads per extraction per sample for flow-through and 3mg beads per extraction per sample for fractions. Beads were washed with 1 ml Phospho elution buffer on a rotating wheel for 2 min and centrifuged at 2600 rpm for 1 min. The supernatant was discarded. Following this, beads were washed with 1 ml 70% ACN and twice with 1 ml Phospho wash buffer in a similar way. Finally, washed beads were resuspended in Phospho binding buffer. The flow-through and fractions obtained from SCX chromatography were vacuum concentrated using a SpeedVac and adjusted to the binding buffer condition by combining 1 part of the sample to 6 parts of 93% ACN / 7% TFA. Flow-through samples were extracted thrice and fractions were extracted twice using the appropriate amount of TiO<sub>2</sub> beads specified earlier. During each extraction step, samples with beads were incubated on a rotating wheel for 25 min at room temperature and centrifuged at 2000g for 2 min to pellet the beads. Supernatant was transferred to a new tube for the next extraction and the pelleted beads were washed with 1ml Phospho binding buffer. C8 StageTips were prepared by stacking one layer of C8 material in pipette tips. Extracted beads were loaded onto the C8 StageTips. In case of flow-through samples, the second and third extractions were pooled together and in case of fractions, both the extractions were pooled together. Beads were washed twice with 200 µl

Phospho binding buffer and twice with 200  $\mu$ l Phospho wash buffer. During each washing step, StageTips were centrifuged at 2600 rpm for 4 min and waste was discarded. Washed beads were eluted thrice with 25  $\mu$ l Phospho elution buffer and the eluates were vacuum concentrated using SpeedVac to 2-3  $\mu$ l. The concentrated phosphopeptides were diluted with 10  $\mu$ l Buffer A for analysis by mass spectrometry.

## **2.13 Liquid Chromatography - Tandem Mass Spectrometry (LC-MS/MS)**

### **2.13.1 Reversed phase liquid chromatography (LC)**

Peptides were eluted from the StageTips by adding 30  $\mu$ l Buffer B to the C18 material and incubating for 15 min. The solvent was pushed through a syringe into a 96-well plate and vacuum evaporated using a SpeedVac to approximately 2  $\mu$ l in order to evaporate the acetonitrile. The concentrated peptides were resuspended with 10  $\mu$ l Buffer A. Reversed phase liquid chromatographic separation of eluted peptides was performed using an Easy nLC 1000 UHPLC system. Peptides were loaded using an Auto sampler onto in-house made 50 cm fused silica emitters (75  $\mu$ m diameter) packed with 1.9  $\mu$ m C18-AQ Reprosil Pur beads, at a flow rate of 750 nl/min. Peptides were eluted using a segmented gradient of 10-38% Buffer B and 38-60% Buffer B at a flow rate of 250 nl/min. The nLC 1000 UHPLC was connected to a Q Exactive instrument.

### **2.13.2 Tandem mass spectrometry (MS/MS)**

Eluted peptides were ionized by electrospray ionization (ESI) using a nano-electrospray ion source and sprayed onto the transfer capillary of the Q Exactive mass spectrometer. The Q Exactive was operated in a data-dependent mode, where full MS scans (300-1750 m/z) were acquired by the Orbitrap at a resolution of R=70,000 with an automated gain control (AGC) target of  $3 \times 10^6$  ions collected within 20 ms. The dynamic exclusion was set to 20s and the 10 most intense peaks ( $z \geq 2$ ) from the full MS scan were fragmented in the high-energy collision induced dissociation (HCD) cell (25% normalized collision energy). MS/MS scans



with a target of  $5 \times 10^5$  ions were collected within a maximum fill time of 120 ms at a resolution of  $R=35,000$ . The isolation width was set to 1.8 m/z. A spray voltage of 1.8 kV and capillary temperature of 280°C were among the general settings applied. The Q Exactive instrument was calibrated once in three days using LTQ Velos ESI positive ion calibration solution, and opened once in a month to clean its parts using methanol.

### **2.13.3 Data processing with MaxQuant**

The raw data were processed and analysed using the MaxQuant software [98]- versions 1.4.1.2 to 1.5.2.8. Andromeda search engine [97] was used to search for peptides against a mouse FASTA database (UniProt, 73,921 entries). SILAC peptide pairs were quantified by setting Lys6 as the heavy label (for SILAC mouse based samples) or Lys8/Arg10 as heavy labels (for SILAC labelled cell culture samples). Enzyme specificity was set to LysC or trypsin with an additional allowance of cleavage N-terminal to proline. A maximum of 2 missed cleavages were allowed. Cysteine carbamidomethylation was set as fixed modification; and oxidation of methionine, acetylation of protein N-terminus and phosphorylation of STY (Serine, Threonine, and Tyrosine), where applicable, were set as variable modifications. The initial precursor ion mass deviation was set to 7 ppm and the maximum allowed mass deviation was set to 20 ppm. MS/MS tolerance was set to 0.5 Da. A false discovery rate of 0.01 and minimum peptide length of 7 amino acids were used for peptide identifications. A minimum ratio count of 2 was used for SILAC quantification. Statistical analysis of data and t-tests were performed using the R package and Perseus (version 1.4.1.3).

## **2.14 Molecular biology methods**

### **2.14.1 Bacterial culture and competent cell preparation**

Single colonies of DH5 $\alpha$  or DH10 $\beta$  bacteria were picked up from LB agar plate and inoculated in 5 ml LB medium overnight at 37°C with shaking at 200 rpm. 1 ml of this bacterial culture was inoculated in 500 ml LB medium and grown at 37°C with shaking at 200 rpm until an optical density of 0.5-0.8 at 600 nm wavelength was attained. The culture was chilled on ice

for 30 min and centrifuged at 4000g at 4°C for 10 min. The bacterial pellet was resuspended in 200 ml cold 10% glycerol and centrifuged at 4000g at 4°C for 10 min. This was repeated another two times and finally the bacterial pellet was resuspended in 3 ml 10% glycerol. 50 µl aliquots were snap frozen in liquid nitrogen and stored at -80°C until use.

### **2.14.2 Polymerase chain reaction**

For cloning, double stranded DNAs of interest were amplified using PCR with specific primers. A 20 µl reaction with 4 µl Phusion HF buffer, 0.6 µl dimethylsulphoxide (DMSO), 0.4 µl 10mM dNTPs, 0.5 µl forward primer, 0.5 µl reverse primer, approximately 10ng template DNA, 0.2 µl Phusion Hot Start DNA polymerase and 12.8 µl sterile water was used for the PCR which was performed in a thermocycler with the appropriate program. Amplified products were purified, digested and cloned into the target vector.

### **2.14.3 A-tailing of PCR product**

For A-tailing the purified PCR product was mixed with 3 µl of 10x Taq Polymerase buffer with MgCl<sub>2</sub>, 1 µl 1mM dATP, 1 µl Taq DNA Polymerase (5PRIME). MilliQ water was added to a final volume of 30 µl. The A-tailing mix was incubated for 30 min at 70°C and then cooled on ice.

### **2.14.4 Enzymatic digestion and ligation**

1-2 µg DNA was used for digestion with 1-2 µl of appropriate restriction enzymes along with their corresponding buffer in a 50 µl reaction. The temperature of incubation was followed as indicated by the manufacturer for the optimal activity of each enzyme. Digested plasmids or DNA fragments were purified after agarose gel electrophoresis. Ligation was performed in a 50 µl reaction with 5 µl 10x T4 DNA ligation buffer, 5 µl T4 DNA ligase and DNA insert and plasmid in the ratio of 3:1. The reaction was incubated overnight at 16°C. 5 µl of this reaction was used for bacterial transformation.

### **2.14.5 Bacterial transformation of plasmid**

Plasmids were transformed into competent cells by heat shock method. Few nanograms of the plasmid were mixed with 10  $\mu$ l 5x KCM buffer and sterile water to a final volume of 50  $\mu$ l. To this, 50  $\mu$ l competent E.coli cells were added, mixed and the tube was placed immediately on ice. The tube was incubated on ice for 10 min and then in room temperature for 20 min. Then, 1 ml LB medium was added and incubated at 37°C for 1.5 h with shaking at 800 rpm. The tube was then centrifuged at 3000g for 1 min, the bacterial pellet was resuspended in 50  $\mu$ l LB medium and spread on a LB agar selection plate made with the appropriate antibiotic. The plate was incubated overnight at 37°C.

### **2.14.6 Plasmid DNA isolation**

Plasmid DNA was isolated on a small-scale using mini preparation (from 5 ml bacterial culture) or on a large-scale using maxi preparation (from 200 ml bacterial culture). Single colonies of bacteria were picked from the LB agar plate and inoculated in LB medium containing 100  $\mu$ g/ $\mu$ l selective antibiotics and grown for 14-18 h at 37°C with shaking at 200 rpm. For mini preparation, bacteria were pelleted by centrifugation at 14000g for 5 min. Supernatant was discarded and the pellet was resuspended with 150  $\mu$ l Miniprep Solution A. 200  $\mu$ l Miniprep Solution B was added and incubated at room temperature for 10 min. Then 175  $\mu$ l Miniprep Solution C was added and incubated for 10 min on ice to precipitate the proteins. The samples were centrifuged at 14000g for 10 min at 4°C and the supernatant was transferred to a new tube containing 500  $\mu$ l isopropanol. The samples were mixed thoroughly and centrifuged at 20000g for 20 min at 4°C. The DNA pellet was washed with 500  $\mu$ l 70% ethanol, dried and resuspended in sterile water. The plasmid concentration and quality was determined using Nanodrop ND-100 Spectrophotometer. Maxi preparation of plasmid DNA was performed using the NucleoBond Xtra Maxi Kit according to the manufacturer's instructions. The DNA was sequenced by the company SeqLab using 1.5 $\mu$ g plasmid and 30 pmol sequencing primer.

### **2.14.7 Agarose gel electrophoresis and DNA purification**

According to the size of DNA, 1-2% agarose gel was prepared by melting the agarose in TAE buffer using a microwave. Once the solution cooled down to ~45°C, 5-10 µl ethidium bromide was added, mixed and the solution was poured into a gel chamber with the appropriate comb. Once the gel polymerized, the DNA solution mixed with loading buffer was loaded on the gel and run for 30-40 min at 160V. DNA was visualized under UV light. The DNA band of interest was excised from the agarose gel with a scalpel and purified using the QIAquick Gel Extraction Kit (QIAGEN) according to the manufacturer's instructions. The DNA was eluted with sterile water and the concentration was measured using Nanodrop ND-100 Spectrophotometer.

### **2.14.8 RNA isolation**

RNA was isolated using the TRIzol reagent. Tissues were homogenized using 1 ml TRIzol per 50-100 mg tissue sample and centrifuged at 12000g for 10 min at 4°C. 200 µl chloroform was added per 1 ml TRIzol reagent, shaken vigorously for 15 seconds and incubated at room temperature for 2-3 min. The samples were centrifuged at 12000g for 15 min at 4°C. The mixture separated into a lower red phenol-chloroform phase, an interphase and a colorless upper aqueous phase. RNA present in the aqueous phase was transferred into a new tube and 500 µl isopropanol per 1 ml TRIzol was added. The samples were incubated at room temperature for 10 min and centrifuged at 12000g for 10 min at 4°C. The pelleted RNA was washed with 1 ml 75% ethanol per 1 ml TRIzol, mixed thoroughly and centrifuged at 7500g for 5 min at 4°C. The RNA pellet was then dried for 5-10 min, resuspended in RNase-free water and incubated at 60°C for 10-15 min. RNA concentration and quality was determined using Nanodrop ND-100 Spectrophotometer.

### **2.14.9 Reverse transcription**

For reverse transcription, ~1 µg RNA was used. Firstly, the RNA was subjected to DNase digestion in an 11 µl reaction with 1 µl 10x RQ1 DNase buffer, 1 µl RQ1 DNase, RNA and

RNase free-water. The reaction was incubated at 37°C for 30 min. To stop the DNase digestion, 1 µl RQ1 DNase stop solution was added and incubated at 65°C for 10 min. Next, 1 µl random primers and 1 µl dNTP mix was added, the mixture was incubated at 65°C for 5 min and quick chilled on ice. Then, 4 µl 5x First Strand buffer, 2 µl 0.1M DTT and 1 µl RNaseIN were added, mixed gently and incubated at room temperature for 2 min. To this, 1 µl Superscript II reverse transcriptase was added and the samples were sequentially incubated at 25°C for 10 min, 42°C for 50 min and 70°C for 15 min. This produced the cDNA. Finally, any remaining RNA was digested using 1 µl RNase H for 20 min at 37°C.

#### **2.14.10 Real-time PCR**

Real-time PCR was performed using the KAPA SYBR Green Fast reagent with quantification curve method on the StepOne Plus real-time PCR system. A 20 µl reaction with 10 µl 2x KAPA SYBR Fast qPCR mix, 0.4 µl forward primer, 0.4 µl reverse primer. The expression levels of this protein were normalized to the levels of 18S rRNA as the endogenous control.

### **2.15 Cell culture and transfection methods**

#### **2.15.1 Culture and sub-culture**

Human embryonic kidney (HEK) 293 cells and C2C12 myoblasts were cultured in Dulbecco's Modified Eagle's Medium (DMEM) with high glucose of 4.5g/L supplemented with 10% Fetal Bovine Serum (FBS) and 1% Penicillin-Streptomycin-L-Glutamine (PSG) at 37°C in 10% CO<sub>2</sub>. For sub-culturing, confluent cells in 10cm dishes were washed once with 5ml Phosphate Buffered Saline (PBS) and incubated with 1ml Trypsin-EDTA for approximately 2 min to enable detachment of adherent cells. Culture medium containing FBS was added to stop the trypsin activity and cells were seeded at 1:3 ratio for HEK or 1:6 ratio for C2C12 for experiments on the following day.

### 2.15.2 SILAC labelling

For SILAC labelling, cells were cultured in SILAC DMEM medium with high glucose of 4.5 g/L supplied with 10% dialyzed FBS and 1% PSG with either L-Lysine (Lys0) and L-arginine (Arg0), or  $^{13}\text{C}_6$   $^{15}\text{N}_2$ -labeled L-lysine (Lys8) and  $^{13}\text{C}_6$   $^{15}\text{N}_4$ -labeled L-arginine (Arg10). Lysine was used at a concentration of 73.5 g/L and arginine at 28.1 g/L. Cells were passaged for 5 cell doublings for complete labelling.

### 2.15.3 Stocking cells

Cells were trypsinized, pelleted and frozen in 40% DMEM, 50% FBS and 10% dimethyl sulphoxide (DMSO). Cells from a confluent 10cm dish were aliquoted in two cryotubes and frozen initially at  $-80^\circ\text{C}$  overnight. On the following day, frozen stocks were transferred to a liquid nitrogen tank maintained at  $-180^\circ\text{C}$  for longer storage. To recover frozen cells, they were thawed slowly on ice, resuspended in growth medium and pelleted to remove DMSO.

### 2.15.4 Calcium phosphate transfection

HEK293 cells were transfected using calcium phosphate method. To transfect a 10cm dish, 10  $\mu\text{g}$  plasmid was precipitated in 61 $\mu\text{l}$  2M  $\text{CaCl}_2$  and filled up to 500  $\mu\text{l}$  sterile water. This 500  $\mu\text{l}$  solution was added to 500  $\mu\text{l}$  2x HEPES buffered saline (HBS) and mixed thoroughly. The 1 ml transfection mixture was added as drops onto the cells. Cells were processed after 24 hours.

### 2.15.5 Transfection with TurboFect

To transfect C2C12 myoblasts, the TurboFect transfection reagent was used. For a 10cm dish, 10  $\mu\text{g}$  plasmid was diluted in 1 ml reduced-serum Opti-MEM medium. 25  $\mu\text{l}$  TurboFect transfection reagent was then added to this mixture, vortexed thoroughly and incubated at room temperature for 20 min. This transfection mixture was added as drops onto the cells. Cells were processed after 24-30 hours.

### 2.15.6 siRNA transfection

For siRNA transfection of mouse neonatal cardiomyocytes, cells were freshly isolated from P1-P3 pups one day before as described in an earlier section. Cells were cultured in normal growth medium and on the following day washed with antibiotic-free growth medium twice before transfection. For a 12-well plate, 5 µl of 5 µM siRNA (scrambled or siRNA against 2310042D19Rik) was diluted in 95 µl serum-free DMEM. In another tube, 3.6 µl DharmaFECT 2 transfection reagent was diluted in 96.4 µl serum-free DMEM. The tubes were left at room temperature for 5 min and then mixed together and incubated for 20 min. Then 800 µl serum containing DMEM was added (making a final siRNA concentration of 25nM) and the total 1 ml transfection medium was added to each well after removing the cell culture medium. Cells were incubated at 37°C in 10% CO<sub>2</sub> for 48 hours and proteins were analysed.

### 2.15.7 Treating cells with inhibitors

Inhibitors were typically administered to cells 24h post transfection, after replacing the transfection medium with fresh growth medium. MG-132 was used at a final concentration of 10 µM and treated for 4 hours. TBB was used at 50 µM concentration and administered for 4 hours. Cycloheximide was used at a final concentration of 20 µg/ml and treated for specific time periods. For control cells without inhibitor treatment, 5 µl DMSO was added as control.

## 2.16 Biochemistry methods

### 2.16.1 Immunoprecipitation

Cells or tissues were lysed in RIPA buffer containing protease inhibitors by incubation on a rotating wheel at 4°C for 30 min. Crude extracts were clarified by centrifugation and protein concentration was measured using the *DC* protein assay. Typically, 1 mg protein lysate was used for immunoprecipitation. 30 µl Sepharose G beads were added to the protein lysate and incubated on a rotating wheel at 4°C for 30 min as a pre-clearing step. Beads were

pelleted by centrifugation at 2000g for 2 min at 4°C and supernatant was incubated with 5-7 µg antibody on a rotating wheel at 4°C for 1h. Finally, fresh 30 µl Sepharose G beads were added and incubated overnight on rotating wheel at 4°C. In case of antibody coupled to beads, this was added directly after the pre-clearing step. On the following day, proteins bound to beads were washed 4 times with RIPA buffer by centrifugation at 2000g for 2 min at 4°C. After washing, proteins were eluted from the beads by boiling with 1.5x Laemmli buffer and 40mM DTT at 70°C for 10 min.

### **2.16.2 Immunoblotting**

Either eluted immunoprecipitate or 20 µg proteins (boiled with 1.5x LDS buffer and 40mM DTT at 70°C for 10 min) were loaded onto 4-12% Bis-Tris gel and SDS-PAGE was performed using MOPS buffer at 175V. Proteins from the gel were then transferred to a nitrocellulose membrane sandwiched between two Whatman papers using transfer buffer at 35V for 2 hours. Water with ice was added to the outer chamber to maintain the system cold. The membrane was then stained with Red Alert for 5 min on a shaker and then washed with Milli-Q water to observe the protein bands. The staining was completely removed by washing with TBS-T buffer and the membrane was blocked with 5% BSA or 5% non-fat dry milk in TBS-T for 1h at room temperature on a shaker. Blocked membrane was incubated with primary antibody diluted in blocking buffer overnight at 4°C with gentle shaking. On the following day, membrane was washed 5 times for 5 min with TBS-T with rigorous shaking and then incubated with horseradish peroxidase-coupled secondary antibody diluted in blocking buffer for 1h room temperature with gentle shaking. Finally, the membrane was washed 5 times for 5 min with TBS-T with rigorous shaking. Proteins in the blot were detected on a VersaDoc using enhanced chemiluminescence method with a 1:1 mixture of peroxide solution and luminol enhancer.

### **2.16.3 Subcellular fractionation**

Isolation of mitochondria from tissues was performed as described earlier [156]. Heart tissue was minced finely in ice-cold Mito Isolation Buffer A and washed to remove blood. Tissues



were homogenized with 8-10 strokes of a tight fitting Teflon/glass pestle. The homogenate was centrifuged at 1000g for 10 min at 4°C to pellet the debris. The supernatant was centrifuged at 12000g for 15 min at 4°C to pellet the crude mitochondria, cytosolic fraction being in the supernatant. Cytosolic proteins were precipitated using acetone and the mitochondrial pellet was washed with Mito Isolation Buffer A and 1mM PMSF, centrifuged at 12000g for 5 min at 4°C. The mitochondrial pellet was resuspended in Mito Isolation Buffer B with 1mM PMSF and protein concentration was determined by lysing a small aliquot.

#### **2.16.4 Submitochondrial fractionation**

To separate membrane and soluble mitochondrial fractions, the carbonate procedure was used [157]. Mouse heart mitochondria were solubilized in 100mM Na<sub>2</sub>CO<sub>3</sub>, pH 11.5 for 30 min on ice and ultracentrifuged at 50,000 rpm for 1 hour at 4°C. The pellet consisted of the membrane fraction and the soluble proteins in the supernatant were precipitated using 10% Trichloroacetic acid.

For submitochondrial localization of mitochondria, swelling experiments combined with proteinase K treatment were performed [158]. 200µg freshly isolated mitochondria were used per condition. For osmotic shock, mitochondria were incubated in 10mM Tris/HCl pH 7.6, 1mM EDTA for 15 min on ice. For proteinase K treatment, mitochondria were resuspended in 250mM sucrose, 10mM Tris/HCl pH 7.6, 1mM EDTA and incubated with 1 µg proteinase K for 5 min on ice. For detergent solubilization, mitochondria were treated with Triton-X at a final concentration of 1% for 10 min on ice.

#### **2.16.5 In vitro kinase assay**

For *in vitro* kinase assay, HEK293T cells were transfected with Flag-tagged Mic85. After 30h, cells were starved overnight and Mic85 was immunoprecipitated using anti-Flag M2 affinity gel. Constitutively active Casein Kinase II (CK2) was incubated with the immunoprecipitate in the presence of CK2 buffer, 10 µM cold ATP, 5 µCi γ<sup>32</sup>-ATP for 1h at 30°C. Casein Kinase I (CK1) and IKK were used as controls. The reaction was stopped using 4x Laemmli buffer and

boiling for 5 min at 95°C. Samples were separated using SDS-PAGE, the gel was dried and exposed to an X-ray film.

## **2.17 Immunostaining methods**

### **2.17.1 Immunofluorescence**

C2C12 cells were transfected with Flag-tagged Mic85 and GFP-tagged Omp25 [159] for 24h, fixed with 4% paraformaldehyde for 10 minutes, permeabilized with 0.1% Triton X-100 in PBS for 10 minutes and stained with anti-Flag antibody for 1-2 hours at room temperature. Alexa dye conjugated secondary antibodies were incubated for 1 hour at room temperature. GFP fluorescence was used for visualization of mitochondria. The coverslips were mounted in Mowiol 4-88 Reagent. Confocal imaging was performed with a Zeiss LSM700 confocal microscope using the ZEN2011 software.

Neonatal cardiomyocytes were cultured on Nunc Lab-Tek II 8-chamber slide, transfected as described in section 2.14.6, fixed with 4% paraformaldehyde for 20 minutes, permeabilized with 0.05% Triton X-100 for 15 min and stained using anti-Tom20 and anti-sarcomeric  $\alpha$ -actinin antibodies. The cover slips were mounted in Mowiol 4-88 reagent and confocal imaging was performed on TCS SP8 confocal microscope (Leica microsystems) using the LASX software.

### **2.17.2 Immunohistochemistry**

Human heart sections were fixed in 4% paraformaldehyde for 15 min, permeabilized in 0.05% Triton X-100 for 20 min followed by incubation of corresponding primary antibodies overnight. Anti-c1orf170 was used to stain Mic85 and mouse Tom20 was used to stain mitochondria. Images were captured on a Leica TCS laser confocal microscope with corresponding filters.

## 2.18 Human heart tissues

For immunoprecipitation and immunohistochemistry analysis of human samples, we used myocardial tissues from five individuals who underwent subvalvular myectomy during surgical aortic valve replacement which served as control samples in a previous study [160]. These samples showed preserved cardiac function (ejection fraction  $\geq 60\%$ ), and the resected myocardial tissue did not show any signs of myocardial hypertrophy or ischemic damage. The study was approved by the ethics committee of the Medical Council of the State of Hessen. Informed consent was obtained from patients complying with the requirements of the Medical Council and institutional ethics guidelines of the Kerckhoff Hospital, Bad Nauheim, Germany.

## 2.19 Metabolic assay – oxygen consumption rate

Oxygen consumption rate was measured using XFe96 Extracellular Flux Analyzer (Seahorse Bioscience) according to the manufacturer's instructions. Neonatal cardiomyocytes were seeded at 70,000 cells/well in XFe96 culture plate after coating the plate with fibronectin solution and then subjected to siRNA knockdown. The concentrations of mitochondrial drugs used were 1.5 $\mu$ M Oligomycin A, 0.5  $\mu$ M carbonyl cyanide 4-(trifluoromethoxy) phenylhydrazone (FCCP), 0.75  $\mu$ M Antimycin A and 0.75  $\mu$ M Rotenone.

## 3. Results

### 3.1 Proteome-wide mapping of phosphorylation sites and quantitative analysis of post-natal heart development

To gain a deep insight into phosphoproteome regulation and changes in protein levels during early post-natal heart development, we employed a combination of spike-in SILAC quantification and high resolution LC-MS/MS analysis using a quadrupole Orbitrap mass spectrometer. We isolated hearts from non-labelled P2, P10 and P20 mice and pooled multiple hearts from each time point to obtain sufficient material for phosphopeptide enrichment. As a spike-in standard we used a pool of age-matched hearts from Lys6 ( $^{13}\text{C}_6$ -Lysine) labelled SILAC mice. Lys6 labelled and non-labelled proteins were mixed equally and part of the lysates (40  $\mu\text{g}$  per sample) was separated by SDS-PAGE gel electrophoresis and in-gel digested with LysC. LysC was used for proteolytic digestion so that all the generated peptides contain lysine (in case of non-labelled proteins) or  $^{13}\text{C}_6$ -Lysine (in case of SILAC labelled proteins), thus enabling quantification of all peptide pairs. To enrich for phosphorylated peptides, ~15 mg of heart lysates from labelled and non-labelled heart tissue were digested with LysC and subsequently by trypsin (for proteins undigested by LysC) using filter aided sample preparation. The arginine containing peptides obtained from tryptic digestion could not be quantified, however this approach led to an increased number of identified phosphorylation sites. Each sample was fractionated using strong cation exchange chromatography to yield flow through and 8-10 fractions. The flow through and early fractions contained mainly phosphorylated peptides. Each sample obtained from SCX chromatography was then subjected to sequential enrichment using  $\text{TiO}_2$  beads to enrich for phosphorylated peptides. The flow through was extracted three times with 5mg  $\text{TiO}_2$  beads and the fractions were extracted twice with 2mg  $\text{TiO}_2$  beads. Finally, phosphopeptides were eluted from the beads using an alkaline buffer ( $\text{pH}>11$ ) and subjected to LC-MS/MS analysis (Fig. 12). These experiments were done in biological duplicates and analysed in 72 LC-MS/MS runs for the proteome and 81 LC-MS/MS runs for phosphoproteome, all on 2.5 h long

chromatographic gradients. The raw files obtained from the Q Exactive mass spectrometer were analysed using MaxQuant.

In total, we identified 21,261 phosphorylation sites mapped to 5,102 proteins. Out of these, 16,593 sites (78%) had a localization probability of 0.75 or higher and were classified as Class

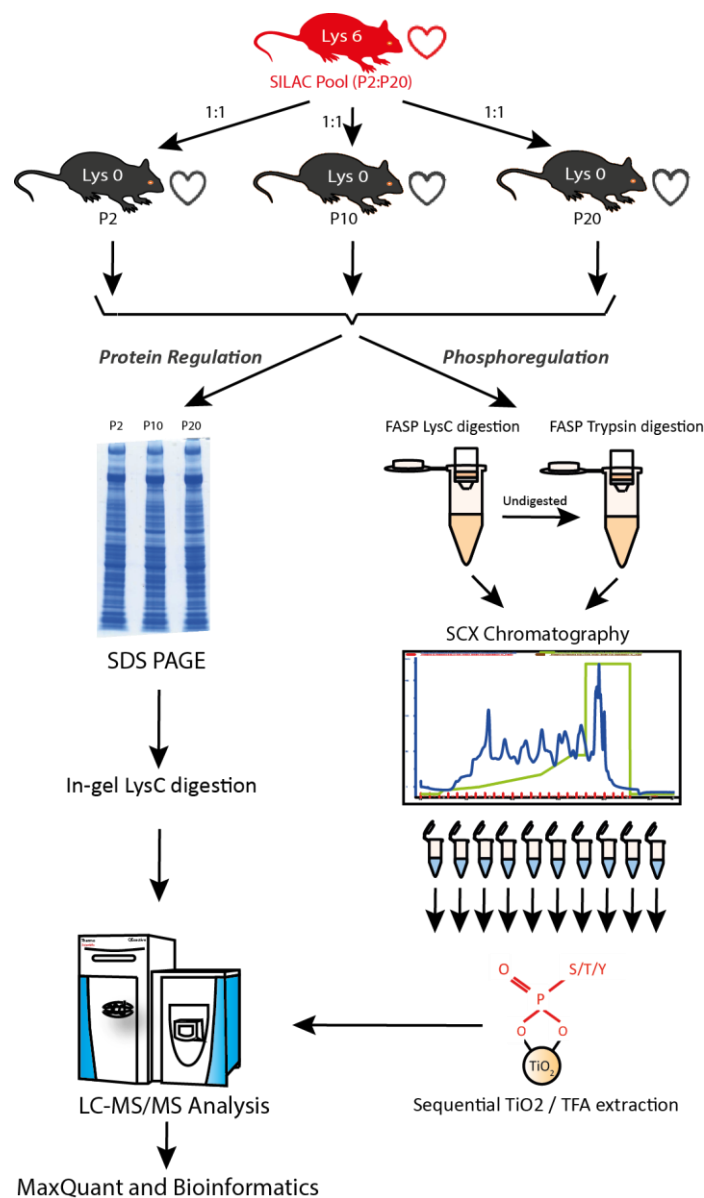


**Figure 12. Schematic experimental workflow for proteome-wide mapping of phosphorylation sites.** Heart tissues were isolated from wild type and SILAC mice, lysed and mixed in a 1:1 ratio. For whole proteome analysis, proteins were separated using SDS PAGE and in-gel digested. For phosphopeptide enrichment, proteins were digested using LysC followed by Trypsin (for undigested proteins). Peptides were separated using SCX chromatography and enriched with TiO<sub>2</sub> beads. Modified and unmodified peptides were subjected to LC-MS/MS analysis on the high-resolution Q Exactive mass spectrometer. Raw files were analysed using MaxQuant.

1 sites. Among all phosphopeptides we identified 84.8% (18,033) to be serine phosphorylated, 14.7% (3130) to be threonine phosphorylated and 0.5% (98) to be tyrosine phosphorylated (Fig. 13A). Notably, 4276 sites were newly identified in our study and not present in publicly available databases [26, 161] (Fig. 13B). Our measurement of the proteome revealed 8985 proteins across all three post-natal time points. Principal Component Analysis showed high similarity among the duplicates of a group. In contrast, the components of different groups were clearly separated showing high differential regulation of proteins between the time points (Fig. 13C). Moreover, 4133 proteins were identified simultaneously at all the three time points indicating that ~50% of the proteome is expressed during P2 and P20 (Fig. 13D). Andromeda score distribution of phosphorylated and unmodified peptides is shown in (Fig. 13E) and the biological duplicates of proteome analysis revealed a Pearson correlation coefficient being greater than 0.8 in all experiments (Fig. 13F).

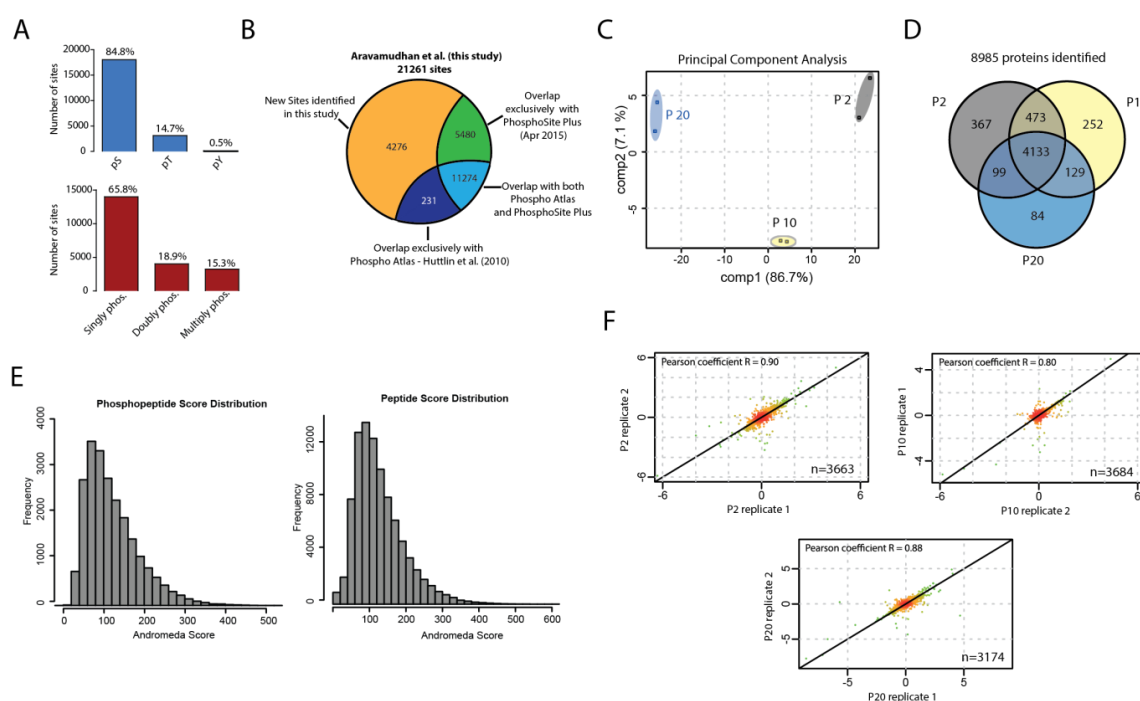


**Figure 13. Phosphoproteomics profiling of post-natal heart development.** (A) Distribution of STY sites and their multiplicity. (B) Overlap of identified phosphorylation sites with PhosphoSite Plus database and mouse phosphorylation atlas showing newly identified sites. (C) Principal component analysis showing high similarity among duplicates and differential regulation of proteins between time points. (D) Venn diagram showing overlap of identified proteins in all time points. (E) Histograms showing the Andromeda score distribution for phosphopeptides and unmodified peptides. (F) Pearson correlation plots of the biological replicates for proteome quantification in P2, P10 and P20.

Due to our parallel measurement of more than 21,000 phosphorylation sites and 9000 proteins, we could investigate a possible correlation between the abundance of a protein and its extent of phosphorylation. Fig. 14A represents a histogram of the frequency of proteins showing a certain degree of phosphorylation. Fig. 14B shows a density scatter plot between protein abundance and number of phosphorylation sites per protein. Examining the distribution of phosphorylated sites per protein, we found a weak but significant tendency (Pearson correlation 0.19,  $p$ -value $<10^{-16}$ ) that highly abundant proteins are more phosphorylated (Fig. 14A and 14B), which is in agreement with a previous study [155].

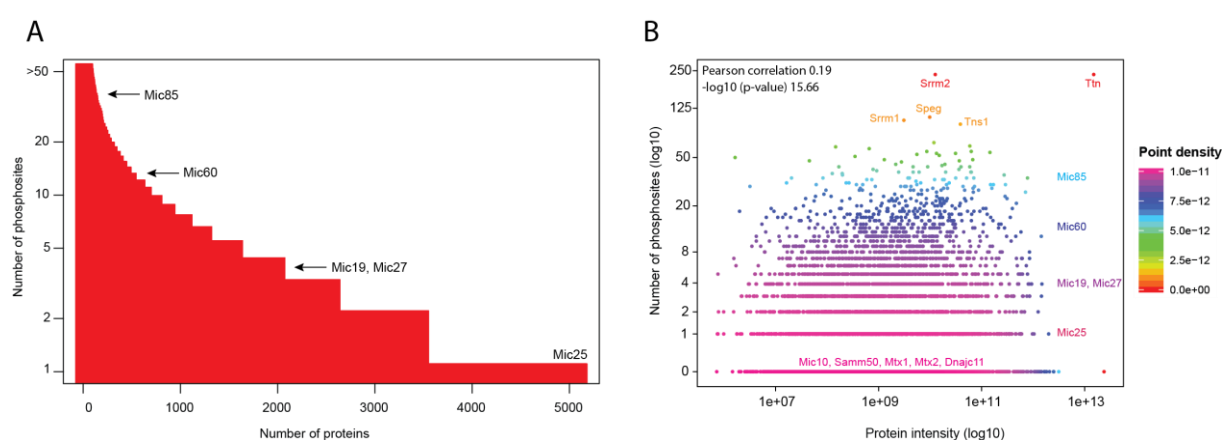


**Figure 14. Overview of phosphorylation sites per protein.** (A) Histogram showing the distribution of phosphoproteins based on number of phosphorylation sites per protein. (B) Density scatterplot between number of phosphorylation sites per protein and protein abundance (colour code depicts the amount of points included in a region of a specific colour).

To identify regulated proteins and phosphopeptides, we filtered our data by fold-change  $\geq 1.5$ -fold, t-test  $p < 0.05$ , and FDR  $< 0.01$  as significantly regulated proteins and phosphorylation sites (Fig. 15A and 15B) at P2 and P20 with respect to P10. To exclude that changes in the abundance of phosphorylation events are due to differential protein expression, we normalized the ratios obtained for phosphorylated peptides against the corresponding parental protein SILAC ratios. As shown in Fig. 15C, phosphorylated Naca, a regulator of protein synthesis is upregulated at P20 compared to P10 while the unmodified protein is unchanged, demonstrating an increase of phosphorylation at position pS524. Conversely, the RNA binding factor Igf2bp3 is equally regulated at the protein and phosphorylation level excluding a relative increase of phosphorylation of Igf2bp3 at position pS184 during development (Fig. 15D). In total we normalized 3413 out of 4620 quantified sites at P2 to protein levels; 5104 out of 7098 quantified sites at P10 to protein levels and

4779 out of 6940 quantified sites at P20 to protein levels. On performing a t-test analysis with normalized phosphorylation ratios in both the biological replicates, we were able to identify 77 and 232 significantly regulated phosphopeptides at P2 and P20, respectively, with reference to P10 (Fig. 15A). In case of total proteome, we quantified 5083 proteins at P2, 5000 proteins at P10 and 4454 proteins at P20. Upon t-test analysis with quantified protein ratios in both biological replicates, we identified 378 and 745 significantly regulated proteins at P2 and P20, respectively, with reference to P10 (Fig. 15B).

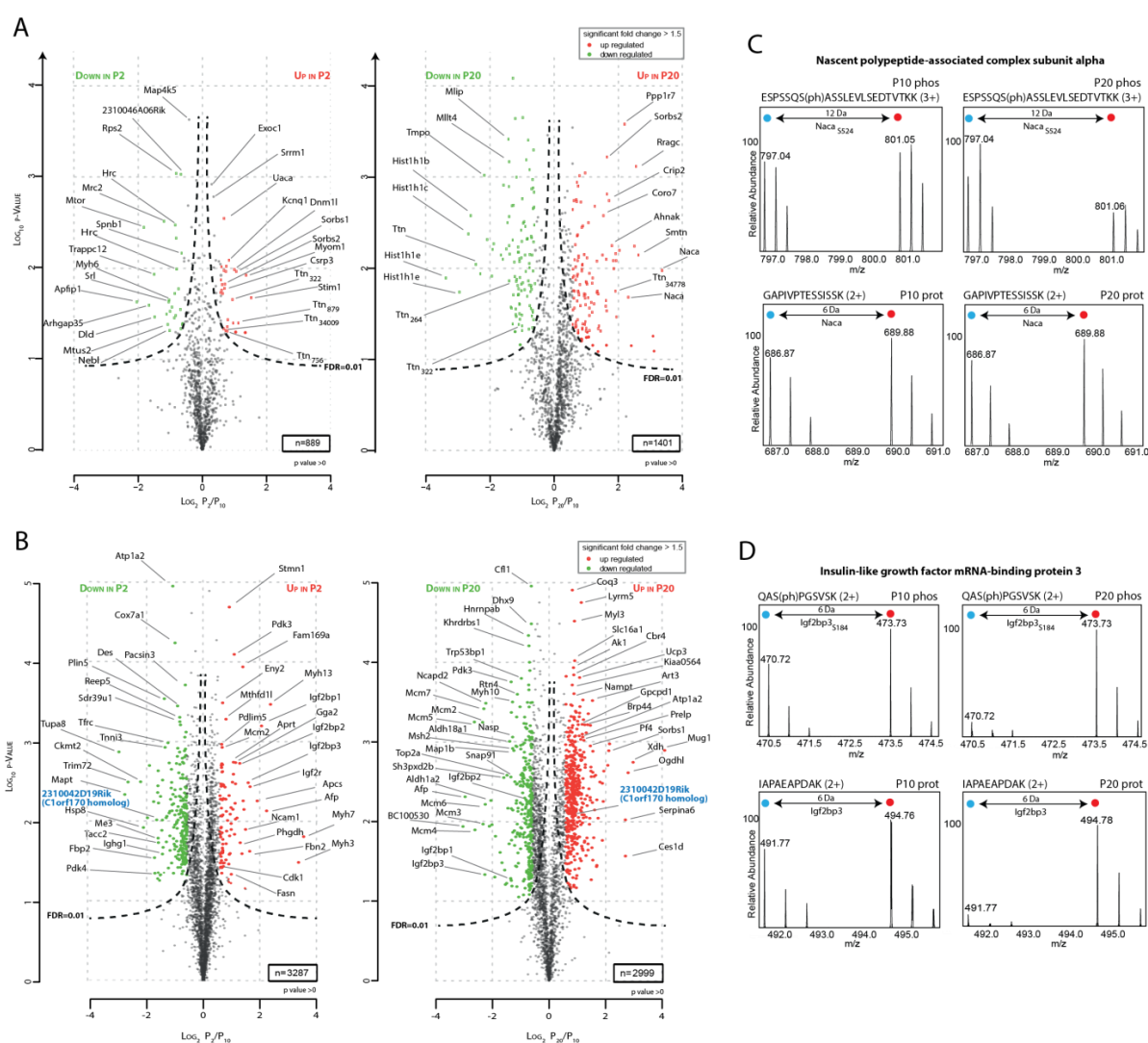


**Figure 15. Integrative quantification of proteins and phosphopeptides.** (A) Volcano plots depicting significantly regulated phosphorylation at P2 and P10 with respect to P20 ( $n=2$ ,  $p<0.05$ ). FDR curve was drawn at a cut-off of 0.01. (B) Volcano plots depicting significantly regulated proteins at P2 and P10 with respect to P20 ( $n=2$ ,  $p<0.05$ ). FDR curve was drawn at a cut-off of 0.01. (C) MS spectra of a phosphorylated and an unmodified peptide of Naca at P10 and P20 showing upregulation of phosphorylation but no change in protein level. (D) MS spectra of a phosphorylated and an unmodified peptide of Igf2bp3 at P10 and P20 showing the importance of normalizing phosphorylation ratios to protein abundance.



### 3.2 Cluster analysis reveals reduced phosphorylation of CDK1/2 substrates after P10

We performed clustering to identify groups of proteins with a similar expression pattern during heart development. All SILAC ratios were z-score normalized before clustering. Z-score or standard score is the number of standard deviations a value is from the mean. Thus, a positive z-score indicates a value above the mean, while a negative score indicates a value below the mean. Z-score normalized ratios were obtained by subtracting the population mean from an individual ratio value and dividing this difference by the standard deviation. K-means clustering was then used to partition these normalized phosphorylation ratios into 9 clusters, in which each ratio belonged to the cluster with the nearest mean, meaning that proteins with similar phosphorylation profiles were grouped in the same cluster (Fig. 16A). Although we found diverse classes of phosphorylation sites assigned to different clusters, the cluster “Unchanged Down” revealed several phosphorylation sites on histones, which were not changed between P2 to P10 but clearly downregulated after P10, the time point of cell cycle arrest and initiation of cellular hypertrophy.

Since modifications on histones are important regulators of cell cycle progression, we focused on the regulation of potential substrates of the cell cycle regulatory kinases CDK1 and CDK2 (Fig. 16B). We observed that the majority of the CDK1/CKD2 substrates showed unchanged phosphorylation from P2 to P10 followed by a clear downregulation (>2 fold change) at P20. Furthermore, a strong preference of proline at position +1 and lysine and arginine at positions +2 and +3 of the phosphorylated site shown by sequence motif analysis (Fig. 16B) indicate phosphorylation by CDK1/2 kinases [162]. We also observed a profound phosphorylation on histones H1.2, H1.4 and H1.5, which was downregulated more than 5-fold at P20. Since phosphorylation on histone H1 has been observed to be at its peak during mitosis [163], such a regulatory pattern might have a negative effect on mitotic progression after P10. It is noteworthy that phosphorylation of the majority of substrates of cell cycle regulatory kinases was highly different before and after 10 days of birth.

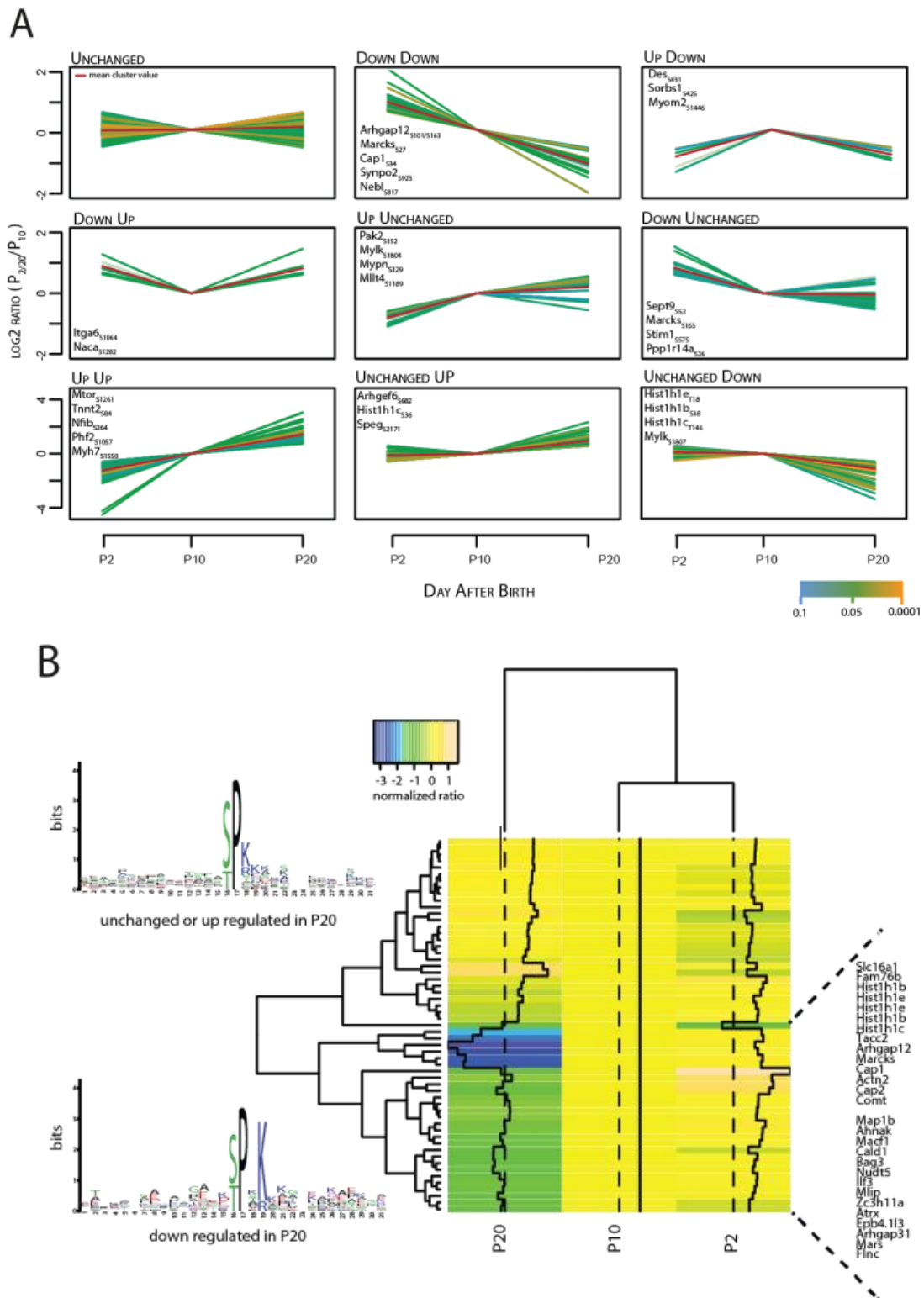
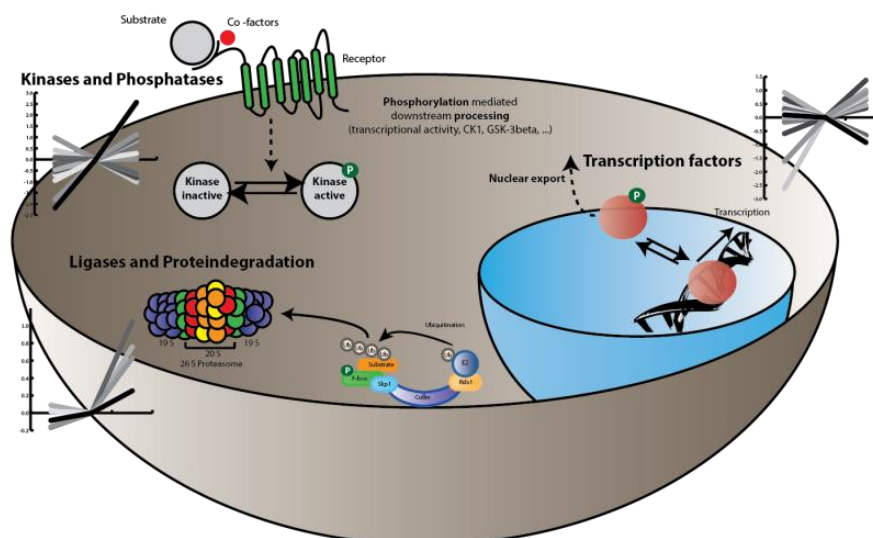


**Figure 16. Cluster analysis shows reduced phosphorylation of CDK1/2 substrates after P10. (A) Nine clusters showing the regulation of phosphorylation between P2, P10 and P20. Ratios at P2 and P20 are normalized to P10. (B) Heat map depicting the phosphorylation status of CDK1/2 substrates at P2 and P20 with respect to P10. Sequence logos show the differential preference of residues in the neighborhood of the phosphorylated residue between upregulated and downregulated sites at P20.**

### 3.3 Key molecular players: kinases, phosphatases, transcription factors and ubiquitin ligases



Gene name	Phosphosite	log <sub>2</sub> (P2/P10)	-log <sub>10</sub> p-value P2/P10	log <sub>2</sub> (P20/P10)	-log <sub>10</sub> p-value P20/P10	Functional annotation
Prkab1	108	-0.475	1.508	1.020	1.345	Hypertrophic cardiomyopathy (HCM)
Prkab2	107	-0.546	1.051	0.952	1.718	Hypertrophic cardiomyopathy (HCM)
Ppip5k2	1005	-0.213	1.077	-0.625	1.434	InsP6 and PP-IP5 kinase 2
Spag9	586	0.082	0.183	1.027	1.840	JUN kinase binding
Pak2	152	-0.691	0.000	0.277	1.701	MAPK signaling pathway
Rras2	186	-0.080	0.616	-0.645	2.882	MAPK signaling pathway
Mtor	1261	-1.803	2.447	1.112	1.946	mTOR signaling pathway
Mylk	1807	0.418	1.804	-1.009	1.827	Myosin light chain phosphorylation, Vascular smooth muscle contraction
Mylk3	432	-0.161	0.323	-1.053	1.900	Myosin light chain phosphorylation, Vascular smooth muscle contraction
Rragc	381	-2.190	0.000	2.572	3.116	positive regulation of TOR signaling cascade
Murc	334	0.071	0.145	0.721	2.730	Rho/ROCK signaling pathway
Prkcd	662	-0.528	0.000	0.738	1.913	Vascular smooth muscle contraction
Ppp1r14a	26	0.977	1.400	0.019	0.000	Vascular smooth muscle contraction
Ppp1r12a	299	-0.121	0.000	-0.823	1.692	Vascular smooth muscle contraction
Tbc1d5	546	-0.944	0.000	2.514	2.241	Vascular smooth muscle contraction
Speg	316	0.145	0.000	0.881	1.195	

Gene name	Phosphosite	log <sub>2</sub> (P2/P10)	-log <sub>10</sub> p-value P2/P10	log <sub>2</sub> (P20/P10)	-log <sub>10</sub> p-value P20/P10	Functional annotation
Actn2	237	0.174	0.554	-0.815	2.325	Arrhythmogenic right ventricular cardiomyopathy (ARVC), Regulation of actin cytoskeleton
Atrx	315	0.095	0.471	-0.922	2.511	Modifies gene expression by affecting chromatin
Atrx	590	0.321	0.738	-0.657	1.138	Modifies gene expression by affecting chromatin
Cnot3	299	0.240	0.662	-0.667	0.562	RNA degradation
Jup	54	-0.179	0.109	0.657	0.476	
Mkl2	77	-2.616	0.794	0.361	0.272	positive regulation of striated muscle tissue development
Naca	1489	-0.008	0.008	0.986	1.129	
Nfib	264	-0.595	0.522	1.370	1.084	CCAAT-box-binding transcription factor
Phf2	1057	-1.617	0.545	0.892	1.341	Phosphorylated by PKA

Gene name	Phosphosite	log <sub>2</sub> (P2/P10)	-log <sub>10</sub> p-value P2/P10	log <sub>2</sub> (P20/P10)	-log <sub>10</sub> p-value P20/P10	Functional annotation
Trip12	1049	-0.085	2.113	0.254	2.420	ubiquitin fusion degradation (UFD) pathway
Stub1	20	0.019	0.040	0.310	2.289	Protein processing in endoplasmic reticulum; Ubiquitin mediated proteolysis
Hectd1	632	-0.157	0.000	0.630	1.913	U3 ubiquitin ligase
Ube2o	836	-0.165	0.000	1.046	1.827	Ubiquitin mediated proteolysis
Ube2o	893	0.089	0.245	0.759	1.747	Ubiquitin mediated proteolysis

**Figure 17. Key molecular players.** Phosphoregulation of kinases, phosphatases, transcription factors and ubiquitin ligases at P2 and P20 with respect to P10. Phosphorylated sites with a p-value <0.05 in at least one of the time intervals are represented. Upregulated ratios are highlighted in green and downregulated ratios are highlighted in red.

We screened for key molecular players which show a differential phosphoregulation between the different stages of development (Fig. 17) and we report here selected phosphorylated sites, phosphopeptide ratios and the p-value for the regulated kinases, phosphatases, transcription factors, and ubiquitin ligases identified in this study. We observed a median phosphoregulation of kinases to be upregulated during development. In addition, the signaling molecule mTOR and the positive regulator of mTOR pathway, Ras-related GTP-binding protein C (Rragc), show a significant 2-fold upregulated phosphorylation during the developmental time points. A similar trend is observed for the Protein Kinase C delta type, with a 1.5-fold upregulation. Conversely, the phosphorylation of MAPK signalling pathway component Rras2 remains unchanged from P2 to P10 but is 1.5-fold downregulated at P20. Similarly, the cardiomyocyte-specific Mylk3 and the Mylk, which are responsible for myosin light chain phosphorylation, are 2-fold less phosphorylated at P20. While the kinases seem to be overall upregulated during development, the phosphatases Ppp1r14a and Ppp1r12a show a downregulation of phosphorylation from P2 to P20. It is striking to observe that several of the low abundant transcription factors were identified and quantified in this study. The global transcriptional regulator Atrx and Cnot3 show unchanged phosphorylation upto P10 but a downregulation at P20. However, we see an opposite trend for Nfib and Naca which are more phosphorylated at P20. The components involved in ubiquitin-mediated proteolysis are more phosphorylated after P10. All of the molecules indicated in Figure 17, Trip12, Stub1, Hectd1 and Ube2o show a highly significant upregulation of phosphorylation during the interval P10 to P20. Understanding the phosphoregulation of such key signalling molecules is valuable for the research communities working on cardiac development at the molecular level. Our approach is sensitive enough to detect low abundant transcription factors and their phosphorylation status.

### **3.4 Titin is dynamically phosphorylated during heart development**

Titin is a major sarcomeric protein which is crucial for the assembly and function of striated muscles. Phosphorylation of titin in various domains is important for the regulation of muscle growth and myocardial stiffness. We identified 233 phosphorylated sites on Titin (of which 85 sites were newly identified in this study), showing that it is a highly phosphorylated

protein, and about 50 sites quantified among all the three time points. A schematic view of the major domains of titin, a scatter plot and line graph showing the regulation of corresponding sites is illustrated in Fig.18 and 18B.

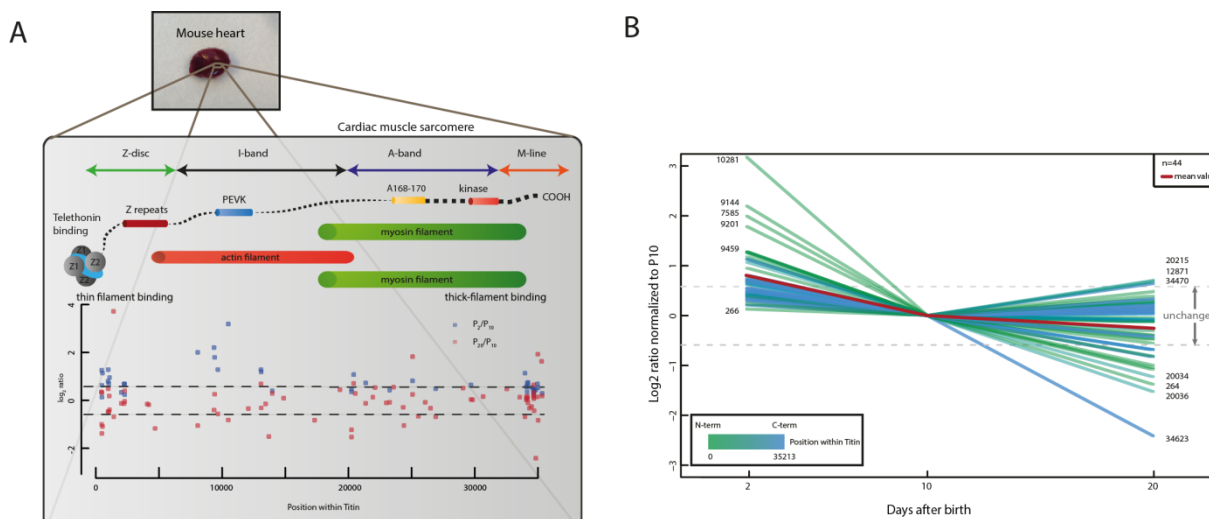


**Figure 18. Phosphorylation of titin during heart development.** (A) Schematic map of the various domains of titin and scatter plot showing the regulation of all the phosphorylated sites quantified in titin. (B) Line graph depicting the regulation of phosphorylated sites in titin with a colour code representing the position of the site within the protein. Red line shows the mean regulation.

Biochemical studies have shown that the titin-cap protein telethonin in conjugation with titin Z1Z2 (a sensor complex at the N-terminal region of titin formed from two IgG domains Z1 and Z2 which are anchored by telethonin) is involved in the progression of muscle growth [164]. We identified S132 to be phosphorylated in the Z1Z2 domain which allows interaction with telethonin [164]. On the other hand, it is shown that phosphorylation on PEVK domain increases titin stiffness [165]. We found S10165, S10281 and S11866 to be phosphorylated in the PEVK domain. Notably, we found S10281 within the PEVK domain being 8-fold less phosphorylated at P10 compared to P2 and further 2-fold downregulated at P20. Strikingly, we also identified two sites in the kinase domain to be phosphorylated- S33086 and S33128. In addition, we observed several phosphorylated sites in the part of titin that localizes to the Z-disk and M-line, which might affect titin's ability to bind to adjacent proteins. In summary, our results revealed strong changes in the phosphorylation status of titin during heart development, which will regulate its activity and protein-protein interaction dynamics.

Moreover, the detailed knowledge of phosphorylation profiles on titin will help to decipher pathobiology during cardiac diseases [166].

### 3.5 Mic85 is up-regulated during heart development and interacts with components of mitochondrial contact site (MICOS) complex

The analysis of gene expression profiles via deep sequencing is a powerful tool to monitor nearly all gene activities in complex biological samples. Cardiomyocytes undergo transition from hyperplasia to hypertrophy after birth, a process known as developmental cardiac hypertrophy. This is characterized by upregulation of mitochondrial biogenesis and increase in mitochondrial mass, morphological changes including increase in myofibril density and mature intercalated discs due to cell differentiation [43]. Recently, a global expression profiling of developing heart tissue revealed a common up regulation of sarcomeric and mitochondrial proteins after birth [167]. Likewise, our quantitative proteomics study showed a clear up-regulation of those compartments, as shown by the Fisher Exact test indicating the enrichment factor and p-value of upregulated gene ontology terms from P10 to P20 (Fig. 19).

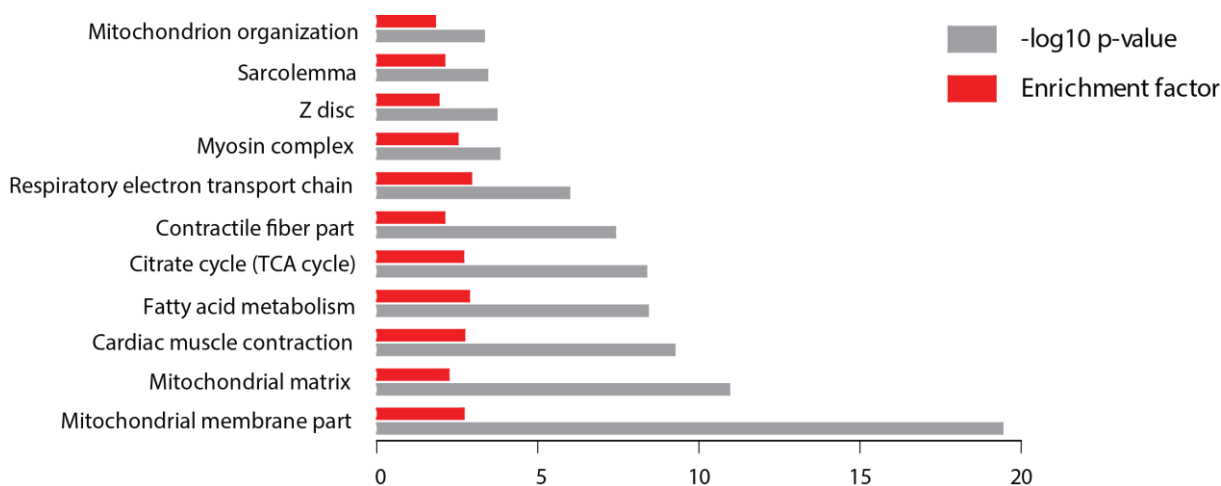


**Figure 19. Enrichment of gene ontology terms upregulated during heart development.** Fischer Exact test showing enrichment factor and p-value of upregulated gene ontology terms from P10 to P20.

The protein Perm1 (Peroxisome proliferator – activated receptor  $\gamma$  coactivator 1 and Estrogen related receptor – induced regulator in muscle 1) [168] raised our particular attention since Perm1 showed a strong up regulation during early heart development (Fig 20A). Interestingly, we found 39 phosphorylation sites in Perm1, including 28 newly identified sites (Fig. 20C). Since we found that this protein is associated with the MICOS

complex (see below), we renamed Perm1 as MICOS complex subunit Mic85, according to its mass of 85 kDa. Among the known MICOS complex-associated proteins, Mic85 showed the highest degree of phosphorylation (Fig. 14A and 14B). Mic85 was strongly up regulated with a  $\sim 3$ -fold increase from P2 to P10 and further with a  $\sim 2$ -fold increase from P10 to P20 ( $p < 0.05$ ), as shown by the MS spectra, line graph and western blot analysis (Fig. 20A and 20B). Protein sequence analysis indicated the presence of two nuclear localization signals, a PEST motif (rich in P, E, S, T amino acids) and several cysteine residues, including two C-terminal CX<sub>13</sub>C motifs (Fig. 20C) [169] [170].

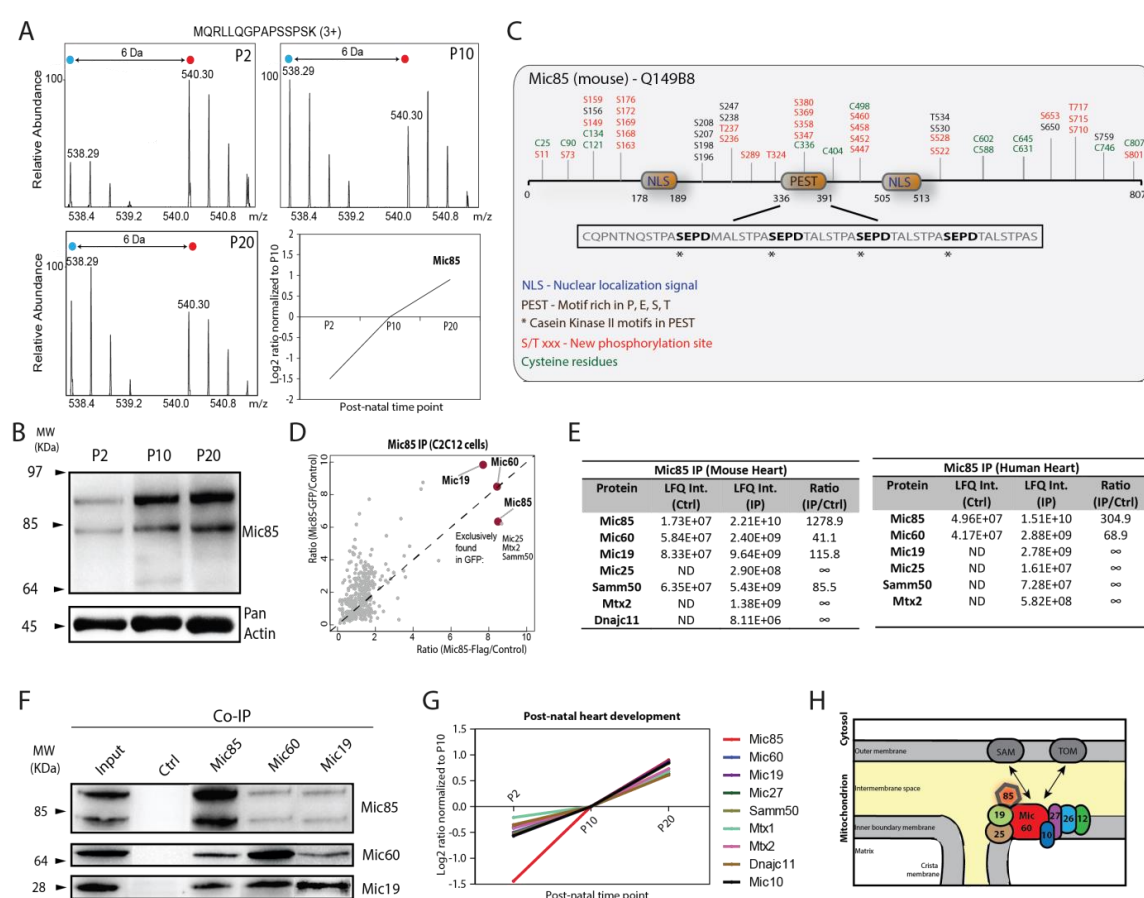


**Figure 20. Mic85 is upregulated during heart development and interacts with the mitochondrial MICOS complex.** (A) MS spectra, line graph and (B) western blot depicting the upregulation of Mic85 from P2 through P20. (C) Sequence landscape of Mic85 indicating nuclear localization signals, casein kinase 2 motifs on the PEST domain, cysteine residues and phosphorylation sites identified. (D) Scatter plot comparing the SILAC ratios of the interaction partners of Flag and GFP tagged Mic85 overexpressed in SILAC-labelled C2C12 myoblasts normalized to the controls, analysed using LC-MS/MS. (E) Interactome screening of endogenous Mic85 in mouse heart and human heart using LC-MS/MS and label-free protein quantification. ND=not detected. (F) Western blot showing the interaction of Mic60 and Mic19 with endogenous Mic85 in mouse heart. (G) Line graph showing the upregulation of Mic85 and other MICOS-associated proteins during heart development. (H) Updated model of MICOS complex indicating Mic85 as a new member.

Next, we performed quantitative RT-PCR to study the endogenous expression of Mic85 in developing embryos and adult mouse tissues. Mic85 showed the highest expression in the heart followed by skeletal muscle and only a weak expression in other tissues (Fig. 21), indicating a specific function in contractile and mitochondrial rich tissues.

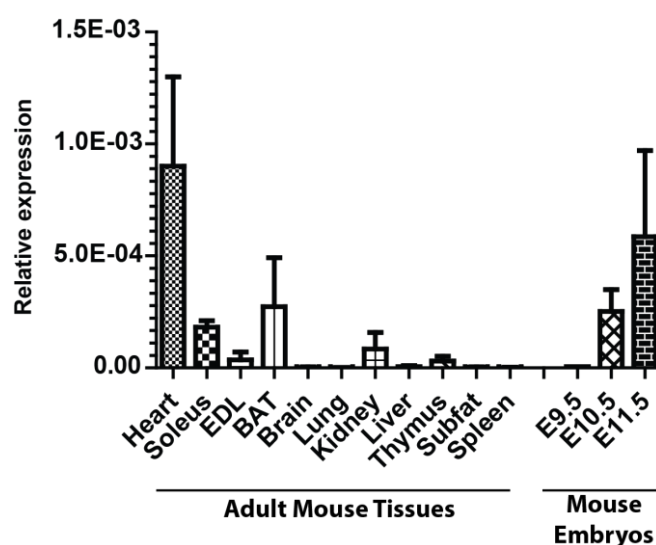


**Figure 21. Tissue-wide expression of Mic85.** Real-time PCR analysis depicting the expression of Mic85 in various adult mouse tissues as well as developing embryos relative to the expression of 18srRNA.

To gain a better insight into the biological function of Mic85, we performed co-immunoprecipitation to identify its interaction partners. To generate expression constructs for Mic85, the FANTOM Riken cDNA clone for the mouse gene 2310042D19Rik was purchased from Source Bioscience and was used as template for Phusion polymerase based PCR amplification by introducing the restriction sites KpnI (5') and XhoI (3') flanking the coding sequence of Mic85. Since Phusion polymerase results in amplification of blunt end fragments, the PCR product was subjected to A-tailing and then ligated into pGEM-T Easy plasmid. The coding sequence of Mic85 was then subcloned into pcDNA5/TO vector containing either a C-terminal Flag or GFP tag using KpnI and XhoI as the restriction enzymes. For accurate quantification, C2C12 cells were SILAC labelled (heavy lysine and arginine) and were transfected with Flag and GFP tagged Mic85, while the unlabeled cells were transfected with control-plasmids (TO5-Flag or TO5-GFP). Twenty four hours post transfection, cells were lysed and immunoprecipitated using Flag/GFP antibody and Sepharose G beads. The heavy and light beads were washed and mixed before elution. Eluted proteins were separated using SDS-PAGE, in-gel digested and subjected to LC-MS/MS



analysis. We found that Mic85 interacts specifically with Mitofilin (Mic60) and Coiled-coil-helix-coiled-coil-helix domain containing 3 (Mic19) as shown by the SILAC ratios in the scatter plot (Fig. 20D). Notably, Mic60 and Mic19 have been reported as the main constituents of the mitochondrial MICOS complex [69, 76].

To identify interaction partners *in vivo*, we performed an immunoprecipitation (IP) of endogenous Mic85 from adult mouse and human hearts using the Mic85 antibody. In this case, beads incubated in the tissue lysate served as control. The control and IP samples were eluted separately and subjected to SDS-PAGE, in-gel digestion and LC-MS/MS analysis. With label-free quantification, this experiment confirmed a strong interaction of Mic85 with Mic60 and Mic19 and uncovered other MICOS complex associated proteins, including Samm50, Mic25, Mtx2 and Dnajc11 (Fig. 20E) [80]. To verify the robustness of the physical interaction of Mic85 with the MICOS complex, we performed reverse immunoprecipitations with Mic60 and Mic19 from human hearts corroborating the interaction of Mic85 with Mic60 and Mic19 (Table 2). Moreover, we validated our SILAC based forward and reverse immunoprecipitations by western blotting (Fig. 20F). Taken together, we conclude that Mic85 is associated with the MICOS complex, which includes Mic60, Mic19 and Mic25. In addition, we found a significant interaction with two proteins from the outer membrane namely the Sorting and assembly machinery component 50 homolog (Samm50) and the mitochondrial outer membrane import complex protein 2 (Mtx2), suggesting that Mic85 is an intermediate connector between the inner and outer membrane.

Mic60 IP (Human Heart)				Mic19 IP (Human Heart)			
Protein	LFQ Int. (Ctrl)	LFQ Int. (IP)	Ratio (IP/Ctrl)	Protein	LFQ Int. (Ctrl)	LFQ Int. (IP)	Ratio (IP/Ctrl)
Mic60	9.03E+08	6.73E+10	74.5	Mic19	3.54E+08	3.66E+10	103.4
Mic85	ND	5.04E+08	∞	Mic85	ND	7.08E+08	∞
Mic19	6.87E+07	9.25E+09	134.6	Mic60	ND	5.35E+08	∞
Mic25	ND	3.94E+07	∞	Mic25	ND	8.43E+08	∞
Samm50	1.69E+07	4.36E+09	258.6	Samm50	3.52E+08	1.60E+10	45.5
Mtx2	ND	1.74E+09	∞	Mtx1	ND	9.65E+06	∞
Dnajc11	ND	3.44E+06	∞	Mtx2	ND	3.91E+09	∞
				Dnajc11	ND	7.65E+08	∞

**Table 2. Reverse interactome screening for Mic85.** Interactome screening of endogenous Mic60 and Mic19 in human heart using LC-MS/MS and label-free quantification showing Mic85 as a robust interactor. ND=not detected.

Next, we wished to compare the up-regulation of Mic85 with other MICOS-associated proteins during heart development. We observed a stronger upregulation of Mic85 compared to other components of the MICOS complex from P2 to P10 indicating that the up-regulation of Mic85 is not simply due to the increase in mitochondrial mass during development (Fig. 20G). An updated model of the MICOS complex with its known subunits and the newly discovered Mic85 is shown in Fig. 20H.

### 3.6 Mic85 is a mitochondrial inner membrane-associated protein facing the intermembrane space

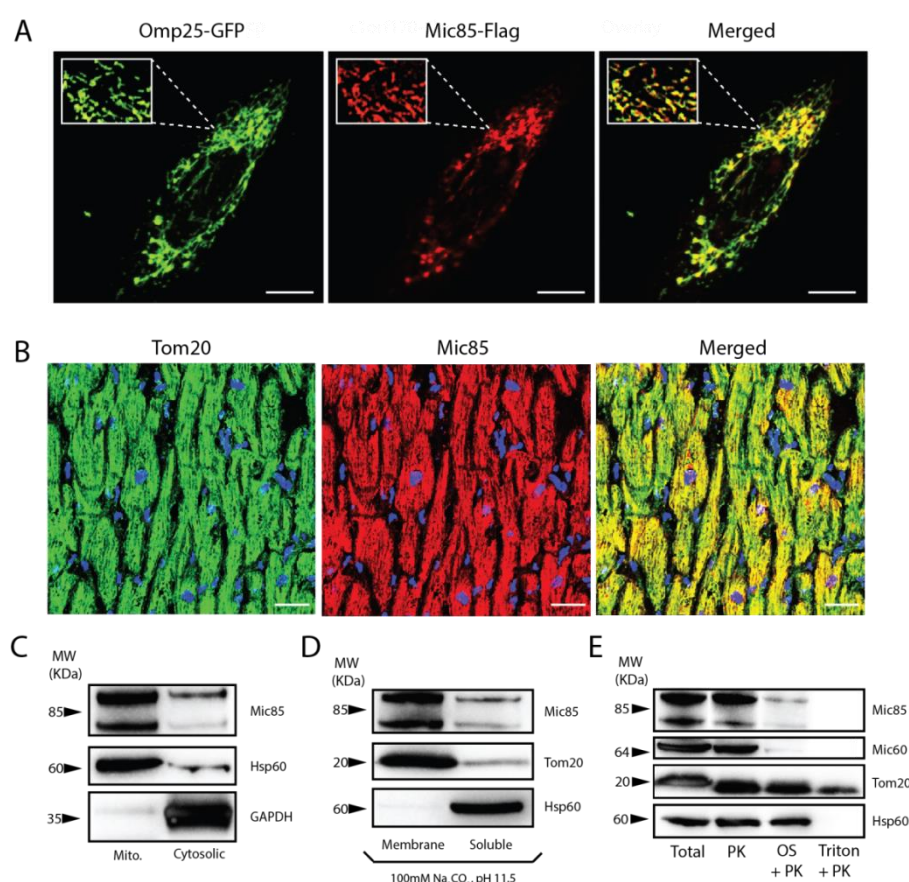


**Figure 22. Mic85 is a mitochondrial inner membrane-associated protein facing the intermembrane space.** (A) Immunofluorescence microscopy of C2C12 myoblasts showing the mitochondrial co-localization of overexpressed Flag-tagged Mic85 (red) with overexpressed Omp25-GFP (green). Scale bars=10 $\mu$ m. (B) Immunohistochemistry of human heart section showing the mitochondrial co-localization of endogenous Mic85 (red) with Tom20 (green). Scale bars=30  $\mu$ m. (C) Biochemical fractionation of cytosolic mitochondrial fractions from mouse heart showing the enrichment of Mic85 in the mitochondrial fraction similar to Hsp60. (D) Sodium carbonate extraction of membrane and soluble fractions of mouse heart mitochondria showing the enrichment of Mic85 in the membrane associated fraction similar to Tom20. (E) Submitochondrial localization of Mic85 using protease digestion assay in mouse heart mitochondria, showing the association of Mic85 to the mitochondrial inner membrane similar to Mic60.

To gain a more detailed view on the subcellular localization of Mic85, we used C2C12 cells transiently transfected with Flag-tagged Mic85 and GFP-tagged Omp25 (outer membrane protein 25) for 24 hours. Omp25 is localized to the mitochondrial outer membrane and plays a role in maintaining the intracellular distribution of mitochondria [159]. The cells were fixed, permeabilized and stained with Flag antibody. Confocal laser scanning microscopy (CLSM) analysis showed a clear punctate co-localization of Mic85 with the mitochondrial marker Omp25-GFP (Fig. 22A). In order to visualize the endogenous localization of Mic85 we used human heart sections (obtained as described in section 2.17) and performed parallel immunostainings with anti-Mic85 and Tom20 antibodies, confirming co-localization of both proteins (Fig. 22B).

We co-stained human heart sections with anti-Mic85 antibody and Phalloidin (for staining F-actin) and consistently, we detected Mic85 only in F-actin positive cells in human heart sections, indicating its cardiomyocyte-specific expression (Fig. 23). F-actin has been widely used in literature as a marker for staining cardiomyocytes [171, 172]. In conclusion, the overlapping signal of Mic85 with mitochondrial marker proteins and its dotted pattern in between myofibrils suggest its localization within mitochondria.

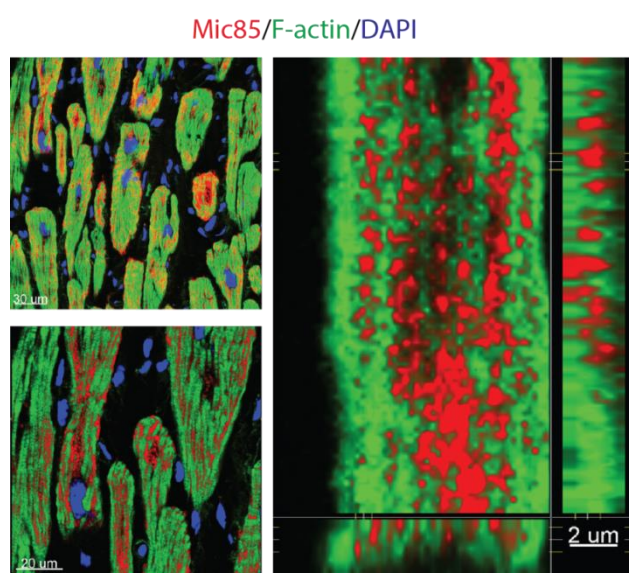


**Figure 23. Cardiomyocyte-specific localization of Mic85 in heart.** Immunohistochemical sections (7  $\mu\text{m}$ ) of human heart showing localization of Mic85 only in F-actin positive cells.

Next, we performed biochemical subcellular fractionation from mouse heart tissue to generate cytosolic and mitochondrial fractions, which were analyzed by western blot analysis using different markers (Fig. 22C). We found a strong enrichment of endogenous

Mic85 in the mitochondrial fraction, similar to the mitochondrial Hsp60 protein. To investigate whether Mic85 is a soluble or membrane-associated protein, we performed alkaline sodium carbonate extraction using mitochondria isolated from mouse heart. Mic85 remained mostly in the membrane fraction similar to the outer membrane protein Tom20, whereas the soluble matrix protein Hsp60 was released efficiently into the soluble fraction (Fig. 22D). This indicates that Mic85 is a mitochondrial membrane-associated protein. To determine the submitochondrial localization of Mic85, we performed swelling experiments combined with protease digestion (Fig. 22E). When intact mitochondria were treated with Proteinase K, the outer membrane receptor Tom20 was accessible to the protease (a band seen at a lower molecular weight indicates the digested Tom20 fragment detected by the antibody), whereas Mic85, the inner membrane protein Mic60 and the matrix protein Hsp60 remained intact. When mitochondria were subjected to osmotic shock by incubation with hypotonic buffer (which leads to opening of the outer membrane) and then treated with Proteinase K, Mic85 was digested. Likewise, the partially inner membrane integrated intermembrane space protein Mic60 showed similar sensitivity to Proteinase K digestion. Hsp60 became accessible to Proteinase K only after detergent solubilization with Triton-X, verifying its matrix localization. Taken together, we conclude that Mic85 is an inner membrane associated protein facing the intermembrane space, consistent with the proposed location of the MICOS complex.

### **3.7 Casein kinase 2 phosphorylation of PEST motif regulates the turnover of Mic85**

In addition to an increasing expression during heart development, we also detected 39 phosphorylation sites on different serine and threonine residues of Mic85. Protein motif analysis of Mic85 indicated the presence of a 56-amino acid PEST motif, with four repeating predicted CK2 substrate motifs (Fig. 20C) [173]. PEST regions are rich in proline (P), glutamine (E), serine (S) and threonine (T) and usually serve as signals for rapid proteasomal degradation [174]. Moreover, phosphorylation on the PEST motifs further regulates the turnover of a protein by leading to the exposure of degrons through induction of a conformational change [175]. In order to monitor the dynamics of Mic85 in cardiomyocytes, we fed adult C57BL/6 mice with a  $^{13}\text{C}_6$  lysine containing mouse diet for 1-6 weeks. Then, we

isolated cardiomyocytes and extracted proteins, which were subjected to LysC digestion and LC-MS/MS analysis, to determine the proteome-wide incorporation rate of  $^{13}\text{C}_6$  lysine. Mic85 showed a faster Lys6 incorporation compared to other MICOS complex associated proteins, indicating higher dynamics (Fig. 24A).

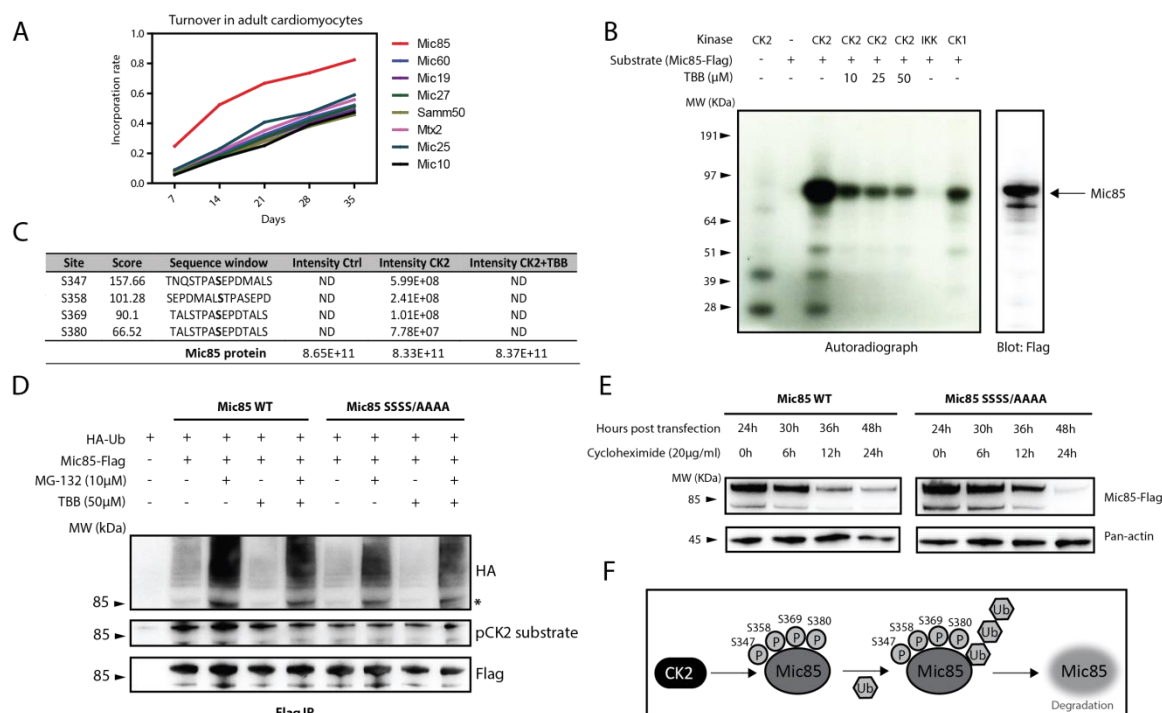


**Figure 24. Rapid turnover of Mic85 is regulated by CK2 phosphorylation on the PEST motif.** (A) Line graph depicting a faster incorporation of Mic85 compared to MICOS complex subunits and associated proteins in adult cardiomyocytes isolated from wild-type mice fed with Lys6-labelled diet for 7, 14, 21, 28 and 35 days. (B) Radioactive kinase assay on Flag-tagged Mic85 overexpressed and immunoprecipitated from HEK293T cells with the kinases CK2, CK1 and IKK and with or without the CK2 inhibitor TBB, indicating that Mic85 is phosphorylated by CK2. (C) CK2 phosphorylation at serines 347, 358, 369 and 380 identified by CK2 kinase assay on Flag-tagged Mic85 followed by elastase digestion and LC-MS/MS analysis with label-free quantification. (D) HEK293T cells were transfected for 24h and then treated with 10  $\mu\text{M}$  MG-132 (Sigma) and/or 50  $\mu\text{M}$  TBB (Sigma) where indicated for 4 hours. TBB reduces ubiquitination of WT Mic85, whereas the mutant is unaffected by TBB. \* indicates the molecular weight of Mic85. (E) Western blot analysis showing the slower degradation of overexpressed mutant Mic85 in comparison to the WT in HEK293T cells upon treatment with 20 $\mu\text{g/ml}$  cycloheximide. (F) Model showing CK2 phosphorylation mediated ubiquitination and degradation of Mic85.

To test the hypothesis of phosphorylation dependent PEST-mediated protein stability, we first performed a radioactive kinase assay on immunoprecipitated Flag-tagged Mic85 with recombinant casein kinase II. Our kinase assay showed that Mic85 is phosphorylated by CK2 kinase while increasing concentrations of the CK2 inhibitor TBB (4,5,6,7-

tetrabromobenzotriazole) reduced phosphorylation of Mic85 (Fig. 24B). IKK (I kappa B kinase) served as a negative control and CK1 as a positive control, since Mic85 harbors several potential CK1 phosphorylation motifs. To identify the predicted phosphorylation sites on the Mic85 PEST motif, we performed *in vitro* kinase assays with immunoprecipitated Flag-tagged Mic85 in the absence of CK2 (control), in the presence of CK2, and in the presence of CK2 and TBB and subjected to LC-MS/MS analysis. After completion of the assay, Mic85 was eluted from the beads and digested in-solution. Although mass spectrometric identification of the phosphorylation sites was challenging due to the absence of lysine or arginine in the 56-amino acid PEST motif (Fig. 20C), we identified all four phosphosites, including S347, S358, S369 and S380 as shown by the MS/MS spectra (Fig. 25) using elastase digestion which cleaves at unspecific sites. Moreover, we observed high peak intensities of these phosphorylation sites only in the presence of CK2 but not in the absence of CK2 or in the presence of TBB (Fig. 24C). These results suggest that CK2 phosphorylates the serine residues within the PEST motif of Mic85, thereby regulating its stability.

Next, we investigated whether the phospho-PEST domain has any influence on proteasomal degradation of Mic85. Notably, the cytosolic ubiquitin-proteasome system mainly acts as protein quality control system for mitochondrial intermembrane space proteins [176]. To detect the degree of ubiquitin proteasomal degradation induced by phosphorylation of the PEST motif, we mutated all the four serines within the PEST domain to alanines and refer to this mutated form as Mic85 SSSS/AAAA. We performed ubiquitination assay in HEK293T cells with the overexpression of Flag-tagged Mic85 and HA-tagged ubiquitin. In the presence of the proteasomal inhibitor MG-132, Mic85 WT showed a reduced ubiquitination after inhibition of CK2 by TBB (Fig. 24D). In contrast, the Mic85 SSSS/AAAA mutant showed reduced ubiquitination even without inhibition of CK2. Further addition of TBB did not affect the degree of ubiquitination of Mic85 SSSS/AAAA. The reduction of phosphorylation after TBB treatment or mutation of serines is shown by pCK2 substrate blot. These results corroborate that CK2 phosphorylation on serines 347, 358, 369 and 380 in the PEST motif regulates the dynamics of the Mic85 precursor protein. To further compare the stability of WT and mutant Mic85, HEK293T cells were transfected independently with Flag-tagged WT and mutant Mic85. Cells were treated 24 hours after transfection with 20 $\mu$ g/ml cycloheximide for 6, 12 and 24 hours to inhibit translation. By immunoblotting using the Flag

antibody, we observed a more rapid degradation of WT Mic85 compared to the mutant form (Fig. 24E). The model of CK2 phosphorylation-mediated degradation of Mic85 is shown in (Fig. 24F).

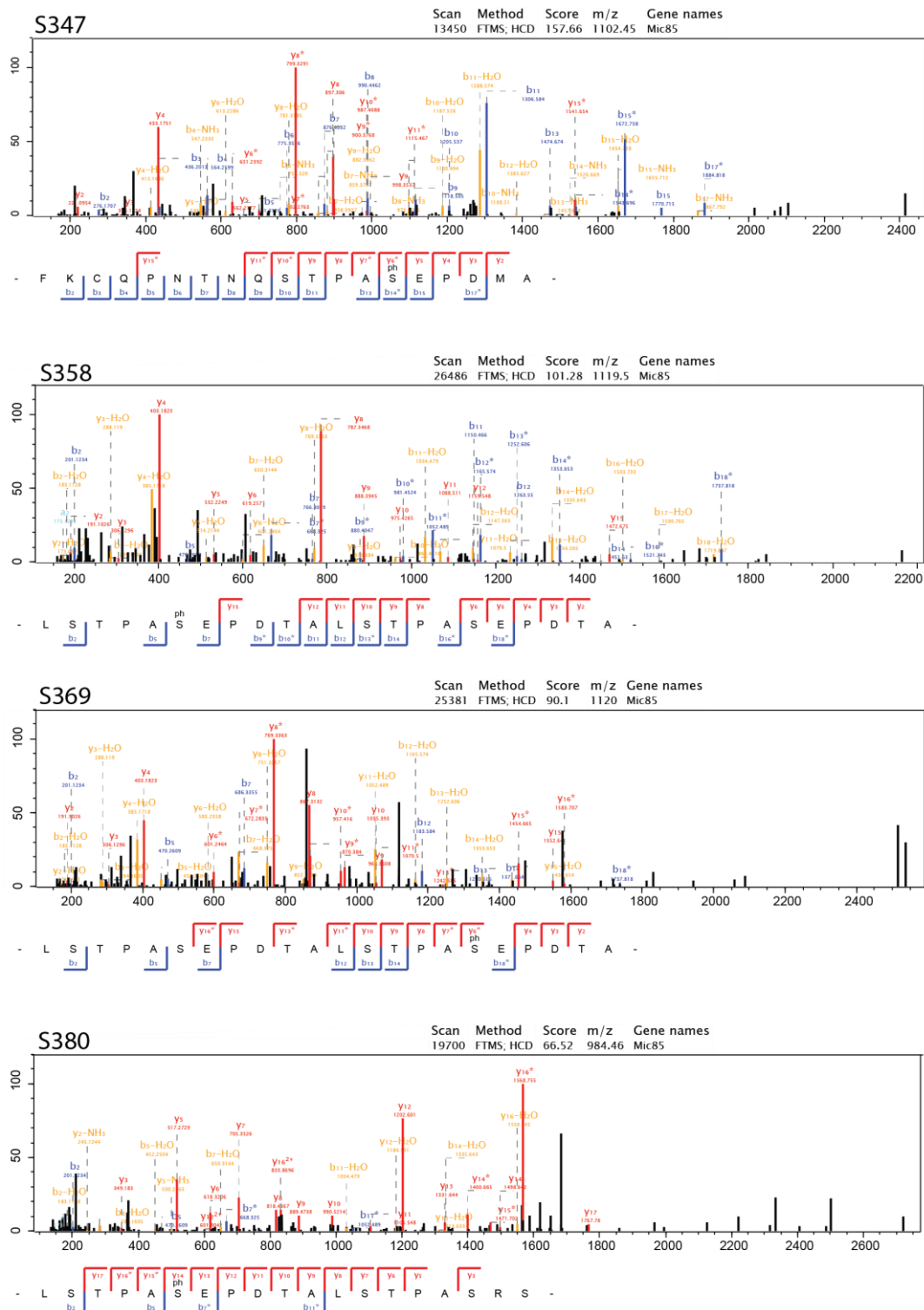


**Figure 25. MS/MS spectra of phosphorylation sites in PEST motif.** MS/MS spectra illustrating the identification of S347, S358, S369 and S380 on the PEST motif of Mic85 using HCD fragmentation on a Q Exactive mass spectrometer.

### 3.8 Loss of Mic85 leads to reduced maximal oxidative capacity and altered mitochondrial morphology

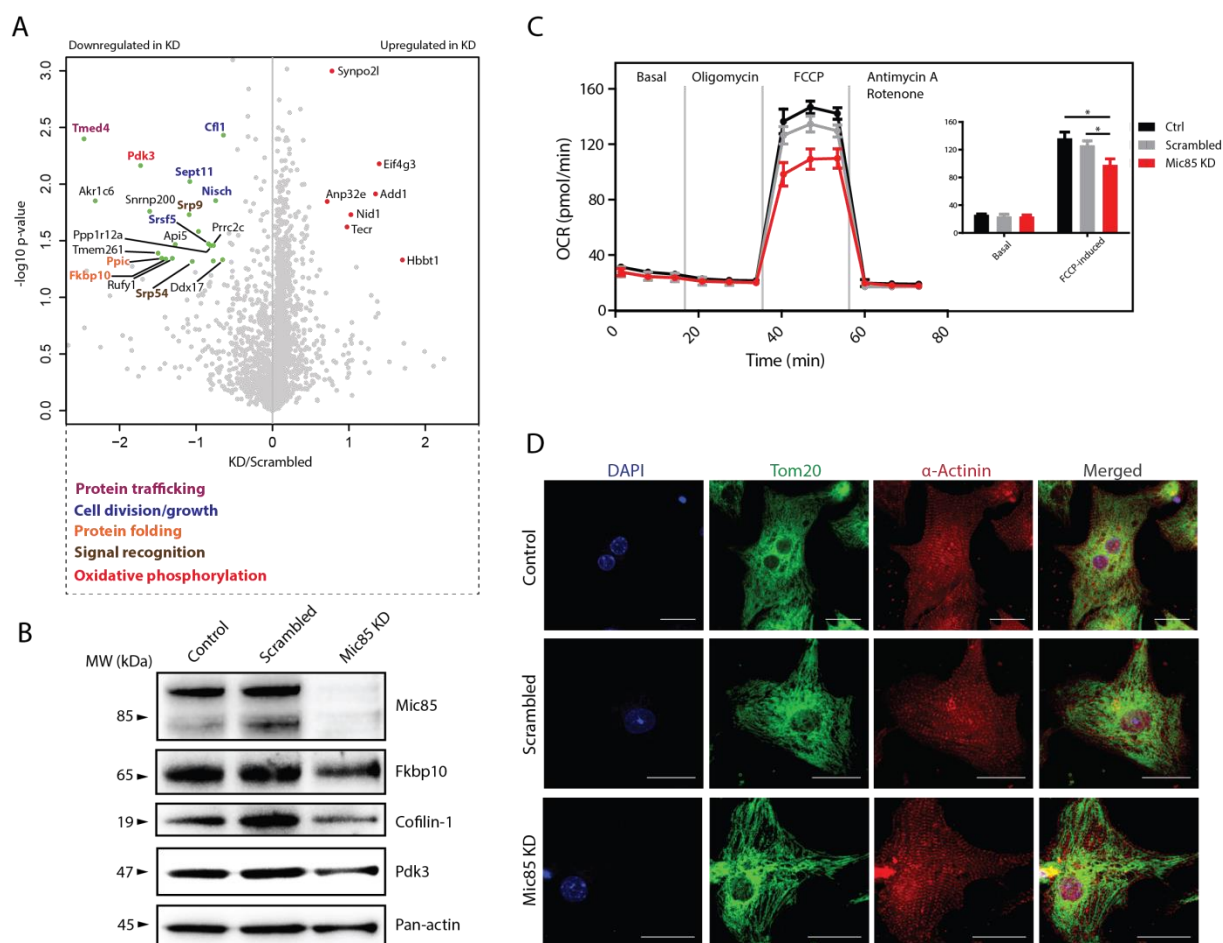


**Figure 26. Mic85 knockdown in mouse neonatal cardiomyocytes leads to altered mitochondrial morphology and reduced maximal oxidative capacity.** (A) Global proteomic analysis of Mic85 KD cardiomyocytes in comparison to scrambled using LC-MS/MS and SILAC-based quantification ( $n=2$ ,  $p<0.05$ ). Downregulated protein associated with specific Gene Ontology annotations are highlighted and indicated in the legend. (B) Western blot showing the knockdown efficiency of Mic85 and downregulation of Fkbp10, Cofilin-1 and Pdk3 upon Mic85 KD. (C) Oxygen consumption rate of neonatal cardiomyocytes measured in the presence or absence of  $1.5\mu\text{M}$  oligomycin,  $0.5\mu\text{M}$  FCCP (uncoupling agent),  $0.75\mu\text{M}$  antimycin A and  $0.75\mu\text{M}$  rotenone, depicting a reduced maximal oxidative capacity upon FCCP injection in Mic85 KD cells compared to scrambled and control cells ( $n=4$  assays with 12 replicates per assay,  $*p<0.05$ ). Error bars indicate SEM. (D) Immunofluorescence microscopy showing altered mitochondrial morphology using Tom20 (green) in Mic85 KD cardiomyocytes compared to scrambled and control cells.  $\alpha$ -actinin (red) was used to stain cardiomyocytes. (E) Electron micrographs of control, scrambled and Mic85 KD neonatal cardiomyocytes.



To investigate the function of Mic85 *in vivo*, we isolated neonatal cardiomyocytes from newborn mouse pups and transfected them with scrambled control siRNA and with siRNA against Mic85. Mic85 knock down efficiency was tested 48h after transfection by western blotting (Fig. 27B). Longer time points were not possible since we observed Mic85 to be rapidly downregulated in culture; moreover cardiomyocytes begin to de-differentiate when kept longer in culture. Next we performed a global unbiased quantitative proteomics analysis, in biological duplicates, with adult cardiomyocytes isolated from the SILAC mouse as a spike-in standard. In total we quantified more than 3000 proteins and identified 27 significantly regulated proteins ( $p < 0.05$ , fold-change  $> 1.5$ ) in Mic85 knockdown (KD) cardiomyocytes compared to the scrambled control. Notably, we found an overrepresentation of Gene Ontology categories for cell division/growth, protein trafficking, protein folding and signal recognition among the down-regulated proteins (Fig. 26A). For example, pyruvate dehydrogenase kinase isoenzyme 3 (Pdk3) which regulates glucose metabolism and aerobic respiration by influencing pyruvate dehydrogenase activity [177, 178] was 3-fold downregulated after knockdown of Mic85. The downregulation of peptidyl-prolyl cis-trans isomerase FKBP10, Cofilin-1 and Pdk3 upon Mic85 KD was also demonstrated by western blot analysis (Fig. 26B).

To investigate the contribution of endogenous Mic85 to the regulation of oxidative phosphorylation, we determined oxygen consumption rates in neonatal cardiomyocytes using an XFe96 Extracellular Flux Analyzer (Seahorse Bioscience). No significant changes of the oxygen consumption rates were measured after knockdown of Mic85 KD under basal conditions and oligomycin (inhibitor of ATP synthesis) treatment in cardiomyocytes. However, we detected a significant reduction in the increase of oxygen consumption rate in the presence of the uncoupling agent FCCP in KD cells in comparison to control cells (Fig. 26C), indicating that Mic85 is required for maximal oxidative capacity in neonatal cardiomyocytes. FCCP is the abbreviation for carbonyl cyanide-p-trifluoromethoxyphenylhydrazone is a mobile ion carrier that disrupts the mitochondrial membrane potential by transporting hydrogen ions across the membrane, thereby causing rapid consumption of energy and oxygen by the cells without the generation of ATP. Upon treatment with Antimycin A and rotenone, mitochondrial respiration was shut down as expected.

To determine whether Mic85 has also a role to establish a normal mitochondrial morphology, we analysed neonatal cardiomyocytes after knockdown of Mic85 by immunofluorescence confocal microscopy. While the control and scrambled siRNA-treated cells showed a dense network of Tom20-stained mitochondria, we observed that the mitochondria in knockdown cells were less dense and elongated (Fig. 26D). In addition, Mic85 knockdown cardiomyocytes showed a tendency of mitochondrial perinuclear accumulation, which is related to mitochondrial dysfunction. Taken together our results suggest that Mic85 regulates mitochondrial respiration and is required to establish normal morphology of mitochondria.

## 4. Discussion

### 4.1 Significance of comprehensive phosphoproteomics analysis of heart development

To date, several anatomical and molecular studies are devoted to heart development in order to address the challenges of cardiovascular diseases and heart regeneration. The regulation of cardiac proteins and signalling events mediated by phosphorylation are important determinants to control crucial signalling pathways during heart development. Likewise, mitochondrial biogenesis was found to represent an important feature of cardiomyocyte maturation [43]. Although the regenerative potential [24] and intracellular energy pathways [179] were studied during post-natal heart development, a comprehensive analysis of protein expression and phosphorylation based on quantitative mass spectrometry events was critically missing.

Here, we employed an unbiased quantitative proteomics approach and present a comprehensive dataset comprising of proteome-wide mapping of phosphorylation sites and their regulatory expression profiles during post-natal heart development in mice. The three post-natal time points (P2, P10, P20) employed in our study covers the stages of development from neonatal stage through the stage of switching to maturation to the matured post-natal stage. Advanced methodologies in mass spectrometry-based proteomics allowed an extensive coverage of more than 20,000 phosphorylation sites and ~9000 proteins which reflects an exhaustive sequencing of the phosphoproteome and proteome of mouse heart and is to our best knowledge the largest quantitative heart tissue dataset reported so far. Our comprehensive analysis allowed us to identify more than 4000 novel phosphorylation sites on 1834 proteins. It is important to note here that whole heart tissues were used for analysis, because isolation of cardiomyocytes from very small heart tissues of P2 or P10 mice would yield significantly insufficient starting material for phosphopeptide enrichment (for which ideally 15mg proteins are required). Out of the total proteome of 8985 proteins, more than 800 proteins (~10%) were gene ontology annotated

as mitochondrial, indicating the abundance and importance of mitochondrial proteins in heart tissue. Interestingly, we identified Mic85 as a protein that is strongly upregulated during postnatal heart development. So far, detailed insights into the physiological function of Mic85 in heart tissue were missing, although Mic85 (Perm1) was recently described as a tissue-specific regulator of oxidative capacity in skeletal muscle cells [168]. Previous results suggested that PGC-1 and ERR-induced regulator in muscle protein 1 (Perm1) is required for expression of selective PGC-1 $\alpha$ /ERR target genes in myotubes and for PGC-1 $\alpha$ -induced mitochondrial biogenesis and maximal oxidative capacity. Here we demonstrate that Mic85 I) is highly expressed in cardiomyocytes (and in skeletal muscle to a significant extent), II) is a novel “dynamic” component associated with the mitochondrial MICOS complex (dynamics is controlled by CK2 phosphorylation on PEST motif), and III) its endogenous levels are essential for optimal mitochondrial morphology and respiration.

## **4.2 SILAC mouse based *in vivo* quantification revealed downregulation of cell cycle progression after P10**

Metabolic labelling using SILAC has been a powerful technique for accurate quantification and the use of SILAC mouse approach in our study enabled robust *in vivo* quantification of protein expression levels, validating previous reports. For instance, we observed a significant downregulation of insulin-like growth factor II mRNA-binding proteins Igf2bp 1-3 during development, proving that these factors are expressed during foetal development and decline towards birth [180]. Though label-free quantification is also a powerful method, only a limited number of PTM quantification analyses have been generated using this method (due to more error-prone steps in the long PTM enrichment protocol), thereby making SILAC labelling the method of choice for quantification of single peptides. Importantly, we identified several factors that might be responsible for the proposed switch from regenerative potential to complete maturation of cardiomyocytes during the course of our proteome study. The strong 5-fold reduction of all six DNA replication licensing factors MCM2-7, belonging to the minichromosome maintenance (MCM) complex, at P20 compared to P10 caught our attention, as this complex is important for eukaryotic DNA replication [181, 182]. MCM complex binds to the origin of DNA replication during the late M phase to early G1 phase of the cell cycle and unwinds the double stranded DNA, recruits DNA

polymerases and begins DNA synthesis. It seems likely that the downregulation of MCM2-7 negatively influences DNA replication and hence cell cycle progression, thereby reducing the proliferative capacity of cardiomyocytes after P10. It is also noteworthy that phosphorylation on histones H1.2, H1.4 and H1.5 was unchanged between P2 to P10 but was more than 5-fold downregulated at P20. Since histone H1 is known to be hyperphosphorylated during mitosis [163], the hypo phosphorylation might reflect the exit from mitosis 10 days after birth at the molecular level. In summary, the use of SILAC-based quantification allowed us to accurately quantify protein levels and phosphorylation changes during post-natal heart development and we present this in-depth quantitative analysis as a valuable and comprehensive resource to the biological community working on heart development, regeneration and disease models.

### **4.3 Mic85 is a novel member of MICOS complex and is possibly imported by the MIA pathway**

The MICOS protein complex is critical for organization of the inner membrane and formation of membrane contact sites in the mitochondria [69-71]. After identification of the core protein Mitofilin (Mic60), a growing number of interaction partners have been reported [74-77, 79, 80]. Using quantitative interactome screenings *in vitro* and *in vivo* coupled to high-resolution mass spectrometry, we discovered that Mic85 constitutes a new component of the mammalian MICOS complex. The interaction of Mic85 with MICOS subunits Mic60, Mic19 and Mic25 and the outer membrane proteins Samm50 and Metaxin-2 indicates an association of Mic85 with MICOS at contact sites between the inner and outer mitochondrial membranes.

Earlier studies showed that Mic60 also supports the translocase machineries TOM and SAM [183]. Thus it is tempting to speculate that Mic85 might be a further component for the import of proteins mediated by the SAM complex. However, at present it is not entirely clear how Mic85 links Mic60 with Samm50 and Mtx2. Since Mic60 does not support the import of precursor proteins across the inner membrane via TIMs (mitochondrial import inner membrane translocases), we did not detect any interaction of Mic85 with translocases. Another transport system is the intermembrane space assembly machinery Mia40, which

imports proteins into the inner membrane and interacts with Mic60 [69]. Our Mic85 motif analysis revealed two adjacent cysteine pairs with CX<sub>13</sub>C motifs at the C-terminus separated by 29 amino acids. Twin CX<sub>3-9</sub>C cysteine residues are responsible for the import of soluble IMS proteins by the mitochondrial disulphide relay system of Mia40 and Erv1 (a sulfhydryl oxidase) [184], which is based on an oxidative folding mechanism. Pre-proteins containing CxC motifs are recognized by Mia40 and translocated through the translocase of outer membrane (TOM complex) into the intermembrane space, where disulphide bonds are transferred from oxidized Mia40 to the reduced substrate, which triggers oxidative folding of the substrate. For further import, the reduced Mia40 is re-oxidized by Erv1. Furthermore, protein import into mitochondria through the TOM complex is regulated by cytosolic kinases like casein kinase 2 (CK2) and protein kinase A (PKA). CK2 promotes biogenesis of the TOM complex through phosphorylation of the receptor Tom22 and import protein Mim1, while PKA inhibits mitochondrial import through phosphorylation and inhibition of the receptor Tom70 [185]. Clearly, most of the proteins imported via the Mia40 machinery are relatively small and the cysteines are separated by either 3 or 9 amino acids. However, there are also examples with CX<sub>10</sub>C motifs and it might be possible that not only typical MIA targeting signals are used by this mitochondrial disulphide system, supporting the view that Mic85 may also be involved in the MIA system [186].

#### **4.4 Mic85 is an important factor for mitochondria within high energy demanding cells**

Another interesting result of our study was the distinct upregulation of Mic85 from P2 to P10 (2.8-fold) compared to other MICOS-associated proteins (1.5-fold). The steep increase of Mic85 during this time period reflects clearly an enhanced expression of this protein and not just an increased abundance due to higher mitochondrial mass (cardiac hypertrophy during post-natal heart development is characterized by an upregulation of mitochondrial biogenesis and an increase in mitochondrial mass [43]). Such a regulation within the first week after birth might also point to the contribution of Mic85 as an important factor to enhance mitochondrial activity and maturation. However, it remains to be determined whether this upregulation actually directly regulates the mitochondrial biogenesis within cardiomyocytes *in vivo*. Notably, using our mass spectrometric approach, Mic85 was only

detectable in skeletal and heart muscle tissue and not in organs like liver and brain. Moreover, the comparison to other large-scale proteomics datasets [26, 27] confirmed our data and suggests a tissue specific function for Mic85. Therefore, we propose that Mic85 is not only a novel MICOS complex member but also an important factor for mitochondria within high energy demanding cells. Future studies on Mic85 in transgenic or knockout animal models are necessary to dissect such a possible function.

#### **4.5 Mic85 is a mitochondrial membrane-associated intermembrane space protein**

The presence of two putative nuclear localization signals in Mic85 and the overexpression of a GFP-Perm1 fusion protein in C2C12 myotubes suggest a nuclear localization, as shown also in a previous study [168]. However, it is important to note that since GFP is itself a protein and rather big, localization studies using GFP-fusion proteins require thorough validation. However, since we detected an association of Mic85 with the MICOS complex, we focused our study on its mitochondrial localization. Immunofluorescence stainings using overexpressed Mic85-Flag and endogenous Mic85 clearly indicate a mitochondrial localization. Whether Mic85 has a dual localization in nucleus and mitochondria, or it shuttles between the two compartments will be an interesting question for future studies. Biochemical fractionation uncovers that Mic85 localizes to the membrane fraction after carbonate extraction, and is exposed to proteinase K only after opening of the outer mitochondrial membrane by swelling, indicating its localization to the inner mitochondrial membrane, which is consistent with the proposed location of the MICOS complex. Since Mic85 is a soluble protein and interacts with the outer membrane protein Samm50, we suggest that Mic85 is a membrane-associated intermembrane space protein involved in the formation of contact sites between the inner and outer membranes. The highly phosphorylated status of Mic85 further reflects a mitochondrial characteristic, since Perm1 expression has been shown to be induced by endurance exercise [168] and previous studies have shown that phosphorylation-dependent regulation of mitochondrial proteins is essential for the adaption of skeletal muscle to stress conditions [187, 188]. Additional methods such as blue native gels or cross-linkers to show the association of Mic85 with

MINOS complex are interesting for future investigations using a loss of function mouse model.

#### **4.6 PEST phosphorylation mediated protein turnover controls Mic85 homeostasis**

To better understand the Mic85 homeostasis in cardiomyocytes, we used a pulsed SILAC approach in living mice which revealed a faster Lys6 incorporation of Mic85 in comparison to other MICOS components in isolated cardiomyocytes. In addition, we observed a fast degradation of Mic85 in skeletal muscle denervation experiments (S.A.; unpublished data), which prompted us to study the role of the Mic85 PEST motif, since PEST motifs and their phosphorylation have been reported to trigger proteasomal protein degradation [174, 175]. Motif analysis revealed four repeating Casein kinase 2 (CK2) substrate motifs within the PEST domain and with radioactive kinase assay in combination with the CK2 inhibitor TBB, we showed that CK2 phosphorylates Mic85. The mass spectrometric identification of the phosphorylation sites was challenging due to the absence of lysine or arginine in the complete 56-amino acid PEST motif, making the use of typically used efficient proteases like LysC or trypsin unfruitful. We accomplished the identification of the four phosphorylation sites using elastase digestion which cleaves a protein at unspecific sites. We showed that Mic85 is phosphorylated on all four CK2 motifs within the PEST domain. Moreover, we found that increased CK2 dependent phosphorylation leads to increased ubiquitination and subsequently to shorter half-life. Importantly, the conversion of all phospho serines to alanine within the PEST domain resulted in reduced protein degradation indicating furthermore the importance of CK2 phosphorylation in respect to Mic85 homeostasis.

It has been shown that the ubiquitin proteasome system is implicated in the degradation of proteins in the mitochondrial outer membrane [189] [190] [191], albeit mitochondrial precursor proteins targeted to the IMS via the MIA system are also controlled by the UPS system [176]. This study by Bragoszewski et al. focused on the biogenesis of intermembrane space proteins at the cytosolic stage and reported that the ubiquitin-proteasome system plays an important role in removing mislocalized IMS proteins under physiological conditions, thereby regulating the influx of proteins into the mitochondrial intermembrane



space. Since we localized Mic85 within the IMS, the most obvious explanation would be that Mic85 precursor protein is either ubiquitinated and quickly degraded, or imported into mitochondria depending on the energy demand and mitochondrial biogenesis of Mic85. Since we have shown Mic85 to be phosphorylated by the cytosolic kinase CK2, we believe that Mic85 is phosphorylated in the cytosol and then imported into the mitochondria, where its level is regulated by the UPS. The increased stability of Mic85 phospho-mutant compared to WT clearly indicates that CK2 phosphorylation of Mic85 on the PEST motif is crucial for the regulation of its turnover. However, the exact mechanism of how Mic85 precursor proteins are imported into mitochondria and which factors favour a mitochondrial or nuclear localization remain to be elucidated.

#### **4.7 Mic85 contributes to increased energy demand of maturing cardiomyocytes**

To gain more insights into the physiological function of Mic85, we used isolated neonatal cardiomyocytes from mouse as the biological system due to its high endogenous expression in these cells. For proteomics analysis, cardiomyocytes isolated from an adult SILAC mouse was used as spike-in standard due to the difficulty in labelling neonatal cardiomyocytes. Though the SILAC ratios were left shifted (due to wide variety of proteins in the adult cells) and were normalized manually, this method of quantification was preferred due to the accuracy and robustness of SILAC. Through our proteomics approach, we identified several proteins essential for proliferation, growth and protein folding, which were downregulated after Mic85 knockdown, suggesting an impaired mitochondrial function in this state. The downregulation of Pdk3 suggests a disturbance in aerobic respiration. Indeed, by measurement of oxygen consumption rate, we showed that Mic85 is essential for maximal oxidative capacity of cardiomyocytes. A similar effect has been reported for Perm1 [168] in C2C12 cells where the endogenous expression of Mic85 is considerably lower. Though we identified and quantified other MICOS components in this study, these were not significantly regulated upon Mic85 knockdown, suggesting that Mic85 is not co-regulated with MICOS components. Here, we emphasize an essential role for Mic85 in the mitochondrial respiration of cardiomyocytes and furthermore mitochondria of Mic85 knockdown cells show an altered morphology with fragmented and less dense mitochondria. Taken together

with the significant expression of Mic85 in heart and muscle in comparison to other tissues, we suggest a specific role for Mic85 in contribution to the enhanced energy demand in those contractile tissues.

Taken together, in this study we propose a specific role for Mic85 to satisfy the increased energy demand in heart and skeletal muscles. We demonstrated an essential role for Mic85 for optimal mitochondrial respiration of cardiomyocytes and show that Mic85 knockdown is required for normal mitochondrial morphology. The interaction of Mic85 with outer and inner mitochondrial membrane proteins suggests the association of Mic85 with MICOS at membrane contact sites. Since we observed robust physical interaction of Mic85 with Mic60 and Mic19 (the core components of MICOS complex), we believe a strong association of Mic85 with the MICOS complex. Use of Mic85 knockout animal model for investigating any effects on the stability and abundance of MICOS and OXPHOS complexes using blue native gel electrophoresis, and measuring differences in mitochondrial function through high resolution respirometry using Oroborus instruments [192] are interesting for future studies. Moreover, the observation that Mic85 is essential for the optimal energetics of cardiomyocyte mitochondria makes it an interesting target of study in heart failure models. In addition, we provide a comprehensive dataset of normalized phosphorylation sites in the mouse heart as a resource for the biological community to support future investigations in mammalian heart development and regeneration.

#### **4.8 Generation of Mic85 knockout mouse for future *in vivo* studies**

Constitutive knockout mouse for Mic85 was generated using a recombineering based method to subclone DNA from bacterial artificial chromosomes (BACs) into high-copy plasmids by gap repair, and together with Flp recombinase to introduce FRT sites into the subcloned DNA. In the first step, two sets of primers were used to amplify two ~500bp regions of the BAC (obtained from mouse bMQ BAC library, Source BioScience). These PCR amplified homology arms were cloned into PKOII vector, which was then linearized and subjected to homologous recombination with the BAC DNA to generate the gap repair (retrieval plasmid) for subcloning. The two homology arms cloned into PKOII mark the ends

of the fragment subcloned by gap repair. In the second step, a minitargeting vector was constructed by ligating two PCR products generated by amplification of BAC DNA with two other primer pairs (located within the fragment subcloned by gap repair) into PL451 vector which contains the Venus-GFP target and the Neo selection cassette bordered by FRT sites. The PL451 plasmid was then linearized to remove its backbone and subjected to homologous recombination with the gap repair (retrieval) plasmid. The region of the BAC now containing the Venus-GFP, Neo cassette and the FRT sites was excised and transformed into ES cells. The Neo positive clones and recombination positive clones of ES cells were confirmed using southern blotting and one was chosen to inject into the mouse. The chimeric mice were then crossed with Flp recombinase mouse to cut out the Neo cassette between the FRT sites. Further breedings and back crossings are being performed to generate heterozygous and homozygous mice and to remove the Flp deleter gene. Such a knockout mouse for Mic85 in combination with a GFP knock-in is a great asset to study the function of Mic85 in cardiac development and to visualize its tissue-wide expression.

#### **4.9 An overview of interdisciplinary collaborative projects**

In an independent study, proteomics analysis revealed partial cross-species conservation of adult zebrafish neutrophils and human neutrophils. Using a gel-based LC-MS/MS approach, we analysed the proteome of primary marrow neutrophils from adult zebrafish. Three-fourth of the identified proteins originated from neutrophils and cross-species comparison with human peripheral blood neutrophils revealed partial conservation of immune related proteins between the two species. Being the first zebrafish neutrophil proteome dataset, this study serves as a valuable resource for future studies on neutrophil biology and innate immunity. This study has been published in *Plos One* [193].

Another study involved the phosphoregulation of the titin-cap protein telethonin in cardiac myocytes. Telethonin is a muscle-specific protein and its mutation is known to be associated with cardiac and skeletal myopathies [194, 195]. In this study, mass spectrometric analysis for site-specific post-translational modifications in an *in vivo* phosphoproteomics approach supported the data from *in vitro* kinase assays that telethonin is doubly phosphorylated on Ser-157 and Ser-161. Identification of these sites was an essential first step before mutating these sites to show that this bis-phosphorylation is important for normal telethonin function,

including maintenance of transverse tubule organization and intracellular calcium transients. This study has been published in *Journal of Biological Chemistry* [196].

In a third study on characterizing the molecular changes on protein level occurring upon sterile inflammation in zebrafish neutrophils, we investigated the protein dynamics in neutrophils of adult zebrafish upon chemically-induced inflammation. Using label-free quantification, we identified several proteins associated with cell cycle, nitric oxide signalling, regulation of intermediate filaments and cytoskeletal rearrangement and several immune responses to be differentially regulated upon inflammation. Being the first proteomics analysis of adult zebrafish neutrophils upon chemically induced inflammation, this study has been published in *Fish & Shellfish Immunology* [197] and serves as a valuable resource for future studies on zebrafish inflammation models.

## 5. Zusammenfassung

### 5.1 Einführung

Die Herzentwicklung bei Säugetieren ist ein komplexer Prozeß und besteht aus einem engen Zusammenspiel von Zellproliferation und Zelldifferenzierung. Es wurde gezeigt, dass kurz nach der Geburt Kardiomyozyten den Zellzyklus verlassen und die Fähigkeit zur Proliferation verlieren. Postmitotische Kardiomyozyten besitzen eine sehr begrenzte Regenerationsfähigkeit und sind daher kaum in der Lage beschädigtes Herzgewebe zu ersetzen [17, 18]. Interessanterweise konnte eine kürzlich durchgeführte Studie zeigen, dass Herzen neugeborener Mäuse die Fähigkeit besitzen geschädigtes Herzgewebe zu regenerieren. Neonatale Kardiomyozyten können vermutlich aufgrund verbleibender proliferativer Kapazität wieder proliferieren und dieser Umbau erfolgt größtenteils ohne Fibrose [24]. Bis heute sind die molekularen Mechanismen und regulatorischen Expressionsprofile von Proteinen und posttranslationalen Modifikationen, die die neonatale Kardiomyozytenproliferation oder die Mechanismen zur Reifung und Differenzierung regulieren, wenig erforscht. Jedoch konnte gezeigt werden, dass Veränderungen der Stoffwechselaktivitäten in Kardiomyozyten zum Übergang in einen postmitotischen Zustand führen [25].

Die reversible Proteinphosphorylierung dient als wichtiger Mechanismus für die Modulation von Proteinfunktionen, Enzymaktivitäten und Regulierung von Protein-Protein Interaktionen. Weiterhin konnten globale Phosphorylierungsstudien in Nagetieren zeigen das unterschiedliche Gewebe spezifische Phosphorylierungsnetzwerke besitzen [26, 27]. Diese Erkenntnisse deuten darauf hin das dynamische Phosphorylierungsmuster eine Schlüsselfunktion bei der Entwicklung des Herzmuskels spielen sowie die Herzmuskelkontraktion und metabolische Prozesse steuern [41]. Aus diesem Grund ist eine genaue Analyse der reversiblen und dynamischen posttranslationalen Modifikationsstellen für die funktionelle Annotation von Proteinnetzwerken während der Herzentwicklung erforderlichlich um Signalwege in Kardiomyozyten besser zu verstehen.

Moderne hochauflösende Massenspektrometer sind heute in Lage nahezu komplette Proteome in Tiefe zu analysieren und zahlreiche posttranslationale Modifikationen zu detektieren [110]. Aufgrund der substöchiometrischen Konzentration der meisten Proteinmodifikationen lassen sich diese nicht ohne eine spezifische Anreicherung darstellen. In der Vergangenheit hat sich eine Kombination aus chromatographischen Trennverfahren und Massenspektrometrie als geeignete Methode für die Darstellung von Phosphopeptiden etabliert [112, 113]. Um akkurat Veränderungen der Phosphorylierung zu bestimmen müssen diese auf das Expressionslevel der jeweiligen Proteine normalisiert werden, um auszuschließen, dass eine veränderte Expression der Proteine die Ursache für die Regulation der Phosphorylierung ist [119].

Bei Mitochondrien handelt es sich um ein zelluläres Kompartiment mit hochdynamischen Proteinveränderungen. Die Funktionsweise des Herzens ist stark abhängig von der in den Mitochondrien erzeugten Energie. Fetale Kardiomyozyten erzeugen ATP hauptsächlich durch Glykolyse und Glukoseoxidation [44]. Nach der Geburt kommt es zu einem Wechsel der Energieerzeugung von der Glykolyse zur  $\beta$ -Oxidation von Lipiden. Hierbei werden größere Mengen an ATP erzeugt [44, 46] und dieser Vorgang geht mit einer Zunahme von Mitochondrien einher [47]. Die oxidative Phosphorylierung findet in der Cristae, der inneren Mitochondrienmembran statt. Diese beinhaltet einen großen Proteinkomplex, der entscheidend für die Anordnung der inneren Membran und die Bildung von Membrankontaktstellen ist. Diesen Komplex bezeichnet man als „*Mitochondrial inner membrane organizing system*“ (MINOS) [69] oder „*Mitochondrial organizing structure*“ (MitOS) [70]. Vor kurzem wurde die Nomenklatur vereinheitlicht, so dass dieser Komplex nun als „*Mitochondrial contact site and cristae organising system*“ (MICOS) bezeichnet wird. Er besteht aus mehreren Untereinheiten, die je nach ihrem Molekulargewicht Mic10 bis Mic60 genannt werden [71]. Mutanten der MICOS-Untereinheiten weisen Veränderungen in der inneren Membranstruktur auf, die mit dem Verlust der Cristaemembran und reduzierter oxidativer Kapazität einhergehen [72, 74-77]. Es wurde gezeigt, dass dieser Komplex mit vielen Kanalproteinen und Protein-Translokasen in der äußeren Membran interagiert. Ein Defekt der Mic-Untereinheiten führt zu einer generellen Verminderung in der Biogenese von

mitochondrialen Proteinen [78-80] und hat einen starken Effekt auf die metabolische Aktivität von Mitochondrien.

## 5.2 Ziele der Studie

Das Ziel dieser Studie ist mittels einer *in vivo* SILAC basierten quantitativen Analyse das globale Proteom und Phosphoproteom während der postnatalen Entwicklung des Herzens im Mausmodell zu untersuchen. Hierbei wurden die drei postnatalen Zeitpunkte P2, P10 und P20 gewählt. Proteine und aktivierte Signalwege in Kardiomyozyten, die unterschiedlich während der neonatalen, proliferierenden und späteren postmitotischen Phase reguliert werden, sollen mittels Massenspektrometrie identifiziert werden.

Darüber hinaus ist die Entwicklung und Funktion des Herzens stark von der Energieproduktion der Mitochondrien abhängig. Aus diesem Grund fokussierte sich diese Studie auf die genauere Charakterisierung eines neuen hochmodifizierten mitochondrialen Proteins, welches im Verdacht steht eine wichtige Rolle bei der Regulierung metabolischer Prozesse in Kardiomyozyten zu spielen.

## 5.3 Ergebnisse

Diese Studie beinhaltet einen umfassenden Datensatz dynamischer Veränderungen in Proteom und Phosphoproteom von Mausherzen während postnataler Entwicklungsstadien. Es wurden drei postnatale Zeitpunkte P2, P10 und P20 gewählt und mittels SILAC basierter *in vivo* quantitativer Proteomics mit hochauflösenden Massenspektrometern analysiert. Dabei wurden 8985 Proteine und 21.261 Phosphorylierungsstellen identifiziert und bemerkenswerterweise konnten 4276 neue Phosphorylierungsstellen detektiert werden, die in zugänglichen Datenbanken bisher nicht annotiert sind [26, 161]. Die hohe biologische Reproduzierbarkeit der Proteom-Analyse zeigt sich durch einen Pearson-Korrelationskoeffizienten größer als 0,8 für alle Experimente. Zusätzlich wurde die Verteilung der Phosphorylierungsstellen auf den jeweiligen Proteinen berechnet und es konnte gezeigt werden, daß hochabundante Proteine eine leichte, aber signifikante Tendenz aufweisen, stärker phosphoryliert zu werden [155]. Nur durch die kombinierte Messung von Protein-

und Phosphopeptidabundanzen konnte eine umfangreiche Normalisierung der Phosphorylierungslevel durchgeführt werden.

In der vorliegenden Arbeit wurde eine Vielzahl von aktivierten Signalwege detektiert, welche an der Zellzyklusregulation beteiligt sind. Zusätzlich konnten mehrere Kinasen und Transkriptionsfaktoren identifiziert werden, die sowohl auf Protein- und Phosphopeptidebene reguliert waren. Darüber hinaus lag der Fokus auf dem Nachweis unterschiedlich regulierter Proteine und Phosphorylierungsstellen, die für den Übergang von regenerativem Potenzial zu vollständig ausgereiften Kardiomyozyten verantwortlich sein könnten. Interessanterweise konnte eine starke Herunterregulierung aller sechs „*DNA replication licensing factors*“, MCM2-7, zwischen P10 und P20 beobachtet werden, welche zum sogenannten „*Minichromosome maintenance (MCM) complex*“ gehören. Dieser Komplex spielt eine bedeutende Rolle in der eukaryotischen DNA-Replikation [181, 182]. Darüber hinaus ergaben Clusteranalysen, dass die Phosphorylierung an den Histonen H1.2, H1.4 und H1.5 zwischen P2 bis P10 unverändert ist. Zehn Tage nach Geburt, wenn die Zellteilung zum Erliegen kommt und die Kardiomyozyten hypertrophieren, zeigt sich eine starke Herunterregulierung der Phosphorylierung dieser Histone. Da die Phosphorylierung von Histon H1 während der Mitose am Höchsten ist, könnte ein solches regulatorisches Muster einen negativen Effekt auf den mitotischen Verlauf nach P10 haben [163]. In dieser Studie zeigte sich, dass Phosphorylierungen an der Mehrzahl aller Substrate von zellzyklusregulierenden Kinasen vor und zehn Tage nach Geburt stark voneinander unterscheiden.

Insgesamt konnte eine deutliche Hochregulierung von sarkomerischen und mitochondrialen Proteinen beobachtet werden und bestätigte somit eindrucksvoll die bereits beschriebenen Mechanismen bei der Herzentwicklung [167]. Während der Anaylisen konnte ein bisher kaum charakterisiertes Protein das bisher unter dem Namen „*PGC-1 and ERR-induced regulator in muscle protein 1*“ (Perm1) annotiert ist, als ein stark phosphoryliertes Protein während der Herzentwicklung identifiziert werden. Perm1 ist bisher als ein Protein, das essentiell für die Expression von selektiven PGC-1 $\alpha$  /ERR Zielgenen in Myotuben beschrieben. Weiterhin ist Perm1 wichtig für die PGC-1 $\alpha$  induzierte Mitochondrienbiogenese und hat einen regulatorischen Einfluß auf die maximale Kapazität der oxidativen Phosphorylierung [168]. Perm1 wurde hier umbenannt zu „*MICOS complex subunit Mic85*“, da es eine robuste physikalische Wechselwirkung mit diversen MICOS-Komplex-Untereinheiten, wie Mitofilin



(Mic60), Chchd3 (Mic19), Chchd6 (Mic25) und dem äußeren Membranprotein Samm50, zeigt. Darüber hinaus ist Mic85 ein kardiomyozyten-spezifisches Protein, das eine stärkere Hochregulation von P2 bis P10 im Vergleich zu anderen MICOS-assoziierten Proteinen aufweist. Aus diesem Grund ist nicht nur eine höhere Mitochondrienmasse während der Herzentwicklung der Grund für eine erhöhte Mic85-Abundanz. Eine solche Regulation innerhalb der ersten Woche nach Geburt lässt demnach den Schluss zu, dass Mic85 einen wichtigen Faktor darstellt, der an der mitochondrialen Aktivität und Reifung beteiligt ist. Biochemische und immunhistochemische Untersuchungen bestätigten die Lokalisierung von Mic85 in den Mitochondrien. Eine submitochondriale Fraktionierung legte zudem offen, dass dieses Protein in der inneren Mitochondrienmembran sitzt und dem Intermembranraum zugewandt ist.

Über ein *pulsed* SILAC Experiment konnte ein hohe Lys6 Inkorporationsrate von Mic85 festgestellt werden. Weiterhin konnte gezeigt werden, dass die Dynamik der Mic85-Proteinexpression über das ubiquitin-proteasomale System durch Phosphorylierung der Caseinkinase 2 an vier Serin-Resten innerhalb des PEST-Motiv reguliert wird. Wenn Mic85 in kultivierten neonatalen Kardiomyozyten ausgeschaltet wird, kommt es zu einer Herunterregulation einiger Proteine, die in Proliferation, Wachstums und Proteinfaltung involviert sind. Darüber hinaus wurde die Beteiligung von endogenem Mic85 an der Regulation von oxidativer Phosphorylierung in Kardiomyozyten untersucht, wobei eine signifikante Verringerung der Sauerstoffverbrauchsrate in Mic85 „Knockdown“-Zellen zu beobachten war. Untersuchungen mittels Immunfluoreszenz-Mikroskopie ergaben, dass die Mitochondrien in „Knockdown“-Zellen morphologisch weniger dicht und länglich wurden. Zudem zeigten Kardiomyozyten mit einem Mic85-knockdown die Tendenz einer mitochondrialen, perinukleären Akkumulation, welche einer mitochondriale Dysfunktion ähnelt. In Zusammenfassung aller hier dargestellten Ergebnisse lässt sich vermuten, dass Mic85 die mitochondriale Atmung reguliert und für die Bildung einer normalen Morphologie von Mitochondrien benötigt wird.

## 5.4 Schlussfolgerung

SILAC basierte Quantifizierung ermöglicht die genaue Quantifizierung von Proteinen und Veränderungen von Phosphorylierung während der Herzentwicklung. Diese Daten zeigen eine dynamische Regulierung der Protein-Expression während der frühen postnatalen Entwicklung des Herzens. Die genaue Erfassung der quantifizierten Phosphopeptide stellt eine wertvolle Ressource für die biologische Forschung dar, auf die zukünftige Studien in der Säugerherzentwicklung und -regeneration zurückgreifen können. Hier konnte nach P10 eine Herunterregulation von verschiedenen Proteinen aufgezeigt werden, die für den Zellzyklus essentiell sind und damit einen möglichen Ursache für die reduzierte proliferative Kapazität von Kardiomyozyten darstellen. Mic85 konnte als ein neues, mitochondriales Protein identifiziert werden, das verstärkt während der postnatalen Entwicklung des Herzens hochreguliert wird, und eine neue Komponente des MICOS Komplex in Säugern darstellt. Es wurde gezeigt, dass Mic85 in Kardiomyozyten stark exprimiert wird und innerhalb des mitochondrialen Intermembranraums lokalisiert ist, in welchem es mit der inneren Membran verknüpft ist. Es wurde auch gezeigt, dass der schnelle Proteinumsatz von Mic85 durch das ubiquitin-proteasomale System über die Phosphorylierung der Casein Kinase 2 auf dessen PEST-Motiv vermittelt wird. Funktionsverlust-Studien zeigen eine eindeutige Rolle für Mic85 bei der Aufrechterhaltung des mitochondrialen Aufbaus und zur Verstärkung der Energetik in entwickelnden und adulten Maus-Kardiomyozyten. Für weitere in vivo Experimente wurde im Rahmen dieser Arbeit die Deletionsmutante von Mic85 generiert. Zur Untersuchung des Expressionsprofil von Mic85 wurde eine knock-in GFP Mausmutante durch homologe Rekombination generiert. Des Weiteren soll die Funktion dieses Proteins sowie die Integrität von Mitochondrien in den Deletionsmutanten analysiert werden.

## 6. References

1. Hall, J.E., *Guyton and Hall textbook of medical physiology*. 2010: Elsevier Health Sciences.
2. Moore, K.L., A.F. Dalley, and A.M. Agur, *Clinically oriented anatomy*. 2013: Lippincott Williams & Wilkins.
3. Carbery, I.D., et al., *Targeted genome modification in mice using zinc-finger nucleases*. *Genetics*, 2010. **186**(2): p. 451-459.
4. Sung, Y.H., et al., *Knockout mice created by TALEN-mediated gene targeting*. *Nat Biotechnol*, 2013. **31**(1): p. 23-4.
5. Yang, H., et al., *One-step generation of mice carrying reporter and conditional alleles by CRISPR/Cas-mediated genome engineering*. *Cell*, 2013. **154**(6): p. 1370-9.
6. Copp, A.J., *Death before birth: clues from gene knockouts and mutations*. *Trends in Genetics*, 1995. **11**(3): p. 87-93.
7. Rossant, J., *Mouse mutants and cardiac development: new molecular insights into cardiogenesis*. *Circ Res*, 1996. **78**(3): p. 349-53.
8. Brandon, E.P., R.L. Idzerda, and G.S. McKnight, *Targeting the mouse genome: a compendium of knockouts (Part III)*. *Curr Biol*, 1995. **5**(8): p. 873-81.
9. Brandon, E.P., R.L. Idzerda, and G.S. McKnight, *Targeting the mouse genome: a compendium of knockouts (Part II)*. *Curr Biol*, 1995. **5**(7): p. 758-65.
10. Brandon, E.P., R.L. Idzerda, and G.S. McKnight, *Knockouts. Targeting the mouse genome: a compendium of knockouts (Part I)*. *Curr Biol*, 1995. **5**(6): p. 625-34.
11. Buckingham, M., S. Meilhac, and S. Zaffran, *Building the mammalian heart from two sources of myocardial cells*. *Nat Rev Genet*, 2005. **6**(11): p. 826-35.
12. Garcia-Martinez, V. and G.C. Schoenwolf, *Primitive-streak origin of the cardiovascular system in avian embryos*. *Dev Biol*, 1993. **159**(2): p. 706-19.
13. Tam, P.P., et al., *The allocation of epiblast cells to the embryonic heart and other mesodermal lineages: the role of ingression and tissue movement during gastrulation*. *Development*, 1997. **124**(9): p. 1631-42.
14. Rawles, M.E., *The heart-forming areas of the early chick blastoderm*. *Physiological Zoology*, 1943: p. 22-43.
15. Li, F., et al., *Rapid transition of cardiac myocytes from hyperplasia to hypertrophy during postnatal development*. *J Mol Cell Cardiol*, 1996. **28**(8): p. 1737-46.
16. Walsh, S., et al., *Cardiomyocyte cell cycle control and growth estimation in vivo--an analysis based on cardiomyocyte nuclei*. *Cardiovasc Res*, 2010. **86**(3): p. 365-73.
17. Mudd, J.O. and D.A. Kass, *Tackling heart failure in the twenty-first century*. *Nature*, 2008. **451**(7181): p. 919-28.
18. Christoffels, V.M. and W.T. Pu, *Developing insights into cardiac regeneration*. *Development*, 2013. **140**(19): p. 3933-3937.
19. Drenckhahn, J.D., et al., *Compensatory growth of healthy cardiac cells in the presence of diseased cells restores tissue homeostasis during heart development*. *Dev Cell*, 2008. **15**(4): p. 521-33.
20. Bergmann, O., et al., *Evidence for cardiomyocyte renewal in humans*. *Science*, 2009. **324**(5923): p. 98-102.
21. Hsieh, P.C., et al., *Evidence from a genetic fate-mapping study that stem cells refresh adult mammalian cardiomyocytes after injury*. *Nature medicine*, 2007. **13**(8): p. 970-974.
22. Pasumarthi, K.B., et al., *Targeted expression of cyclin D2 results in cardiomyocyte DNA synthesis and infarct regression in transgenic mice*. *Circulation research*, 2005. **96**(1): p. 110-118.
23. Quaini, F., et al., *Chimerism of the transplanted heart*. *N Engl J Med*, 2002. **346**(1): p. 5-15.

24. Porrello, E.R., et al., *Transient regenerative potential of the neonatal mouse heart*. Science, 2011. **331**(6020): p. 1078-80.
25. Puente, B.N., et al., *The oxygen-rich postnatal environment induces cardiomyocyte cell-cycle arrest through DNA damage response*. Cell, 2014. **157**(3): p. 565-79.
26. Huttlin, E.L., et al., *A tissue-specific atlas of mouse protein phosphorylation and expression*. Cell, 2010. **143**(7): p. 1174-89.
27. Lundby, A., et al., *Quantitative maps of protein phosphorylation sites across 14 different rat organs and tissues*. Nat Commun, 2012. **3**: p. 876.
28. Wheeler-Jones, C.P., *Cell signalling in the cardiovascular system: an overview*. Heart, 2005. **91**(10): p. 1366-74.
29. Olsen, J.V., et al., *Quantitative phosphoproteomics reveals widespread full phosphorylation site occupancy during mitosis*. Sci Signal, 2010. **3**(104): p. ra3.
30. Manning, G., et al., *The protein kinase complement of the human genome*. Science, 2002. **298**(5600): p. 1912-34.
31. Woodgett, J.R. *Regulation and functions of the glycogen synthase kinase-3 subfamily*. in *Seminars in cancer biology*. 1994.
32. Avruch, J., et al., *Ras activation of the Raf kinase: tyrosine kinase recruitment of the MAP kinase cascade*. Recent Progress in Hormone Research, 2001(56): p. 127-55.
33. Ruehr, M.L., M.A. Russell, and M. Bond, *A-kinase anchoring protein targeting of protein kinase A in the heart*. J Mol Cell Cardiol, 2004. **37**(3): p. 653-65.
34. Rockman, H.A., W.J. Koch, and R.J. Lefkowitz, *Seven-transmembrane-spanning receptors and heart function*. Nature, 2002. **415**(6868): p. 206-12.
35. Lincoln, T.M., N. Dey, and H. Sellak, *Invited review: cGMP-dependent protein kinase signaling mechanisms in smooth muscle: from the regulation of tone to gene expression*. Journal of applied physiology, 2001. **91**(3): p. 1421-1430.
36. Gray, M.O., J.S. Karliner, and D. Mochly-Rosen, *A selective  $\epsilon$ -protein kinase C antagonist inhibits protection of cardiac myocytes from hypoxia-induced cell death*. Journal of Biological Chemistry, 1997. **272**(49): p. 30945-30951.
37. Pyle, W.G., Y. Chen, and P.A. Hofmann, *Cardioprotection through a PKC-dependent decrease in myofilament ATPase*. American Journal of Physiology-Heart and Circulatory Physiology, 2003. **285**(3): p. H1220-H1228.
38. Hahn, H.S., et al., *Protein kinase Ca negatively regulates systolic and diastolic function in pathological hypertrophy*. Circulation research, 2003. **93**(11): p. 1111-1119.
39. Yin, G., C. Yan, and B.C. Berk, *Angiotensin II signaling pathways mediated by tyrosine kinases*. Int J Biochem Cell Biol, 2003. **35**(6): p. 780-3.
40. Crone, S.A., et al., *ErbB2 is essential in the prevention of dilated cardiomyopathy*. Nature medicine, 2002. **8**(5): p. 459-465.
41. Raju, R.V., et al., *Biological significance of phosphorylation and myristoylation in the regulation of cardiac muscle proteins*. Mol Cell Biochem, 1997. **176**(1-2): p. 135-43.
42. Heineke, J. and J.D. Molkentin, *Regulation of cardiac hypertrophy by intracellular signalling pathways*. Nat Rev Mol Cell Biol, 2006. **7**(8): p. 589-600.
43. Pohjoismaki, J.L., et al., *Postnatal cardiomyocyte growth and mitochondrial reorganization cause multiple changes in the proteome of human cardiomyocytes*. Mol Biosyst, 2013. **9**(6): p. 1210-9.
44. Lopaschuk, G.D., M.A. Spafford, and D.R. Marsh, *Glycolysis is predominant source of myocardial ATP production immediately after birth*. American Journal of Physiology-Heart and Circulatory Physiology, 1991. **261**(6): p. H1698-H1705.
45. Agata, Y., et al., *Changes in left ventricular output from fetal to early neonatal life*. J Pediatr, 1991. **119**(3): p. 441-5.
46. Lopaschuk, G.D. and J.S. Jaswal, *Energy metabolic phenotype of the cardiomyocyte during development, differentiation, and postnatal maturation*. J Cardiovasc Pharmacol, 2010. **56**(2): p. 130-40.

47. Lai, L., et al., *Transcriptional coactivators PGC-1alpha and PGC-1beta control overlapping programs required for perinatal maturation of the heart*. *Genes Dev*, 2008. **22**(14): p. 1948-61.
48. Bach, D., et al., *Mitofusin-2 determines mitochondrial network architecture and mitochondrial metabolism. A novel regulatory mechanism altered in obesity*. *J Biol Chem*, 2003. **278**(19): p. 17190-7.
49. McBride, H. and L. Scorrano, *Mitochondrial dynamics and physiology*. *Biochim Biophys Acta*, 2013. **1833**(1): p. 148-9.
50. Papanicolaou, K.N., et al., *Mitofusins 1 and 2 are essential for postnatal metabolic remodeling in heart*. *Circ Res*, 2012. **111**(8): p. 1012-26.
51. Hales, K., *Mitochondrial fusion and division*. *Nature Education*, 2010. **3**(9): p. 12.
52. Rowe, G.C., A. Jiang, and Z. Arany, *PGC-1 coactivators in cardiac development and disease*. *Circ Res*, 2010. **107**(7): p. 825-38.
53. Jornayvaz, F.R. and G.I. Shulman, *Regulation of mitochondrial biogenesis*. *Essays Biochem*, 2010. **47**: p. 69-84.
54. Morita, M., et al., *mTORC1 controls mitochondrial activity and biogenesis through 4E-BP-dependent translational regulation*. *Cell metabolism*, 2013. **18**(5): p. 698-711.
55. Lombard, D.B., D.X. Tishkoff, and J. Bao, *Mitochondrial sirtuins in the regulation of mitochondrial activity and metabolic adaptation*. *Handb Exp Pharmacol*, 2011. **206**: p. 163-88.
56. Senyilmaz, D., et al., *Regulation of mitochondrial morphology and function by stearylolation of TFR1*. *Nature*, 2015.
57. Fvasconcellos. *Schematic diagram of the mitochondrial electron transport chain*. 2007 12 July 2015]; Available from: [https://en.wikipedia.org/wiki/File:Mitochondrial\\_electron\\_transport\\_chain%E2%80%944.svg](https://en.wikipedia.org/wiki/File:Mitochondrial_electron_transport_chain%E2%80%944.svg).
58. Lowenstein, J.M., *Methods in Enzymology: Citric Acid Cycle*. 1969: Academic Press.
59. Mayes, P.A. and K.M. Botham, *The respiratory chain & oxidative phosphorylation*. Harper's Biochemistry. 23rd ed. East Norwalk, Connecticut: Appleton and Lange, Prentice-Hall International, Inc, 1993: p. 119-130.
60. Mitchell, P. and J. Moyle, *Chemiosmotic hypothesis of oxidative phosphorylation*. *Nature*, 1967. **213**(5072): p. 137-9.
61. Palade, G.E., *The fine structure of mitochondria*. *Anat Rec*, 1952. **114**(3): p. 427-51.
62. Schatz, G., *The protein import system of mitochondria*. *J Biol Chem*, 1996. **271**(50): p. 31763-6.
63. Neupert, W. and J.M. Herrmann, *Translocation of proteins into mitochondria*. *Annu. Rev. Biochem.*, 2007. **76**: p. 723-749.
64. Chacinska, A., et al., *Importing mitochondrial proteins: machineries and mechanisms*. *Cell*, 2009. **138**(4): p. 628-44.
65. Frey, T.G. and C.A. Mannella, *The internal structure of mitochondria*. *Trends Biochem Sci*, 2000. **25**(7): p. 319-24.
66. Hoppins, S., L. Lackner, and J. Nunnari, *The machines that divide and fuse mitochondria*. *Annu. Rev. Biochem.*, 2007. **76**: p. 751-780.
67. Perkins, G., et al., *Electron tomography of neuronal mitochondria: three-dimensional structure and organization of cristae and membrane contacts*. *J Struct Biol*, 1997. **119**(3): p. 260-72.
68. Connerth, M., et al., *Intramitochondrial transport of phosphatidic acid in yeast by a lipid transfer protein*. *Science*, 2012. **338**(6108): p. 815-8.
69. von der Malsburg, K., et al., *Dual role of mitofilin in mitochondrial membrane organization and protein biogenesis*. *Developmental cell*, 2011. **21**(4): p. 694-707.

70. Hoppins, S., et al., *A mitochondrial-focused genetic interaction map reveals a scaffold-like complex required for inner membrane organization in mitochondria*. J Cell Biol, 2011. **195**(2): p. 323-40.
71. Pfanner, N., et al., *Uniform nomenclature for the mitochondrial contact site and cristae organizing system*. J Cell Biol, 2014. **204**(7): p. 1083-6.
72. John, G.B., et al., *The mitochondrial inner membrane protein mitofilin controls cristae morphology*. Mol Biol Cell, 2005. **16**(3): p. 1543-54.
73. Rabl, R., et al., *Formation of cristae and crista junctions in mitochondria depends on antagonism between Fcj1 and Su e/g*. The Journal of cell biology, 2009. **185**(6): p. 1047-1063.
74. Alkhaja, A.K., et al., *MINOS1 is a conserved component of mitofilin complexes and required for mitochondrial function and cristae organization*. Molecular biology of the cell, 2012. **23**(2): p. 247-257.
75. An, J., et al., *CHCM1/CHCHD6, novel mitochondrial protein linked to regulation of mitofilin and mitochondrial cristae morphology*. J Biol Chem, 2012. **287**(10): p. 7411-26.
76. Darshi, M., et al., *ChChd3, an inner mitochondrial membrane protein, is essential for maintaining crista integrity and mitochondrial function*. Journal of biological chemistry, 2011. **286**(4): p. 2918-2932.
77. Weber, T.A., et al., *APOOL is a cardiolipin-binding constituent of the Mitofilin/MINOS protein complex determining cristae morphology in mammalian mitochondria*. PloS one, 2013. **8**(5): p. e63683.
78. Körner, C., et al., *The C-terminal domain of Fcj1 is required for formation of crista junctions and interacts with the TOB/SAM complex in mitochondria*. Molecular biology of the cell, 2012. **23**(11): p. 2143-2155.
79. Ott, C., et al., *Sam50 functions in mitochondrial intermembrane space bridging and biogenesis of respiratory complexes*. Mol Cell Biol, 2012. **32**(6): p. 1173-88.
80. Xie, J., et al., *The mitochondrial inner membrane protein mitofilin exists as a complex with SAM50, metaxins 1 and 2, coiled-coil-helix coiled-coil-helix domain-containing protein 3 and 6 and DnaJC11*. FEBS letters, 2007. **581**(18): p. 3545-3549.
81. Karas, M., D. Bachmann, and F. Hillenkamp, *Influence of the wavelength in high-irradiance ultraviolet laser desorption mass spectrometry of organic molecules*. Analytical Chemistry, 1985. **57**(14): p. 2935-2939.
82. Karas, M., et al., *Matrix-assisted ultraviolet laser desorption of non-volatile compounds*. International journal of mass spectrometry and ion processes, 1987. **78**: p. 53-68.
83. Dole, M., et al., *Molecular beams of macroions*. The Journal of Chemical Physics, 1968. **49**(5): p. 2240-2249.
84. Pramanik, B.N., A.K. Ganguly, and M.L. Gross, *Applied electrospray mass spectrometry: practical spectroscopy series*. Vol. 32. 2002: CRC Press.
85. Alves, P., et al. *Advancement in protein inference from shotgun proteomics using peptide detectability*. in *Pacific Symposium on Biocomputing*. 2007. World Scientific.
86. Wolters, D.A., M.P. Washburn, and J.R. Yates, *An automated multidimensional protein identification technology for shotgun proteomics*. Analytical chemistry, 2001. **73**(23): p. 5683-5690.
87. Nesvizhskii, A.I., *Protein identification by tandem mass spectrometry and sequence database searching*. Methods Mol Biol, 2007. **367**: p. 87-119.
88. O'Farrell, P.H., *High resolution two-dimensional electrophoresis of proteins*. Journal of biological chemistry, 1975. **250**(10): p. 4007-4021.
89. Fournier, M.L., et al., *Multidimensional separations-based shotgun proteomics*. Chem Rev, 2007. **107**(8): p. 3654-86.
90. Foster, L.J. and M. Mann, *Protein identification and sequencing by mass spectrometry*. Cell Biology: A Laboratory Handbook. Volume, 2005. **4**(3).
91. Shevchenko, A., et al., *Mass spectrometric sequencing of proteins silver-stained polyacrylamide gels*. Anal Chem, 1996. **68**(5): p. 850-8.

92. Shevchenko, A., et al., *In-gel digestion for mass spectrometric characterization of proteins and proteomes*. Nat Protoc, 2006. **1**(6): p. 2856-60.
93. Aebersold, R. and M. Mann, *Mass spectrometry-based proteomics*. Nature, 2003. **422**(6928): p. 198-207.
94. Ens, W., et al., *Archived polyacrylamide gels as a resource for proteome characterization by mass spectrometry*. Electrophoresis, 2001. **22**: p. 1194-1203.
95. Wisniewski, J.R., et al., *Universal sample preparation method for proteome analysis*. Nat Methods, 2009. **6**(5): p. 359-62.
96. Rappsilber, J., M. Mann, and Y. Ishihama, *Protocol for micro-purification, enrichment, pre-fractionation and storage of peptides for proteomics using StageTips*. Nature protocols, 2007. **2**(8): p. 1896-1906.
97. Cox, J., et al., *Andromeda: a peptide search engine integrated into the MaxQuant environment*. Journal of proteome research, 2011. **10**(4): p. 1794-1805.
98. Cox, J. and M. Mann, *MaxQuant enables high peptide identification rates, individualized p.p.b.-range mass accuracies and proteome-wide protein quantification*. Nat Biotechnol, 2008. **26**(12): p. 1367-72.
99. Wu, C.C. and M.J. MacCoss, *Shotgun proteomics: tools for the analysis of complex biological systems*. Curr Opin Mol Ther, 2002. **4**(3): p. 242-50.
100. Bantscheff, M., et al., *Quantitative mass spectrometry in proteomics: a critical review*. Anal Bioanal Chem, 2007. **389**(4): p. 1017-31.
101. Ong, S.E. and M. Mann, *Mass spectrometry-based proteomics turns quantitative*. Nat Chem Biol, 2005. **1**(5): p. 252-62.
102. Zhang, B., et al., *Detecting differential and correlated protein expression in label-free shotgun proteomics*. J Proteome Res, 2006. **5**(11): p. 2909-18.
103. Bantscheff, M., et al., *Quantitative mass spectrometry in proteomics: critical review update from 2007 to the present*. Anal Bioanal Chem, 2012. **404**(4): p. 939-65.
104. Ong, S.-E., et al., *Stable isotope labeling by amino acids in cell culture, SILAC, as a simple and accurate approach to expression proteomics*. Molecular & cellular proteomics, 2002. **1**(5): p. 376-386.
105. Beynon, R.J. and J.M. Pratt, *Metabolic labeling of proteins for proteomics*. Mol Cell Proteomics, 2005. **4**(7): p. 857-72.
106. Geiger, T., et al., *Use of stable isotope labeling by amino acids in cell culture as a spike-in standard in quantitative proteomics*. Nature protocols, 2011. **6**(2): p. 147-157.
107. Gouw, J.W., J. Krijgsveld, and A.J. Heck, *Quantitative proteomics by metabolic labeling of model organisms*. Molecular & cellular proteomics, 2010. **9**(1): p. 11-24.
108. Krüger, M., et al., *SILAC mouse for quantitative proteomics uncovers kindlin-3 as an essential factor for red blood cell function*. Cell, 2008. **134**(2): p. 353-364.
109. Olsen, J.V., et al., *Global, in vivo, and site-specific phosphorylation dynamics in signaling networks*. Cell, 2006. **127**(3): p. 635-648.
110. Choudhary, C. and M. Mann, *Decoding signalling networks by mass spectrometry-based proteomics*. Nat Rev Mol Cell Biol, 2010. **11**(6): p. 427-39.
111. Beausoleil, S.A., et al., *Large-scale characterization of HeLa cell nuclear phosphoproteins*. Proc Natl Acad Sci U S A, 2004. **101**(33): p. 12130-5.
112. Zarei, M., et al., *Comparison of ERLIC-TiO<sub>2</sub>, HILIC-TiO<sub>2</sub>, and SCX-TiO<sub>2</sub> for global phosphoproteomics approaches*. J Proteome Res, 2011. **10**(8): p. 3474-83.
113. Michalski, A., et al., *Mass spectrometry-based proteomics using Q Exactive, a high-performance benchtop quadrupole Orbitrap mass spectrometer*. Molecular & Cellular Proteomics, 2011. **10**(9): p. M111. 011015.
114. Olsen, J.V., et al., *Global, in vivo, and site-specific phosphorylation dynamics in signaling networks*. Cell, 2006. **127**(3): p. 635-48.

115. Rigbolt, K.T., et al., *System-wide temporal characterization of the proteome and phosphoproteome of human embryonic stem cell differentiation*. *Sci Signal*, 2011. **4**(164): p. rs3.
116. Di Palma, S., et al., *Zwitterionic hydrophilic interaction liquid chromatography (ZIC-HILIC and ZIC-CHILIC) provide high resolution separation and increase sensitivity in proteome analysis*. *Analytical chemistry*, 2011. **83**(9): p. 3440-3447.
117. Hao, P., et al., *Novel application of electrostatic repulsion-hydrophilic interaction chromatography (ERLIC) in shotgun proteomics: comprehensive profiling of rat kidney proteome*. *Journal of proteome research*, 2010. **9**(7): p. 3520-3526.
118. Batth, T.S., C. Francavilla, and J.V. Olsen, *Off-line high-pH reversed-phase fractionation for in-depth phosphoproteomics*. *J Proteome Res*, 2014. **13**(12): p. 6176-86.
119. Wu, R., et al., *Correct interpretation of comprehensive phosphorylation dynamics requires normalization by protein expression changes*. *Mol Cell Proteomics*, 2011. **10**(8): p. M111009654.
120. Michalski, A., J. Cox, and M. Mann, *More than 100,000 detectable peptide species elute in single shotgun proteomics runs but the majority is inaccessible to data-dependent LC-MS/MS*. *Journal of proteome research*, 2011. **10**(4): p. 1785-1793.
121. Köcher, T., R. Swart, and K. Mechtler, *Ultra-high-pressure RPLC hyphenated to an LTQ-Orbitrap Velos reveals a linear relation between peak capacity and number of identified peptides*. *Analytical chemistry*, 2011. **83**(7): p. 2699-2704.
122. Domon, B. and R. Aebersold, *Mass spectrometry and protein analysis*. *science*, 2006. **312**(5771): p. 212-217.
123. Mann, M. and N.L. Kelleher, *Precision proteomics: the case for high resolution and high mass accuracy*. *Proceedings of the National Academy of Sciences*, 2008. **105**(47): p. 18132-18138.
124. Wolf-Yadlin, A., et al., *Multiple reaction monitoring for robust quantitative proteomic analysis of cellular signaling networks*. *Proceedings of the National Academy of Sciences*, 2007. **104**(14): p. 5860-5865.
125. Addona, T.A., et al., *Multi-site assessment of the precision and reproducibility of multiple reaction monitoring-based measurements of proteins in plasma*. *Nature biotechnology*, 2009. **27**(7): p. 633-641.
126. Picotti, P., et al., *Full dynamic range proteome analysis of *S. cerevisiae* by targeted proteomics*. *Cell*, 2009. **138**(4): p. 795-806.
127. Louris, J.N., et al., *Instrumentation, applications, and energy deposition in quadrupole ion-trap tandem mass spectrometry*. *Analytical Chemistry*, 1987. **59**(13): p. 1677-1685.
128. Hardman, M. and A.A. Makarov, *Interfacing the orbitrap mass analyzer to an electrospray ion source*. *Anal Chem*, 2003. **75**(7): p. 1699-705.
129. Makarov, A., *Electrostatic axially harmonic orbital trapping: a high-performance technique of mass analysis*. *Analytical chemistry*, 2000. **72**(6): p. 1156-1162.
130. Scigelova, M. and A. Makarov, *Orbitrap mass analyzer--overview and applications in proteomics*. *Proteomics*, 2006. **6 Suppl 2**: p. 16-21.
131. Syka, J.E., et al., *Novel linear quadrupole ion trap/FT mass spectrometer: performance characterization and use in the comparative analysis of histone H3 post-translational modifications*. *Journal of proteome research*, 2004. **3**(3): p. 621-626.
132. Makarov, A., et al., *Dynamic range of mass accuracy in LTQ Orbitrap hybrid mass spectrometer*. *J Am Soc Mass Spectrom*, 2006. **17**(7): p. 977-82.
133. Makarov, A., et al., *Performance evaluation of a hybrid linear ion trap/orbitrap mass spectrometer*. *Anal Chem*, 2006. **78**(7): p. 2113-20.
134. Olsen, J.V., et al., *A dual pressure linear ion trap Orbitrap instrument with very high sequencing speed*. *Molecular & cellular proteomics*, 2009. **8**(12): p. 2759-2769.
135. Olsen, J.V., et al., *Higher-energy C-trap dissociation for peptide modification analysis*. *Nat Methods*, 2007. **4**(9): p. 709-12.



136. Macek, B., et al., *Top-down protein sequencing and MS3 on a hybrid linear quadrupole ion trap-orbitrap mass spectrometer*. Mol Cell Proteomics, 2006. **5**(5): p. 949-58.
137. McAlister, G.C., et al., *A proteomics grade electron transfer dissociation-enabled hybrid linear ion trap-orbitrap mass spectrometer*. J Proteome Res, 2008. **7**(8): p. 3127-36.
138. McAlister, G.C., et al., *Higher-energy collision-activated dissociation without a dedicated collision cell*. Molecular & Cellular Proteomics, 2011. **10**(5): p. O111. 009456.
139. Geiger, T., J. Cox, and M. Mann, *Proteomics on an Orbitrap benchtop mass spectrometer using all-ion fragmentation*. Molecular & Cellular Proteomics, 2010. **9**(10): p. 2252-2261.
140. Lange, O., et al. *Accelerating spectral acquisition rate of Orbitrap mass spectrometry*. in *Proc. 58th Conf. Amer. Soc. Mass Spectrom.* 2010.
141. Scheltema, R.A., et al., *The Q exactive HF, a benchtop mass spectrometer with a pre-filter, high-performance quadrupole and an ultra-high-field orbitrap analyzer*. Molecular & Cellular Proteomics, 2014. **13**(12): p. 3698-3708.
142. Lowry, O.H., et al., *Protein measurement with the Folin phenol reagent*. J Biol Chem, 1951. **193**(1): p. 265-75.
143. Villen, J., et al., *Large-scale phosphorylation analysis of mouse liver*. Proc Natl Acad Sci U S A, 2007. **104**(5): p. 1488-93.
144. Kawahara, M., H. Nakamura, and T. Nakajima, *Titania and zirconia: possible new ceramic microparticulates for high-performance liquid chromatography*. Journal of Chromatography A, 1990. **515**: p. 149-158.
145. Tani, K. and Y. Suzuki, *Syntheses of spherical silica and titania from alkoxides on a laboratory scale*. Chromatographia, 1994. **38**(5-6): p. 291-294.
146. Tani, K. and Y. Suzuki, *Investigation of the ion-exchange behaviour of titania: Application as a packing material for ion chromatography*. Chromatographia, 1997. **46**(11-12): p. 623-627.
147. Jiang, Z.-T. and Y.-M. Zuo, *Synthesis of porous titania microspheres for HPLC packings by polymerization-induced colloid aggregation (PICA)*. Analytical chemistry, 2001. **73**(3): p. 686-688.
148. MATSUDA, H., H. NAKAMURA, and T. NAKAJIMA, *New ceramic titania: Selective adsorbent for organic phosphates*. Analytical sciences, 1990. **6**(6): p. 911-912.
149. Ikeguchi, Y. and H. NAKAMURA, *Selective Enrichment of Phospholipids by Titania*. Analytical sciences, 2000. **16**(5): p. 541-543.
150. Ikeguchi, Y. and H. Nakamura, *Determination of Organic Phosphates by Column-Switching High Performance Anion-Exchange Chromatography Using On-Line Preconcentration on Titania*. Analytical sciences, 1997. **13**(3): p. 479-483.
151. KAWAHARA, M., H. NAKAMURA, and T. NAKAJIMA, *Group separation of ribonucleosides and deoxyribonucleosides on a new ceramic titania column*. Analytical sciences, 1989. **5**(6): p. 763-764.
152. Pinkse, M.W., et al., *Selective isolation at the femtomole level of phosphopeptides from proteolytic digests using 2D-NanoLC-ESI-MS/MS and titanium oxide precolumns*. Analytical chemistry, 2004. **76**(14): p. 3935-3943.
153. Larsen, M.R., et al., *Highly selective enrichment of phosphorylated peptides from peptide mixtures using titanium dioxide microcolumns*. Molecular & Cellular Proteomics, 2005. **4**(7): p. 873-886.
154. Thingholm, T.E., et al., *Highly selective enrichment of phosphorylated peptides using titanium dioxide*. Nature protocols, 2006. **1**(4): p. 1929-1935.
155. Sharma, K., et al., *Ultradeep human phosphoproteome reveals a distinct regulatory nature of Tyr and Ser/Thr-based signaling*. Cell Rep, 2014. **8**(5): p. 1583-94.
156. Pohjoismäki, J.L., et al., *Human heart mitochondrial DNA is organized in complex catenated networks containing abundant four-way junctions and replication forks*. Journal of Biological Chemistry, 2009. **284**(32): p. 21446-21457.
157. Fujiki, Y., et al., *Isolation of intracellular membranes by means of sodium carbonate treatment: application to endoplasmic reticulum*. J Cell Biol, 1982. **93**(1): p. 97-102.

158. Kozjak-Pavlovic, V., et al., *C1orf163/RESA1 Is a Novel Mitochondrial Intermembrane Space Protein Connected to Respiratory Chain Assembly*. Journal of molecular biology, 2014. **426**(4): p. 908-920.
159. Nemoto, Y. and P. De Camilli, *Recruitment of an alternatively spliced form of synaptojanin 2 to mitochondria by the interaction with the PDZ domain of a mitochondrial outer membrane protein*. EMBO J, 1999. **18**(11): p. 2991-3006.
160. Lörchner, H., et al., *Myocardial healing requires Reg3 [beta]-dependent accumulation of macrophages in the ischemic heart*. Nature medicine, 2015. **21**(4): p. 353-362.
161. Hornbeck, P.V., et al., *PhosphoSitePlus, 2014: mutations, PTMs and recalibrations*. Nucleic Acids Res, 2015. **43**(Database issue): p. D512-20.
162. Songyang, Z., et al., *Use of an oriented peptide library to determine the optimal substrates of protein kinases*. Curr Biol, 1994. **4**(11): p. 973-82.
163. Sarg, B., et al., *Histone H1 Phosphorylation Occurs Site-specifically during Interphase and Mitosis IDENTIFICATION OF A NOVEL PHOSPHORYLATION SITE ON HISTONE H1*. Journal of Biological Chemistry, 2006. **281**(10): p. 6573-6580.
164. Lee, E.H., et al., *Mechanical strength of the titin Z1Z2-telethonin complex*. Structure, 2006. **14**(3): p. 497-509.
165. Kotter, S., et al., *Differential changes in titin domain phosphorylation increase myofilament stiffness in failing human hearts*. Cardiovasc Res, 2013. **99**(4): p. 648-56.
166. Hidalgo, C. and H. Granzier, *Tuning the molecular giant titin through phosphorylation: role in health and disease*. Trends Cardiovasc Med, 2013. **23**(5): p. 165-71.
167. Dobрева, G. and T. Braun, *The transcriptional landscape of regenerating newborn mouse hearts*. Circ Res, 2015. **116**(5): p. 767-9.
168. Cho, Y., et al., *PGC-1 and ERR-induced Regulator in Muscle 1 (PERM1) is a tissue-specific regulator of oxidative capacity in skeletal muscle cells*. Journal of Biological Chemistry, 2013: p. jbc. M113. 489674.
169. Kosugi, S., et al., *Systematic identification of cell cycle-dependent yeast nucleocytoplasmic shuttling proteins by prediction of composite motifs*. Proc Natl Acad Sci U S A, 2009. **106**(25): p. 10171-6.
170. Rechsteiner, M. and S.W. Rogers, *PEST sequences and regulation by proteolysis*. Trends Biochem Sci, 1996. **21**(7): p. 267-71.
171. Polyakova, V., et al., *Distinct structural and molecular features of the myocardial extracellular matrix remodeling in compensated and decompensated cardiac hypertrophy due to aortic stenosis*. IJC Heart & Vessels, 2014. **4**: p. 145-160.
172. Srinivasan, S., *A method to fix and permeabilize isolated adult mouse cardiomyocytes for immuno-staining and confocal imaging*. Nature Protocol Exchange, 2011. **235**.
173. Blom, N., et al., *Prediction of post-translational glycosylation and phosphorylation of proteins from the amino acid sequence*. Proteomics, 2004. **4**(6): p. 1633-49.
174. Rogers, S., R. Wells, and M. Rechsteiner, *Amino acid sequences common to rapidly degraded proteins: the PEST hypothesis*. Science, 1986. **234**(4774): p. 364-8.
175. Garcia-Alai, M.M., et al., *Molecular basis for phosphorylation-dependent, PEST-mediated protein turnover*. Structure, 2006. **14**(2): p. 309-19.
176. Bragoszewski, P., et al., *The ubiquitin-proteasome system regulates mitochondrial intermembrane space proteins*. Mol Cell Biol, 2013. **33**(11): p. 2136-48.
177. Patel, M.S. and L.G. Korotchkina, *Regulation of mammalian pyruvate dehydrogenase complex by phosphorylation: complexity of multiple phosphorylation sites and kinases*. Exp Mol Med, 2001. **33**(4): p. 191-7.
178. Roche, T.E. and Y. Hiromasa, *Pyruvate dehydrogenase kinase regulatory mechanisms and inhibition in treating diabetes, heart ischemia, and cancer*. Cell Mol Life Sci, 2007. **64**(7-8): p. 830-49.
179. Piquereau, J., et al., *Postnatal development of mouse heart: formation of energetic microdomains*. J Physiol, 2010. **588**(Pt 13): p. 2443-54.

180. Nielsen, J., et al., *A family of insulin-like growth factor II mRNA-binding proteins represses translation in late development*. Mol Cell Biol, 1999. **19**(2): p. 1262-70.
181. Labib, K., J.A. Tercero, and J.F. Diffley, *Uninterrupted MCM2-7 function required for DNA replication fork progression*. Science, 2000. **288**(5471): p. 1643-7.
182. Bell, S.P. and A. Dutta, *DNA replication in eukaryotic cells*. Annu Rev Biochem, 2002. **71**: p. 333-74.
183. Qiu, J., et al., *Coupling of mitochondrial import and export translocases by receptor-mediated supercomplex formation*. Cell, 2013. **154**(3): p. 596-608.
184. Hell, K., *The Erv1-Mia40 disulfide relay system in the intermembrane space of mitochondria*. Biochim Biophys Acta, 2008. **1783**(4): p. 601-9.
185. Schmidt, O., et al., *Regulation of mitochondrial protein import by cytosolic kinases*. Cell, 2011. **144**(2): p. 227-39.
186. Herrmann, J.M. and J. Riemer, *Mitochondrial disulfide relay: redox-regulated protein import into the intermembrane space*. Journal of Biological Chemistry, 2012. **287**(7): p. 4426-4433.
187. Kanamaru, Y., et al., *The phosphorylation-dependent regulation of mitochondrial proteins in stress responses*. J Signal Transduct, 2012. **2012**: p. 931215.
188. Zhao, X., et al., *Phosphoproteome analysis of functional mitochondria isolated from resting human muscle reveals extensive phosphorylation of inner membrane protein complexes and enzymes*. Mol Cell Proteomics, 2011. **10**(1): p. M110 000299.
189. Escobar-Henriques, M., B. Westermann, and T. Langer, *Regulation of mitochondrial fusion by the F-box protein Mdm30 involves proteasome-independent turnover of Fzo1*. J Cell Biol, 2006. **173**(5): p. 645-50.
190. Margineantu, D.H., et al., *Hsp90 inhibition decreases mitochondrial protein turnover*. PLoS One, 2007. **2**(10): p. e1066.
191. Karbowski, M. and R.J. Youle, *Regulating mitochondrial outer membrane proteins by ubiquitination and proteasomal degradation*. Curr Opin Cell Biol, 2011. **23**(4): p. 476-82.
192. Burtscher, J., et al., *Differences in mitochondrial function in homogenated samples from healthy and epileptic specific brain tissues revealed by high-resolution respirometry*. Mitochondrion, 2015. **25**: p. 104-112.
193. Singh, S.K., et al., *Proteome mapping of adult zebrafish marrow neutrophils reveals partial cross species conservation to human peripheral neutrophils*. PloS one, 2013. **8**(9): p. e73998.
194. Hayashi, T., et al., *Tcap gene mutations in hypertrophic cardiomyopathy and dilated cardiomyopathy*. Journal of the American College of Cardiology, 2004. **44**(11): p. 2192-2201.
195. Moreira, E.S., et al., *Limb-girdle muscular dystrophy type 2G is caused by mutations in the gene encoding the sarcomeric protein telethonin*. Nature genetics, 2000. **24**(2): p. 163-166.
196. Candasamy, A.J., et al., *Phosphoregulation of the titin-cap protein telethonin in cardiac myocytes*. J Biol Chem, 2014. **289**(3): p. 1282-93.
197. Singh, S.K., et al., *Proteome dynamics in neutrophils of adult zebrafish upon chemically-induced inflammation*. Fish & shellfish immunology, 2014. **40**(1): p. 217-224.

## 7. Curriculum Vitae

### SRIRAM ARAVAMUDHAN

Alexander Dubcekplaats 50, 2332 HX Leiden, The Netherlands  
(31) 657579316 • sriram.aravamudhan@cellsignal.com

#### Work Experience

---

**Sep 2015-present**      **Cell Signaling Technology Europe, Leiden, The Netherlands**  
*Field Application Specialist*

#### Education

---

**Expected Early 2016**      **Max Plank Institute for Heart and Lung Research, Bad Nauheim, Germany**  
*PhD, Mass Spectrometry-based Proteomics*

**Sep 2011**      **University of Edinburgh, United Kingdom**  
*MSc, Drug Discovery and Translational Biology*  
Second-class honours, upper division (2:1)

**May 2010**      **SASTRA University, Thanjavur, India**  
*B.Tech (Hons.), Bioinformatics*  
First class with distinction

#### Research Experience

---

**Nov 2011-Aug 2015**      **Max Plank Institute for Heart and Lung Research, Bad Nauheim, Germany**  
*PhD thesis*

- Investigated the regulation of global proteome and phosphorylation during post-natal heart development in mice using *in vivo* SILAC based quantification
- Characterized a novel mitochondrial protein regulated during heart development based on localization, interactome screening, biochemical assays and loss of function studies
- Performed an integrated quantitative analysis of proteome, ubiquitinome and protein turnover of skeletal muscle following denervation-induced atrophy in mice

**May-Aug 2011**      **University of Edinburgh, United Kingdom**  
*Postgraduate thesis*  
Applied computer-aided drug design methodologies to study the binding specificity of cyclophilin inhibitors

**Dec 2009-Mar 2010**      **National University of Singapore, Singapore**  
*Undergraduate thesis*  
Constructed support vector machine models to predict dual inhibitors of GSK3 and CDK1/CDK2 as an *in silico* approach to multi-target drug discovery

**Summer 2009**      **Indian Institute of Science, Bangalore, India**  
**Summer research fellow**  
 Mathematically modelled enfuvirtide pharmacokinetics, adherence and resistance to study viral load decay under antiretroviral therapy

## Achievements

---

- Accomplished the graduate program of International Max Planck Research School for Heart and Lung Research in 2014 that comprised of lecture series, methods seminars, soft skills, progress reports and annual retreats
- Best outgoing student of the Department of Bioinformatics among the Class of 2010 in SASTRA University
- Ranked first in the B.Tech Bioinformatics program and attained the Dean's merit list of top 2% students in the school
- Granted summer research fellowship for short term project in the Indian Institute of Science
- Won the first prize for the presentation on 'Focus on genomics as a tool to eradicate Vitiligo' at a symposium held in Dr. MGR Educational and Research Institute, Chennai, India in 2008

## Conferences and Meetings

---

- 2014**      **HUPO Annual World Congress, Madrid, Spain**  
 Oral presentation on 'Phosphoproteomic profiling of post-natal heart development unravels a novel mitochondrial protein associated with the MINOS complex'
- 2013**      **ASMS Annual Conference for Mass Spectrometry, Minneapolis, USA**  
 Poster presentation on 'Integrated analysis of proteome and ubiquitinome of skeletal muscle following denervation-induced atrophy'
- 2012**      **Computational Mass Spectrometry-Based Proteomics, Munich, Germany**  
 MaxQuant summer school – hands on training in computational analysis of proteomics data generated by high-resolution mass spectrometry
- 2012**      **Keystone Symposium on Proteomics and Interactomics, Stockholm, Sweden**  
 Poster presentation on 'Quantitative proteomic analysis of denervation-induced muscle atrophy using *in vivo* SILAC'
- 2011**      **ScotCHEM Computational Chemistry Symposium, Edinburgh, United Kingdom**  
 Poster presentation on 'Computational study of the binding specificity of cyclophilin inhibitors'

## Technical Skills

---

**Mass spectrometry:** Handling, cleaning and calibration of Thermo Q Exactive Plus, Q Exactive and LTQ Orbitrap Velos, experience with Proxeon Easy nLC-II and Easy nLC-1000 HPLC systems, pulling and packing reversed-phase columns for LC-MS

**Biochemistry:** Sample preparation methods for mass spectrometry - protein digestions in solution, in gel and FASP, phosphopeptide enrichment, antibody-based peptidome enrichment, SDS-PAGE, western blotting, immunoprecipitation, kinase assay, Seahorse assay

**Visualization:** Immunofluorescence, immunohistochemistry, confocal microscopy

**Analytical chemistry:** SCX, RPLC and isoelectric focussing chromatographic techniques

**Molecular biology:** RNA extraction, reverse transcription, PCR, cloning, plasmid isolation

**Cell culture:** Primary and secondary cell culture, SILAC labelling, transfections

**Data analysis:** Qualitative and quantitative proteomics data, MaxQuant, Perseus, R programming language, Adobe Illustrator, MS Office, online bioinformatics tools

## Teamwork/Leadership Experience

---

- Organised a Proteomics Workshop at the Max Planck Institute for Heart and Lung Research in Bad Nauheim in July 2014 for doctoral scholars of the CARDIONET Marie Curie fellowship program in Europe. Held lecture series and hands-on practical courses together with peers.
- Supervised a university student for bachelor thesis, supported colleagues with technical help and edited scientific writings in English.
- Worked with group peers in contributing towards the mass spectrometry facility service at the Max Planck Institute in supporting inter-departmental colleagues in their proteomics projects with experimental design and data analysis, and maintenance of instruments.

## Languages

---

**Proficient**                      English, Tamil and Hindi

**Medium advanced**        German (took up evening language courses during PhD)

## Voluntary Service

---

**2011**                      **Cancer Research UK, Edinburgh, United Kingdom**

Worked at a clothing store to refurbish and sell donated clothes towards contribution to the funding for cancer research

**2009**                      **SASTRA Community Outreach Program, Thanjavur, India**

Participated in providing free education and organizing social activities for poor village children

## Personal details

---

**Surname, name:** Aravamudhan, Sriram

**Marital status:** Married

**Date of birth:** 27<sup>th</sup> September 1988

**Nationality:** Indian

**Place of birth:** Chennai, India

## 8. Publications

1. **Aravamudhan S**, et al. Comprehensive phosphoproteomics of heart development identifies Mic85 as a new component of mitochondrial MICOS complex. (*Manuscript in progress*)
2. Singh SK, **Aravamudhan S**, Armant O, Krüger M, Grabher C. (2014). Proteome dynamics in neutrophils of adult zebrafish upon chemically-induced inflammation. *Fish Shellfish Immunol.* 40(1):217-24
3. Candasamy AJ, Haworth RS, Cuello F, Ibrahim M, **Aravamudhan S**, Krüger M, Holt MR, Terracciano CM, Mayr M, Gautel M, Avkiran M. (2014). Phosphoregulation of the titin-cap protein telethonin in cardiac myocytes. *J Biol Chem.* 289(3):1282-93
4. Singh SK, Sethi S, **Aravamudhan S**, Krüger M, Grabher C. (2013). Proteome mapping of adult zebrafish marrow neutrophils reveals partial cross species conservation to human peripheral neutrophils. *PLoS One.* 8(9):e73998